

MODELING AND PLUME TRACKING STUDY
OF A NEWFOUNDLAND COASTAL OUTFALL

JIHAD SHANAA



**Modeling and Plume Tracking Study
of a Newfoundland Coastal Outfall**

by

© Jihad Shanaa

**A Thesis Submitted to the School of Graduate Studies in Partial
Fulfilment of the Requirements for the Degree
of Master of Engineering**

Faculty of Engineering and Applied Science
Memorial University of Newfoundland

June 2008

St. John's

Newfoundland

Abstract

Marine pollution is a serious environmental problem facing many industrialized and developing countries. It has short-term and long-term impacts on the ecological systems, human health, and economy. These impacts can be minimized through proper offshore and coastal zone management, continuous monitoring, and enforcement of regulations. Outfall disposal can be an effective environmental and economical method for discharging treated industrial and municipal effluents to the marine environment. This is because the dynamic nature of the ocean can enhance the dilution process of the effluent. However, if the outfall is not properly designed and monitored, it may have negative impacts on the marine biota and public health. Well designed outfalls result to better effluent mixing within the ambient water.

In this work, the performance of an existing staged diffuser outfall design, at Spaniard's Bay, was evaluated using the Cornell Mixing Zone Expert Model (CORMIX) length scale model and compared with an alternative T-Shape riser design using Roberts, Snyder and Baumgartner (RSB) length scale model. The existing staged outfall design provided a better near-field dilution than the T-Shape riser for shallow coastal waters. For model validation and water quality assessment, an environmental monitoring experiment was carried out around the Spaniard's Bay outfall. An Autonomous Underwater Vehicle (AUV) and towed sensor platforms were used for monitoring salinity, temperature, turbidity, chlorophyll *a*, and dissolved oxygen. The data were statistically analyzed and mapped for plume tracking and water column assessment purposes. Turbidity and salinity observations were investigated as a natural tracer of the effluent. The turbidity values

were decreasing while moving from the effluent boil to a downstream direction. The salinity variations were also decreasing while moving from the outfall to a downstream direction. The low salinity and high turbidity results of more than 13000 *in-situ* observations were positively correlated. As for the water quality status, the dissolved oxygen percent saturation and chlorophyll *a* concentrations were not significant indicating a good water circulation in the bay. The experiment results demonstrated that effluent plume can be traced by *in-situ* monitoring of turbidity and salinity as natural tracers. These parameters were also applied for near-field hydrodynamic model validation.

Acknowledgements

I would like to thank my supervisors, Dr. Tahir Husain and Dr. Neil Bose for their excellent supervision, encouragement, and financial support through the development of this work. I gratefully acknowledge Dr. Brian Veitch and Dr. Kelly Hawboldt for their academic guidance.

I highly appreciate the help of Sara Adams, Ron Lewis, Manoj Issac, Moqin He and Haibo Niu during my experiments.

Finally, this work would have not been accomplished without the support of my wife Reema during my study period.

Table of Contents

Abstract	ii
Acknowledgements	iv
List of Tables	x
List of Figures	xi
List of Symbols	xv
Chapter 1. Introduction	1
1.1. Marine Pollution	1
1.2. Marine Outfalls	2
1.3. Outfall Modeling.....	2
1.4. Water Quality Monitoring	3
1.5. Autonomous Underwater Vehicle (AUV).....	6
1.6. Thesis Overview	8
Chapter 2. Outfall Modeling and Plume Monitoring.....	10
2.1. Outfalls Modeling.....	10
2.1.1. Effluent Entrainment.....	10
2.1.2. Diffuser Configuration.....	12
2.1.3. Ambient Conditions	14
2.1.3.1. Current	14
2.1.3.2. Stratification.....	14
2.1.3.3. Tides.....	16
2.1.3.4. Depth.....	16
2.1.4. Mixing Zone.....	16
2.1.4.1. Length Scale Near-Field Mixing Zone Models	19
2.1.4.1.1. RSB Near-Field Model	20
2.1.4.1.2. CORMIX Model	25
2.1.4.2. Far-Field Mixing Zone Model	28
2.2. Outfall disposal Regulations.....	28
2.2.1. Outfall Design.....	28
2.2.2. Dilution Ratio and Mixing Zone Regulations.....	29

2.3.	<i>In-Situ</i> Environmental Monitoring.....	30
2.3.1.	Sensor Selection Criteria.....	31
2.3.2.	<i>In-Situ</i> Water Quality Sensor and Analyzers	33
2.3.2.1.	CTD.....	33
2.3.2.2.	Dissolved Oxygen.....	37
2.3.2.2.1.	Electrochemical Technique.....	37
2.3.2.2.2.	Fiber Optic Technique	40
2.3.2.3.	Chlorophyll <i>a</i> Fiber Optic Technique	42
2.3.2.4.	Turbidity	44
2.3.2.4.1.	Optical Backscattering Sensor	45
2.3.2.4.2.	Acoustic Backscatter Sensor.....	46
2.3.2.4.3.	Laser Diffraction	47
2.3.2.5.	Nutrient Sensors.....	48
2.3.2.5.1.	Potentiometric Technique	48
2.3.2.5.2.	Flow Injection Analyzer	49
2.3.2.5.3.	UV Absorption Analyzer	52
2.3.2.6.	Hydrocarbons	54
2.3.2.6.1.	Fiber Optic Sensor	54
2.3.2.6.2.	Flow Injection Analyzer	57
Chapter 3.	Experiment	60
3.1.	Objective	60
3.2.	Study Area	60
3.3.	Site Selection	60
3.4.	Previous Work	63
3.5.	Instrumentation	63
3.5.1.	CTD.....	64
3.5.2.	Chlorophyll	64
3.5.3.	Turbidity	65
3.5.4.	Dissolved Oxygen.....	65
3.5.5.	Current Meters	66

3.5.6.	GPS	68
3.6.	Apparatus	69
3.6.1.	MUN Explorer	69
3.6.2.	Boats	71
3.6.3.	Sensor Towing Platform	71
3.7.	Experimental Design.....	72
3.7.1.	Site Survey	72
3.7.2.	Sensor Calibration.....	73
3.7.3.	AUV Sampling Plan	75
3.7.4.	Alternative Sensor Towing Plan	76
3.8.	AUV Monitoring Experiments	76
3.8.1.	AUV Experiment 1	77
3.8.2.	AUV Experiment 2	78
3.9.	Sensor Towing Experiments.....	80
3.9.1.	Water Column Monitoring Plan.....	80
3.9.2.	Towed Sensor Experiment 1	82
3.9.3.	Towed Sensor Experiment 2.....	84
Chapter 4.	Results.....	86
4.1.	Outfall Modeling.....	86
4.1.1.	Outfall Effluent	86
4.1.2.	Diffuser Geometry	87
4.1.3.	Ambient Conditions	89
4.1.3.1.	Current	89
4.1.3.2.	Tidal Data.....	91
4.1.3.3.	Stratification.....	91
4.1.4.	Model Inputs	92
4.1.4.1.	CORMIX Model	93
4.1.4.2.	RSB Model.....	96
4.2.	Data Management.....	100
4.2.1.	Data Transformation	101

4.2.2.	Data Correlation.....	102
4.2.3.	Data Integration	102
4.2.4.	Multivariate Data Analysis	102
4.2.5.	Smoothing.....	108
4.2.6.	Data Validation	109
4.3.	Environmental Monitoring and Plume Tracking.....	109
4.3.1.	AUV Experiment 1	110
4.3.2.	AUV Experiment 2	112
4.3.3.	Sensor Towing Experiment 1.....	112
4.3.3.1.	Salinity	113
4.3.3.2.	Temperature	117
4.3.3.3.	Dissolved Oxygen.....	120
4.3.3.4.	Turbidity	123
4.3.4.	Sensor Towing Experiment 2.....	126
4.3.4.1.	Salinity	126
4.3.4.2.	Temperature	130
4.3.4.3.	Dissolved Oxygen.....	133
4.3.4.4.	Chlorophyll a	137
Chapter 5.	Discussion	141
5.1.	Outfall Modeling.....	141
5.1.1.	CORMIX Model	141
5.1.2.	CORMIX Outfall Design Recommendations	142
5.1.3.	Alternative T-Shape Diffuser Risers Design	143
5.2.	Water Quality Monitoring	144
5.3.	Plume Tracking.....	145
5.4.	Water Quality Assessment.....	147
5.5.	Model Validation	151
Chapter 6.	Conclusions and Recommendations	155
6.1.	Conclusions.....	155
6.2.	Recommendations.....	157

References.....159
Appendix A. CORMIX Model Prediction File168

List of Tables

Table 1.1. AUV Development Milestone	7
Table 2.1. Mixing Zone Regulations of Different States (Doneker and Jirka, 1991).....	18
Table 2.2. Depth and Length relationship of Outfall Design (Section 5.2.15).....	29
Table 2.3. Comparison of Commonly Used CTD Sensors (Zhaoying, 2004).....	37
Table 3.1. MUN Explorer AUV Specifications.....	70
Table 3.2. Proposed AUV Environmental Monitoring Plan.....	76
Table 3.3. Sensor Towing Design Parameters	82
Table 3.4. Experiment 1 Data Summary.....	83
Table 3.5. Experiment 2 Data Summary.....	85
Table 4.1. Spaniard's Bay Outfall Model Input Summary.....	93
Table 4.2. CORMIX Near-Field Dilution Summary	94
Table 4.3. Moving Average Smoothing Technique.....	108
Table 5.1. Comparison between Stage and T- Risers Diffuser Design	143
Table 5.2. Comparison between AUV and Towed Sensor Platforms.....	145
Table 5.3. CORMIX Model & Field Data Comparison	153

List of Figures

Figure 2.1. Development Zone Profile (Davis,1999)	12
Figure 2.2. Diffuser Geometry of Unidirectional and Staged Diffuser Design (Jirka et al., 1991)	13
Figure 2.3. Effluent Discharge in a Stratified and Current Flowing Environment.....	15
Figure 2.4. USEPA Regulatory Mixing Zone Criteria (Doneker and Jirka,2004)	17
Figure 2.5. Multiport T-Shape Diffuser Design (Tian et al.,2006).....	21
Figure 2.6. CORMIX Diagram for Surface Discharges (Doneker and Jurka,2001).....	27
Figure 2.7. Parallel Plate Arrangement for Conductivity Measurement (Arvamudhan et al., 2005)	35
Figure 2.8. Piezoresistive Sensor (a) Side View (b) Top View (Mohan et al., 2004)	36
Figure 2.9. Cross Section of Clark Type DO Sensor (Farhar et al., 1998).....	38
Figure 2.10. Schematic Diagram of DO Optical Sensor (Tengberg et al., 2006).....	41
Figure 2.11. Schematic Diagram of Chlorophyll <i>a</i> FO Sensor (Wenson et al., 1998)	43
Figure 2.12. Schematic Diagram of Conventional OBS Turbidity Sensor.....	46
Figure 2.13. Schematic Diagram of ABS Turbidity Sensor (Thome et al., 1991).....	47
Figure 2.14. Schematic Diagram of a Typical ISE (Malinowska et al., 1995).....	49
Figure 2.15 FIA Process Diagram for Determining Nitrate (Worsfold, 2006).....	50
Figure 2.16 Schematic Diagram of Mark I UV Sensor (Finch et al., 1998).....	53
Figure 2.17. A Standing Wave and Evnacent Field Established Near Reflecting Interfaces (Kraft et al., 2003).....	56
Figure 2.18. Schematic Diagram of UMS (Short et al., 1999)	58

Figure 3.1. Aerial Map of Spaniard’s Bay Outfall.....	61
Figure 3.2. Spaniard’s Bay Outfall Layout.....	62
Figure 3.3 Cyclops 7 Chlorophyll <i>a</i> Sensor (Turner Design).....	65
Figure 3.4 RCM 9 LW Current Meter (Aanderaa Instruments, Inc)	67
Figure 3.5. S-4 Current Meter (InterOceans).....	68
Figure 3.6. Handheld GPS (Garmin)	69
Figure 3.7. MUN Explorer at Spaniard’s Bay Wharf	70
Figure 3.8. Fishing Boat used for the Deployment of Current Meter.....	71
Figure 3.9. Sensor Towing Platform.....	72
Figure 3.10. Chlorophyll <i>a</i> Calibration Curve.....	73
Figure 3.11. Turbidity Calibration Curve	74
Figure 3.12. Proposed Horizontal Trajectory	75
Figure 3.13. AUV Experiment 1 Trajectory	78
Figure 3.14. Experiment 2 AUV Rescue	79
Figure 3.15. Experiment 2 AUV Trajectory	79
Figure 3.16. Towed Sensor Environmental Monitoring Experiment Design	81
Figure 3.17 Current Meter Deployment - Looking Down.....	82
Figure 3.18. Left the Boat Mechanical Poly and Right is the Towed Sensor Platform....	84
Figure 3.19. Experiment 2 Horizontal Trajectory at 0.5 m depth.....	85
Figure 4.1. Spaniard's Bay Outfall Effluent Turbidity Sampling Plot, July 20, 2007	87
Figure 4.2. Spaniards Bay Outfall Design (Sharp, 1989)	88
Figure 4.3. Spaniards Bay Outfall Diffuser Design (Sharp, 1989).....	89
Figure 4.4. Outfall Diffuser Port Geometry.....	89

Figure 4.5. Current Rose Diagram - May 16-18, 2007.....	90
Figure 4.6. Spaniard's Bay Tidal Current. July 18, 2007.....	91
Figure 4.7. Spaniard's Bay Density (a) and Temperature (b) Profile. July 20, 2007.....	92
Figure 4.8. CORMIX Near-field Dilution	95
Figure 4.9. CORMIX 3-D Turbidity Concentration Graph	95
Figure 4.10. Alternative T-Shape Risers Diffuser Geometry	96
Figure 4.11. <i>In-Situ</i> Data Management and Analysis Diagram.....	101
Figure 4.12. AUV Experiment 1 Raw Data Analysis.....	104
Figure 4.13. AUV Experiment 2 Raw Data Analysis.....	105
Figure 4.14. Sensor Towing Experiment 1 Raw Data Analysis	106
Figure 4.15. Sensor Towing Experiment 2 Raw Data Analysis	107
Figure 4.16. AUV Experiment 2 Salinity Smoothing Technique.....	109
Figure 4.17. AUV Experiment 1 Vertical Profiling at the Center of the Bay.....	111
Figure 4.18. AUV Experiment 2 Surface Contour Maps.....	112
Figure 4.19. Geographical Distribution Grids	113
Figure 4.20. Sensor Towing Experiment 1 Salinity - Depth Correlation	113
Figure 4.21. Sensor Towing Experiment 1 Downstream Salinity Distribution Plots.....	115
Figure 4.22. Sensor Towing Experiment 1 Water Column Salinity Contour Maps.....	116
Figure 4.23. Sensor Towing Experiment 1 Temperature - Depth Correlation Plot.....	117
Figure 4.24. Sensor Towing Experiment 1 Downstream Temp Distribution Plots	118
Figure 4.25. Sensor Towing Experiment 1 Water Column Contour Maps	119
Figure 4.26. Sensor Towing Experiment 1 DO-Depth Correlation Plot.....	120
Figure 4.27. Sensor Towing Experiment 1 Downstream DO Distribution Plots.....	121

Figure 4.28. Sensor Towing Experiment 1 Water Column DO Contour Maps.....	122
Figure 4.29. Sensor Towing Experiment 1 Turbidity - Depth Correlation Plot	123
Figure 4.30. Sensor Towing Experiment 1 Downstream Turbidity Distribution Plots ..	124
Figure 4.31. Sensor Towing Experiment 1 Water Column Turbidity Contour Maps	125
Figure 4.32. Sensor Towing Experiment 2 Salinity - Depth Correlation Plot.....	127
Figure 4.33. Sensor Towing Experiment 2 Downstream Salinity Distribution Plots.....	128
Figure 4.34. Sensor Towing Experiment 2 Water Column Salinity Contour Maps	129
Figure 4.35. Sensor Towing Experiment 2 Temperature - Depth Correlation Plot	130
Figure 4.36. Sensor Towing Experiment 2 Downstream Temp Distribution Plots.....	131
Figure 4.37. Sensor Towing Experiment 2 Water Column Temperature Contour Maps	132
Figure 4.38. Sensor Towing Experiment 2 DO - Depth Correlation Plot.....	133
Figure 4.39. Sensor Towing Experiment 2 DO Distribution Plots.....	135
Figure 4.40. Sensor Towing Experiment 2 Water Column DO Contour Maps.....	136
Figure 4.41. Sensor Towing Experiment 2 Chlorophyll <i>a</i> - Depth Correlation Plot.....	137
Figure 4.42. Sensor Towing Experiment 2 Chlorophyll Distribution Plots	139
Figure 4.43. Experiment 4 Water Column Chlorophyll <i>a</i> Contour Maps.....	140
Figure 5.1. Sensor Towing Experiment 1 Turbidity - Salinity Correlation	147
Figure 5.2. Sensor Towing Experiment 1 Salinity and Turbidity Distribution Plots	147
Figure 5.3. 3-D DO % Saturation Concentration.....	149
Figure 5.4. 3-D Chlorophyll <i>a</i> Concentration	150
Figure 5.5. Downstream Turbidity Observations	152
Figure 5.6. Field Data and CORMIX Model Plots	154
Figure 5.7. Field Data and CORMIX Model Correlation.....	154

List of Symbols

\bar{f}	the vector diffusion flux;
D_i	the diffusion coefficient of tracer i ;
∇C_i	the gradient of the concentration of tracer i ;
u_{cl}	the centerline velocity;
b	the partial plume radius;
b'	the plume radius;
L	the diffuser length;
Q_T	the total discharge;
Q_j	the port discharge;
g	gravity force;
g'_o	modified acceleration due to gravity
q	the discharge per unit length;
ρ_a	the ambient density;
ρ_0	the effluent density;
Q_T	the total discharge;
q	the discharge per unit length;
L	the diffuser length;
F	froude number;
BV	the top-hat thickness measured vertically in X-direction;
BH	the top-hat half-width measured horizontally in Y-direction;
d	the port diameter;
s	the risers spacing;
n	the total number of ports;

u_j the port exist velocity;
 N buoyancy frequency;
 q the discharge per unit length;
 Sn the near-field dilution;
 X_n the near-field length;
 l_b the near-field length scale;
 s/l_b the diffuser port spacing length scale;
 Z_n the near-field centerline height;
 Z plume height;
 u_j the port exist velocity;
 U current speed;
 H depth;

Chapter 1. Introduction

1.1. Marine Pollution

According to the United Nations Environmental Program (UNEP, 2002), nearly 40 percent of the world population lives in coastal areas less than 60 kilometers from the shore, most of which are being threatened by untreated sewage and industrial discharges. Disposal of raw sewage to the marine environment may have an adverse impact on the marine habitats and human health. Shannon et al. (2003) reported that estrogen concentrations were found higher near to a coastal sewage source than the open ocean.

The focus of much research in the past has been on the impact of human activities on the oceans, particularly through anthropogenic pollution and exposure risks. Marine pollutants are characterized as biological, chemical, and physical. Some of the important anthropogenic sources of marine pollution are municipal discharges and offshore operations, such as produced water and drilling mud. Human exposure can be through direct contact, such as swimming, or indirect contact, such as consumption of contaminated seafood.

Ocean disposal is a common practice for discharging effluent wastes into the marine environment. The dynamic nature of the ocean constantly dilutes pollutants and minimizes stagnant conditions. However, disposal of excessive quantities of toxic pollutants can cause adverse impacts on the marine environment. In order to minimize these impacts, it has been regulated by authorities. Several socioeconomically and

environmental criteria are considered when establishing these regulations, such as the current and future intended use of marine resources, ecological vulnerability, bathymetric formation, and ambient conditions.

1.2. Marine Outfalls

Ocean outfalls are submerged structures designed to enhance the effluent dilution in the ambient. The design of these structures varies depending on economical and environmental considerations. A careful investigation of the ambient environment should be carried out before selecting the outfall location. The investigation should consider the ambient conditions, including depth, currents, and density stratification. Continuous monitoring programs should be carried out on regular bases to assure that outfalls are working properly and have minimal environmental impacts. Hydrodynamic models are important tools used for predicting the performance of proposed outfall designs.

1.3. Outfall Modeling

Outfall designs are evaluated through hydrodynamic models. In general, these models are developed to predict what changes may occur during some events in nature. Reasons for constructing mathematical models are as follows:

- (1) to gain a better understanding of the transport mechanism of a pollutant;
- (2) to determine exposure concentration to aquatic life or humans; and
- (3) to predict future conditions under different scenarios for supporting management decisions.

For outfall discharges, these models combine hydrodynamic and oceanographic equations obtained from a series of experiments. In order to develop a realistic model, it is important to integrate three components controlling the fate and transport mechanism of the plume. These components are:

- Effluent characteristics,
- Diffuser geometry, and
- Ambient conditions

1.4. Water Quality Monitoring

Environmental monitoring programs are undertaken to provide information to answer questions related to the quality of the water body. They may be a single exercise to examine a particular issue or may be ongoing programs to ensure that the water quality criteria are met. Effective monitoring programs obtain useful information and are not just data collection practices. They require collection of physical, chemical, and biological information and the interpretation of the measurements. Maher and Batley (2002) have addressed the following questions regarding to the need of environmental monitoring;

- What type of information is required?
- What specific data is needed?
- When, where and how the data is to be collected?
- What are the occupational health and safety issues?
- How is the data to be analyzed and interpreted?
- How is the quality of data to be assessed?
- What procedures are needed to ensure that data are of defined standards?

- How data is to be managed?
- How is information to be presented and communicated to those who need it?

Water quality programs are often designed for monitoring rivers, lakes, underground aquifers, and marine environments. As a common practice, random field sampling and laboratory analysis may indicate the presence of a problem in a water body, but does not provide information on the extent or boundaries of these pollutants, particularly in a rapidly changing environment, such as the ocean. These variations can highly affect the fate and transport mechanism of contaminants. *In-situ* monitoring is considered an emerging technology for water quality monitoring and plume tracking. It can be performed through simple sensors such as fiber optics or more complicated analytical systems, such as mass spectrometers.

Three approaches are being used for water quality assessment. These are laboratory analysis, *on-site* analysis and *in-situ* monitoring.

The first approach is conducted through a land based laboratory. This approach involves sample collection, preservation, storage and transportation prior to laboratory analysis. For quality control and assurance objectives, a chain of custody procedures are performed to track the sample from its source to its final destination. The United States Environmental Protection Agency (USEPA) has developed detailed procedures to preserve the integrity of the sample during its collection and storage. Nevertheless, uncontrollable chemical, biological and physical processes may occur and change the nature of the sample before its analysis. Furthermore, this method is often costly and does not provide information on spatial and temporal distribution.

The second approach of analysis is called *on-site* analysis. This approach minimizes many artifacts in comparison with the first one. Collected samples are immediately analyzed on the shipboard or facility equipped with necessary laboratory instruments. Technically, this method still does not correlate between the sample and its surrounding physical environment, such as temperature and hydrostatic pressure. In addition, it is not economically feasible to mobilize sophisticated laboratory equipments (e.g. gas chromatography, mass spectrometry) and trained staff to perform analysis at different locations (Buffle and Horvai, 2000).

The third method is the *in-situ* environmental monitoring. This method minimizes most of the artifacts occurring during collection, storage and transportation. It has the following advantages over the first two methods;

- Performs real-time measurements in locations difficult to reach, such as great depth,
- Minimizes the cost of data collection and analysis,
- Accommodates temporal data banks of complete ecosystems,
- Measures concentration gradients at environmental interfaces at high spatial resolutions, and
- Eliminates biochemical and physical changes occurring during sample collection and storage.

As for the disadvantages, this method is a relatively new and covers few parameters compared to laboratory analysis.

1.5. Autonomous Underwater Vehicle (AUV)

AUV is an unmanned submersible robot that is capable of carrying out missions autonomously. It is powered by batteries or fuel cells and can operate in deep waters. This device can autonomously perform pre-programmed missions for several hours without any human interference. They have various research and industrial applications. One of its promising applications is environmental monitoring. The AUV can be integrated with environmental and oceanographic sensors to provide high resolution spatial and temporal environmental data. These data can provide researchers and regulators a better understanding of the changes occurring in the marine environment. Table 1.1 demonstrates the milestone of some important events during the development of AUVs. A number of vehicles are commercially available including, Hugin (Norway), Maridian 600 (Denmark), AQUA EXPLORER 2 (Japan), Sea Oracle (U.S.), Explorer (Canada) and CETUS II (U.S.) (Wernli, 2000).

The vehicle can be integrated with *in-situ* environmental and oceanographic monitoring sensors to collect spatial and temporal information simultaneously. Siccardi et al. (1997) carried out a mission using multiple input fiber optic fluorometers on the AUV to identify the main features of marine plants growing on the sea bottom. On-board, a submersible microscope and a CTD equipped with multiple sensors were mounted on AUV to measure lake water quality (Kumgai et al., 2002). Ramos et al. (2001) integrated *in-situ* sensors and UM3 near-field model with an AUV to predict outfall plume characteristics. A survey of oxygen concentrations near the bed of a lake has been conducted through “TanTan” AUV (Ura et al., 2002).

Table 1.1. AUV Development Milestone

Date	AUV	Milestone
1969	University of Washington SPURV and UARS	1 st under-ice operations
1976	EAVE East-West testbeds	1 st systems integration- East-West testbeds
1980	Epaulard JL Michel	1 st seabed surveys.
1986	ARCS, AUSS JL Michel, ISE	1 st Real time operating system
	PTEREOA. Twin Burger Tamaki Ura – IIS,	New hull forms
1992	Odysey, ABE	Low cost AUVs
1992	IMTP, SEA LION	Lake science
1992	MARIUS	Integrated navigation
1994	THESEUS	Longest mission under-ice
1995	HUGIN - Karsten Vestgard	Commercial development
1996	AUTOSUB	Science missions
1997	ISE	1 st working fuel cell
1998- 2000	FUGRO, C and C, DEBEERS, and REMUS	Applications
2001	SWIMMERS	1 st Hybrid AUVs
2002	Solar Powered AUVs	Alternative power
2004	URASHIMA, LR AUV	Longest missions

The long endurance solar powered AUV was used to measure DO concentration using fast-response galvanic oxygen micro-sensor in Greenwich Bay, Rhode Island, U.S.A (Crimmins et al., 2005).

Recognizing the importance of this technology, Memorial University of Newfoundland (MUN) has recently acquired an AUV for oceanographic and environmental research applications. The vehicle known as “Explorer” is designed and constructed by International Submarine Engineering Ltd (ISE). It consists of three sections. The rear section contains the propeller and four maneuvering planes, the middle section consist of electronics and control system and two maneuvering planes, and the front section is reserved as a pay load for sensors or analytical monitoring system. More specific details on AUV will be discussed in the later sections.

1.6. Thesis Overview

The organization of the thesis is as follows:

Chapter 2 addresses a literature review on length scale hydrodynamic outfall modeling, an overview of existing outfall disposal regulations, and technical specifications of currently available *in-situ* monitoring sensors and analytical systems.

Chapter 3 describes the different components involved in the design and organization of the environmental monitoring experiment.

Chapter 4 demonstrates the modeling results of an existing staged diffuser design and an alternative T-Shape riser design. Also, the field experimental data were analyzed and mapped for plume tracing and water quality assessment.

Chapter 5 further discusses the results for plume tracking, water quality assessment and model validation, and Chapter 6 provides a conclusion and recommendations obtained from this study.

Chapter 2. Outfall Modeling and Plume Monitoring

2.1. Outfalls Modeling

Hydrodynamic models can be used to better understand the fate and transport of pollutants, determine exposure concentration to aquatic life or humans, and evaluate the outfall dilution mechanism. Three basic factors contribute to the dilution process of effluent in the ambient. These factors are the effluent characteristics, the diffuser geometry, and the ambient conditions.

2.1.1. Effluent Entrainment

Many factors contribute to the mixing of effluent when discharged into an ambient body of water. The mixing process occurs during two important phases: a jet and a plume. The term “jet” is usually associated with the effluents high velocity relative to the ambient; where the “plume” is associated with the buoyancy forces of the ambient. Entrainment is defined as the process of entraining ambient fluid into a jet or a plume. Around the discharge point, where the relative velocity between the jet and the ambient is high, the entrainment is also high. As the jet moves through the ambient and loses its momentum, the entrainment rate decreases. Turbulent eddies also contribute to the mixing process by grabbing large quantities of ambient fluid and carrying it along with the jet (Davis, 1999). When the discharge fluid is less dense than the ambient, the buoyancy affect forces the plume up to the ambient surface. During this process, the effluent is also entrained due to viscosity and turbulent shear. Molecular diffusion resulting from the random motion of

the molecules in the fluid also causes additional mixing where the higher concentration flows to the direction of the lower concentration. This process is governed by Ficks law as follows: (Davis, 1999).

$$\bar{f}_i = D_i \nabla C_i \quad (2.1)$$

where \bar{f} is the vector diffusion flux, D_i is the diffusion coefficient of tracer i , and ∇C_i is the gradient of the concentration of tracer i .

Initially, the diffusion process produces a shear layer, where the jet penetrates the ambient causing it to increase its velocity and the ambient penetrates the jet causing it to decrease its velocity. Ultimately, the ambient penetrates the jet's centerline causing it to lose its momentum. During this process, the centerline velocity and concentration are constant until they are penetrated by the ambient (Figure 2.1). This region is expressed by the Gaussian Probability Function (Davis, 1999).

$$\frac{u}{u_{cl}} = e^{-r^2/b^2} \quad (2.2)$$

where u_{cl} is the centerline velocity, and b is the partial plume radius given by the standard deviation of the profile. A close approximation to this function is 2/3 power profiles (Davis, 1999).

$$\frac{u}{u_{cl}} = [1 - (r/b')^{2/3}]^2 \quad (2.3)$$

where b' is the plume radius.

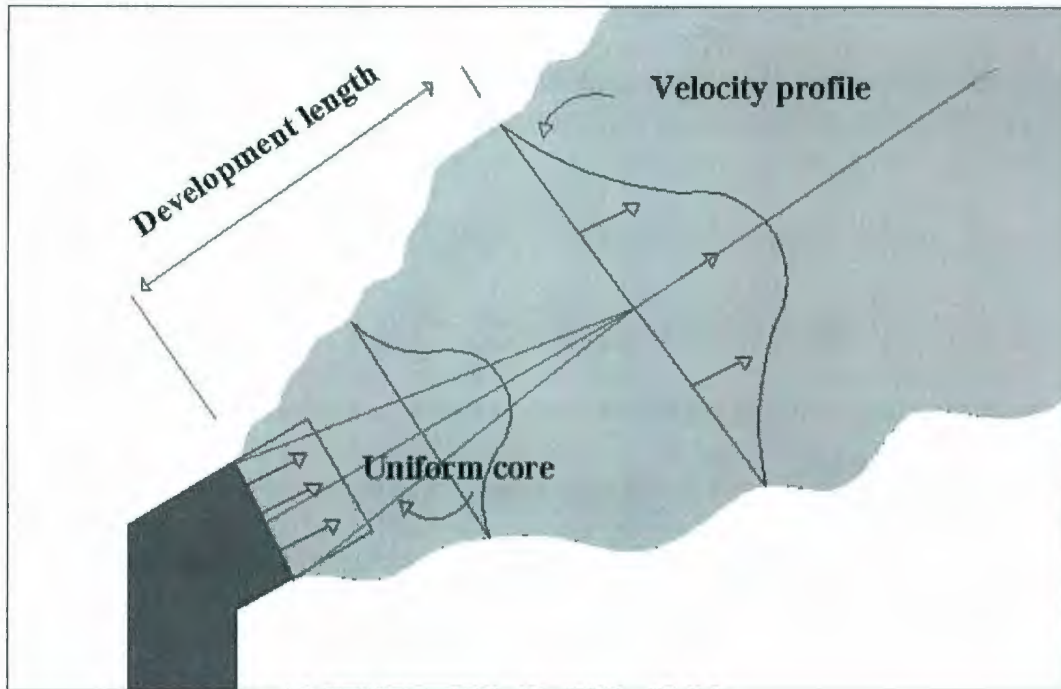


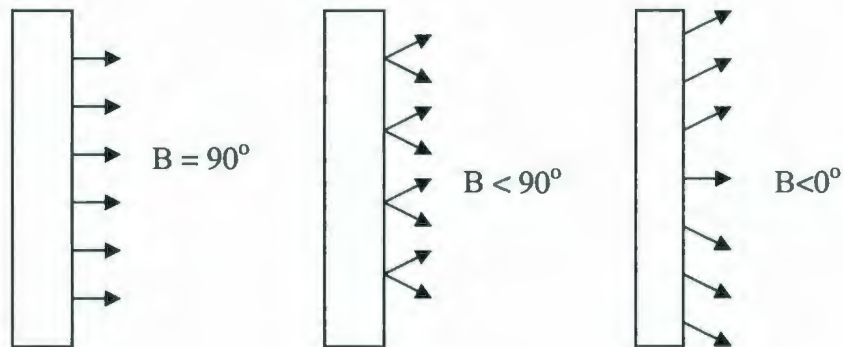
Figure 2.1. Development Zone Profile (Davis, 1999)

2.1.2. Diffuser Configuration

A diffuser is defined as an extended part of the outfall submerged by ambient water and closed at the end. The diffuser may contain two or more discharge ports. These ports can simply be holes or risers. Risers are vertical or inclined extensions of a diffuser, which is most often buried under the seabed. Each riser may consist of one or more discharge ports. The most common types of diffusers are unidirectional and staged (Figure 2.2). Outfall designers make diffusers in a way to enhance the near-field mixing process to meet regulator's objectives and minimize environmental impacts. Port orientation, spacing and discharge velocity highly influence the near-field mixing process. It is commonly believed that more discharge ports allow faster dilution and longer spacing

prevents plumes from merging. Considering regulatory requirements and economy, outfall designers often manipulate designs to combine both factors. In coastal areas dominated by currents and tides, alternating diffusers on both sides are recommended over other types (Mendez-Diaz et al., 1996).

Unidirectional Diffuser Design



Staged Diffuser Design

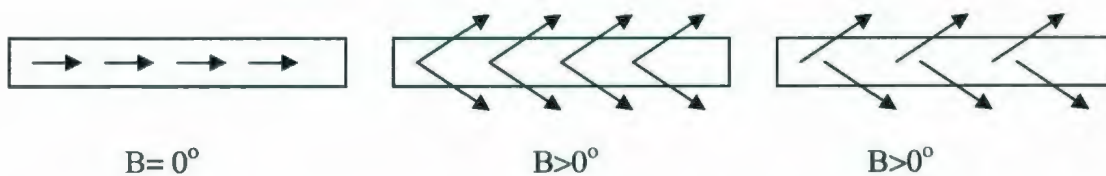


Figure 2.2. Diffuser Geometry of Unidirectional and Staged Diffuser Design (Jirka et al., 1991)

To avoid flooding during peak hours, it is recommended to have the head loss within the diffusers as low as possible and maintain a constant upstream pumping. On the other hand, it is preferable to have high discharge velocities for more rapid mixing (Davis, 1999).

2.1.3. Ambient Conditions

Ambient conditions are the external factors contributing to the effluent dilution process. They highly control the dilution process of an effluent through buoyant spreading motions, passive diffusion due to ambient turbulence, and passive advection by ambient velocity (Doneker and Jirka, 2004). The most dominating ambient conditions are current speed and direction, stratification, tidal movement, and ambient depth.

2.1.3.1. Current

In most cases, the current carries the plume in its direction and causes downstream advection. In stagnant environments, the buoyancy plume will tend to rise to the surface and spread in all directions. Currents can be considered as low, moderate or high. The higher the magnitude of the current, the more dilution is achieved. The configuration of the discharge ports and the current can highly affect the initial dilution process. Effluent dilution can be enhanced when discharge angles are perpendicular to the current. Tian et al. (2004-a) conducted an experiment using a multiport diffuser in unstratified flowing water; they concluded that in a flowing current, port spacing plays a lesser role in the dilution process.

2.1.3.2. Stratification

Ambient stratification can significantly affect the plume dynamics. When a low density effluent is discharged into a higher density ambient, the buoyancy force can cause the plume to rise up until it approaches the same density of the ambient “positive buoyancy”. When the effluent density is higher than the ambient, the plume tends to sink down

“negative buoyancy” until it approaches the same density of the ambient or hits the seabed. The level where the plume has the same density of the ambient is called trapping level. When the plume reaches this level, it starts moving horizontally along the current (Figure 2.3). A Pycnocline phenomenon occurs in lakes when a temperature variation between the lower layer and the surface layer is high and in coastal areas when density variation between these layers is also high. The stratification is expressed as a linear or two layers stratification.

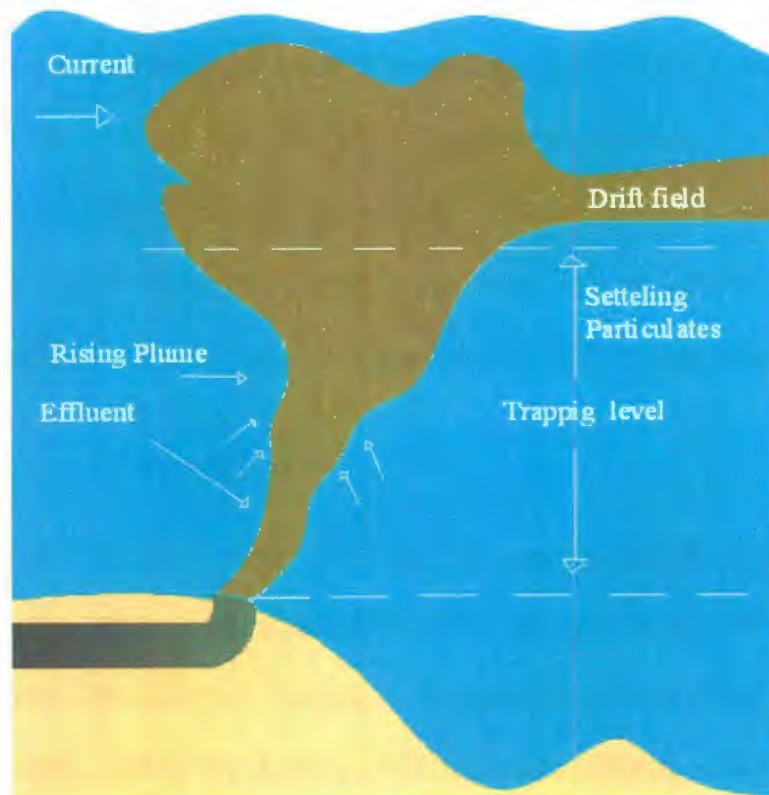


Figure 2.3. Effluent Discharge in a Stratified and Current Flowing Environment.

2.1.3.3. Tides

During the 24-hour daily cycle, tidal changes cause variations in depth, current speed and direction. In shallow coastal areas, tidal currents also cause minor variations to salinity, as the water moves in and out of the bay.

2.1.3.4. Depth

Depth can enhance the vertical mixing process. For this reason, regulators restrict the outfall discharge depth. It is recommended to install outfalls at maximum possible depth to allow better vertical mixing and minimize surface spreading. Discharges into shallow water often results in incomplete dilution and spread of pollutants at the surface layer. Often, interaction of the plume with the surface water and seabed can cause instabilities. Coanda effects occur when the plume sinks down to the bottom causing bottom interaction, which may cause a negative impact on the benthic communities.

2.1.4. Mixing Zone

A mixing zone is an area where effluent discharge undergoes initial dilution and secondary mixing in the ambient water. The USEPA has defined this zone as where water quality criteria can be exceeded, conditional that acutely toxic conditions are prevented (Doneker and Jirka, 2004). By applying this approach, ambient water can be used to dilute pollutants and minimize environmental impacts. Two mixing zones occur when effluent is discharged into the ambient water. The first zone is called the near-field mixing zone or Regulatory Mixing Zone (RMZ) and the second zone is called the far-field mixing zone. In the near-field, the mixing process is controlled by the jet

momentum and plume vertical buoyancy effects. Within this zone another zone is allocated for toxic substances, and it is called the Toxic Dilution Zone (TDZ). The USEPA has set a national water quality criterion for effluents containing toxic contaminants; the Criterion Continuous Concentration (CCC) recommends the highest in stream concentration of a toxicant to which organisms can be exposed without causing unacceptable effect. The Criterion Maximum Concentration (CMC) is another USEPA criterion for the highest in stream concentration of toxicants to which organisms can be exposed for a short period of time without causing an acute effect (Figure 2.4).

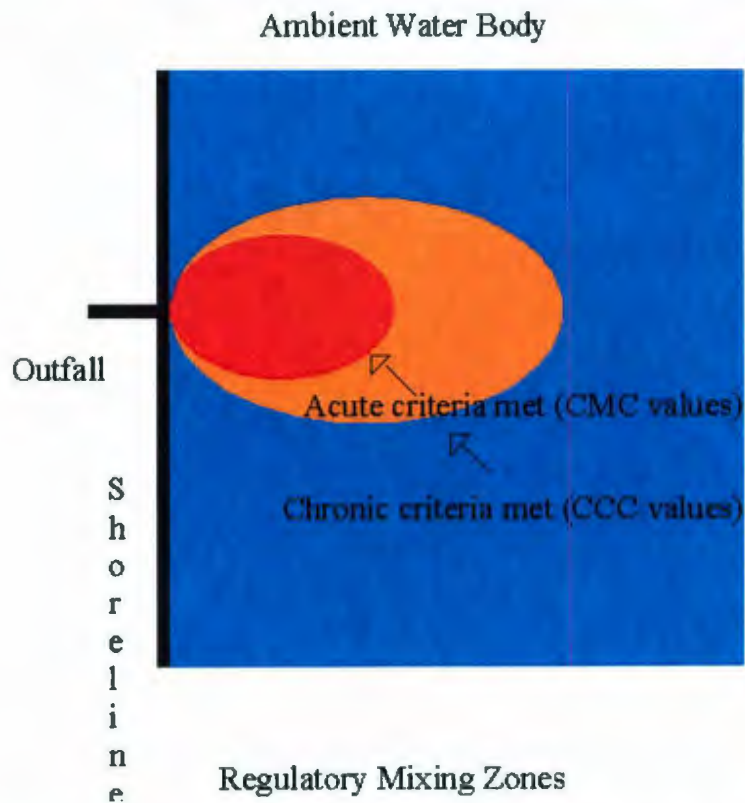


Figure 2.4. USEPA Regulatory Mixing Zone Criteria (Doneker and Jirka,2004)

In the far-field, the mixing process is dominated by ambient conditions, including current speed and direction, through which the dilution process occurs through advection. The

definition of a mixing zone varies widely from one place to another, depending on the ambient conditions and vulnerability of the marine ecosystem. For example, Table 2.1 demonstrates different mixing zone regulations in the United States (Doneker et al., 1991).

Table 2.1. Mixing Zone Regulations of Different States (Doneker and Jirka, 1991)

State	Water body	Dimensions
Florida	Streams, rivers	≤ 800 m and $\leq 10\%$ total length
Florida	Lakes, estuaries	$\leq 125,600\text{m}^2$ (600 ft radius) and $\leq 10\%$ surface area
Michigan	Streams	$\leq \frac{1}{4}$ cross-sectional area
Michigan	Lake Michigan	≤ 1000 ft radius
West Virginia	Warm-water fish streams	$\leq 33\%$ cross-sectional area and $\leq 10^*$ width
West Virginia	Cold-water fish streams	$\leq 20\%$ cross-sectional area and $\leq 5^*$ width
West Virginia	Lakes	≤ 300 ft any direction

In a highly dynamic environment such as a coastal area, the near-field mixing process is complicated and changes rapidly with time and space. Since regulators are more concerned with the near-field mixing zone, the dilution or the mixing process can be predicted using appropriate dispersion models. The most important characteristics of near-field prediction models are the dilution rate, near-field length and width, and plume

rise. The end of the near-field is where no significant dilution changes with distance. Davis (1999) has reported this location as where the dilution does not exceed 10 % of its ultimate value. One of the most commonly used models for predicting the near-field dilution are length scale models.

2.1.4.1. Length Scale Near-Field Mixing Zone Models

Considering the short time period in which the mixing process occurs in the near-field zone, chemical and biological transformations are considered negligible and are only limited to conservative or linear decay. Therefore, it is presumed that the dilution process mainly occurs due to advection and diffusion processes (Bleninger and Jerka, 2004). The length scale models are based on laboratory experiments and a dimensional analysis concept. Davis (1999) has summarized the concept as many variables contributing to the near-field mixing process; these variables can be arranged in groups that have dimensions of length, and the magnitude of these scales reflect how significant the mixing process is. Therefore, the different variables contributing to the mixing process can be expressed in a dimensional length scale to demonstrate those occurring in the field. Often, many experiments are conducted to characterize the behavior of these plumes. When the dilution collapses at a particular distance or length, this length is set as a boundary between the near-field and far-field mixing zone. If the objective is to characterize the dilution at a particular length, the length scale variable (e.g. $L1/L2$) is considered as the independent variable, and dilution rate is considered as the dependent variable (Q/Q_0) that falls through the center of the experiment data. Best fit equations are derived from these bench scale experiments to describe the relationship between these variables. Davis

(1999) has described the advantages of this method as easy to characterize and includes boundary interactions, which do not exist in other mathematical models. The author described its limitation, as extrapolation of field data may lead to prediction errors, where the best fit data do not necessarily represent all boundary sides of the plume. Furthermore, it is not always possible to have the same boundary conditions obtained from lab experiments as those in field. RSB and CORMIX are commonly used length scale models for near-field prediction.

2.1.4.1.1. RSB Near-Field Model

The RSB model is an empirical length scale model designed by Roberts, Snyder and Baumgartner. The model predicts the near-field mixing zone of a submerged multiport T-Shape riser. The model was constructed based on series of laboratory experiments, considering different ambient and discharge conditions. These experiments were conducted in both unstratified and stratified stationary and flowing waters. Figure 2.5 demonstrates a multiport T-Shape riser discharging in a stratified flowing ambient.

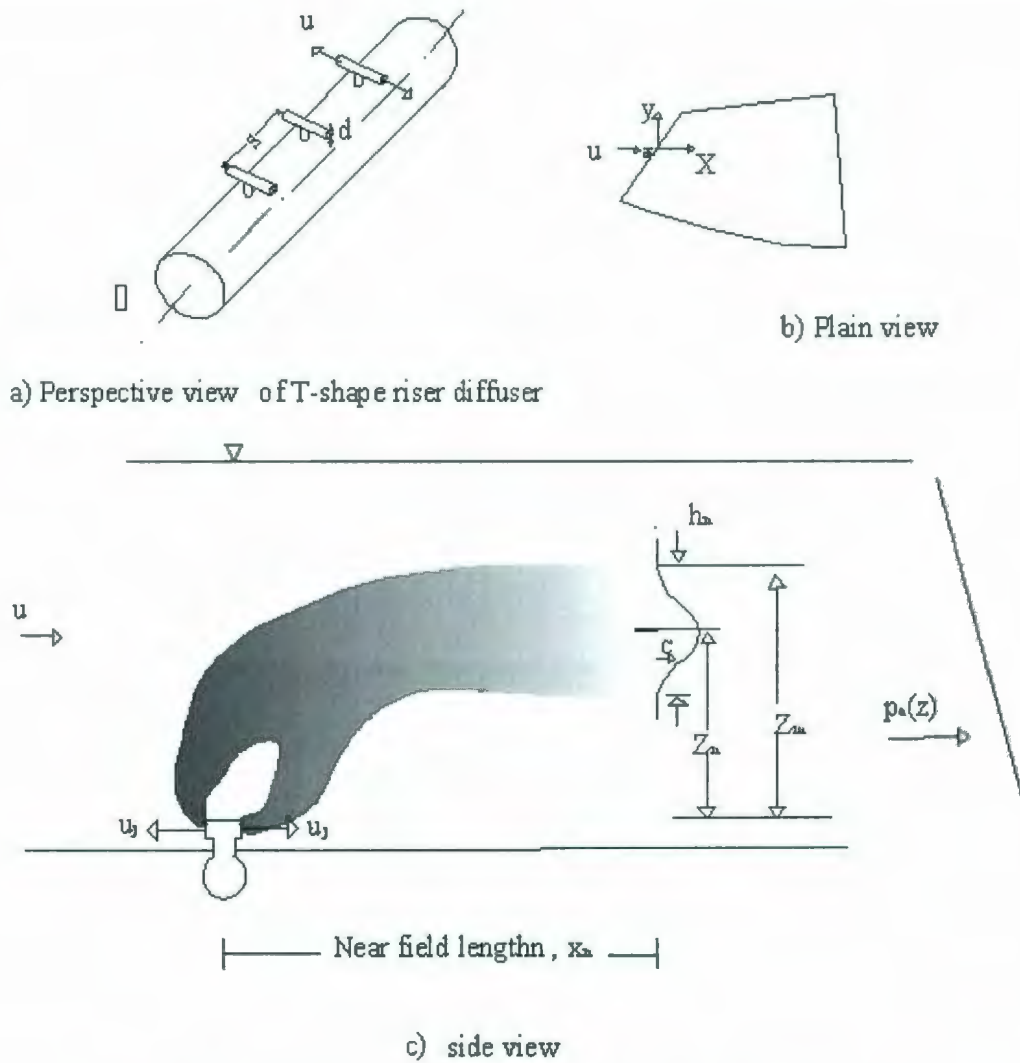


Figure 2.5. Multiport T-Shape Diffuser Design (Tian et al.,2006)

where x is the coordinate system origin extending from the center of the diffuser to a downstream direction, y is the transverse distance, Z is the height from the port, S is the spacing between ports, n is the total number of ports, d is the round port diameter, u_j is the port exit velocity, u is the uniform current flow at angle Θ to the diffuser axis, ρ_o is the horizontal buoyant effluent of density at velocity u_j , ρ_a is the ambient density at the

level of the port, ρ is the ambient density decreasing linearly with height, Z_m is the height to top of spreading layer, and Z_n is the height of the near-field dilution.

Tian et al. (2004-a) have characterized the discharge as a point source when the initial dilution is controlled by ports geometry and as line source when the discharge is controlled by the buoyancy force. They have defined the source fluxes per unit diffuser length of volume, momentum, and buoyancy, b as:

$$Q_j = (\pi/4)d^2u_j \text{ for point source, and} \quad (2.4)$$

$$q = \frac{Q_j}{L} \text{ for line source} \quad (2.5)$$

where Q_j is the flow per port, L is the diffuser length, and Q_T is the total discharge

The authors characterized the momentum flux as:

$$M = u_j Q_j \text{ for point source, and} \quad (2.6)$$

$$m = u_j q \text{ for line source} \quad (2.7)$$

They have described the buoyancy flux as:

$$B = g'_o Q_j \text{ for point source, and} \quad (2.8)$$

$$b = g'_o q \text{ for line source} \quad (2.9)$$

where B is the point source buoyancy flux, g'_o is the modified acceleration due to gravity, b is the line source buoyancy flux, and q is the flow rate per diffuser length. The line source length scales for the volume, momentum and buoyancy flux can be expressed in the following equations respectively (Tian et al., 2004-b).

$$l_q = \frac{q^2}{m} \quad (2.10)$$

$$l_m = \frac{m}{b^{2/3}} \quad (2.11)$$

$$l_b = \frac{b^{1/3}}{N}. \quad (2.12)$$

In a stratified environment, Daviero and Roberts (2006) have considered the buoyancy frequency as:

$$N = \sqrt{(-g / \rho_a)(d\rho_a / d_z)} \quad (2.13)$$

where g is the gravity force and $d\rho_a/d_z$ is the stratification difference at the discharge depth. They calculated the modified acceleration due to gravity using the following equation:

$$g'_a = g(\rho_a - \rho_0) / \rho_a, \quad (2.14)$$

and the discharge per unit diffuser length was calculated by (Tian et al., 2004-a):

$$Q_T = qL. \quad (2.15)$$

The buoyancy flux per unit length is computed by:

$$b = g_0 q. \quad (2.16)$$

Therefore, the length scale for a linear stratified environment can be obtained from (Daviero and Roberts, 2006):

$$l_b = b^{1/3} / N \quad (2.17)$$

Tian et al. (2006) conducted an experiment under stratified and current flowing environment. As a result of their experiment, they concluded that for a line source length

scale, the near- field mixing is effected by port spacing. When $s/l_b < 2$ the near-field dilution can be predicted by:

$$\frac{S_n q N}{b^{2/3}} = 1.23 F^{1/6} \quad (2.18)$$

when $s/l_b \geq 6$ the near-field dilution can be applied using:

$$\frac{S_n q N}{b^{2/3}} = 1.66 (s/l_b)^{-1/3} F^{1/9} \quad (2.19)$$

For a stationary environment when $s/l_b < 2$ the near-field equation becomes:

$$\frac{S_n q N}{b^{2/3}} = C1 \quad (2.20)$$

where the dilution coefficient $C1 = 0.86$.

Considering a flowing ambient, the effect of the current can be calculated using:

$$F = U^3 / b \quad (2.21)$$

From a series of laboratory experiments conducted in stratified flowing environments (Tian et al., 2006) found that when $s/l_b < 2$ the near-field length is obtained using:

$$X_n / l_b = 8.0 F^{1/3} \quad (2.22)$$

For a weak current when $F < 0.1$ Tian et al. (2006) suggested using equation 2.23 for computing the waste field rise heights

$$Z_m / l_b = 3.2m \quad (2.23)$$

and equation 2.24 for centerline height

$$Z_n / l_b = 1.7 \quad (2.24)$$

In unstratified flowing water, Tian et al. (2004-a) reported that the upstream dilution and merging are more rapid than the downstream. The authors concluded from this experiment that current plays a more important role than port spacing. Daviero and Roberts (2006) reported that in a stratified stationary ambient condition, where the port spacing was varied along the diffuser length, the end of the near-field occurs at a distance equivalent to one plume rise height from the diffuser. Tian et al. (2006) found that the discharge can be predicted as line plume when $s/l_b < 1.0$ and as point plume when $s/l_b \geq 6.0$ in a stratified flowing environment. In such conditions, the authors emphasized that the plume dynamics become more complex. They concluded that depending on the port spacing, upstream plumes may merge with themselves more than with downstream plumes.

2.1.4.1.2. CORMIX Model

Doneker and Jirka (2001) have described the Cornell Mixing Zone Expert System (CORMIX) as a series of programs developed to analyze and predict aqueous conventional and toxic discharges into water bodies. The system was developed for the USEPA by Cornell University during the period of 1985 to 1995. Since then, the software has been upgraded for more advanced applications. However, its main emphasis is on the diffuser geometry and dilution characteristics of the initial mixing zone for regulatory compliance applications. The program consists of three subsystems: CORMIX1, for single submerged discharges; CORMIX2, for multiple port discharges; and CORMIX3, for surface discharges. CORMIX methodology is based on the concept of boundary interactions. Boundary interactions occur when the effluent interacts with the surface or

bottom or with ambient density. From these interactions, the mixing is characterized as stable or unstable. Doneker and Jirka (1991) have reported that CORMIX has built in 80 different classification schemes for submerged single port, multiport and surface flow discharges. The classification schemes use the length scale argument to predict the near-field mixing zone. The system uses 20 different length scales to describe all possible discharges. Doneker and Jirka (2002) have reported that CORMIX 1 applies to more than 90% of submerged single port discharges; CORMIX2 applies to more than 80% of multiport diffusers; and CORMIX3 applies to more than 90% of positively buoyant surface discharges. The early versions predict the mixing zone under steady-state conditions. However, new versions can be applicable to highly unsteady environments including tidal reversal (Doneker and Jirka, 2002). An artificial intelligence technique is used to check for data consistency, calculate basic length scale parameters and determine flow classes for simulation (Doneker and Jirka, 1991). Figure 2.6 illustrates a length scale diagram used by CORMIX for hydrodynamic classification of dense near surface single port discharges (Doneker and Jirka, 2002). The EPA has recommended CORMIX as an analysis tool for permitting industrial, municipal, thermal, and other point source discharges (Doneker and Jirka, 2002). The system can also be used as a design tool for ocean outfall to improve its near-field mixing process.

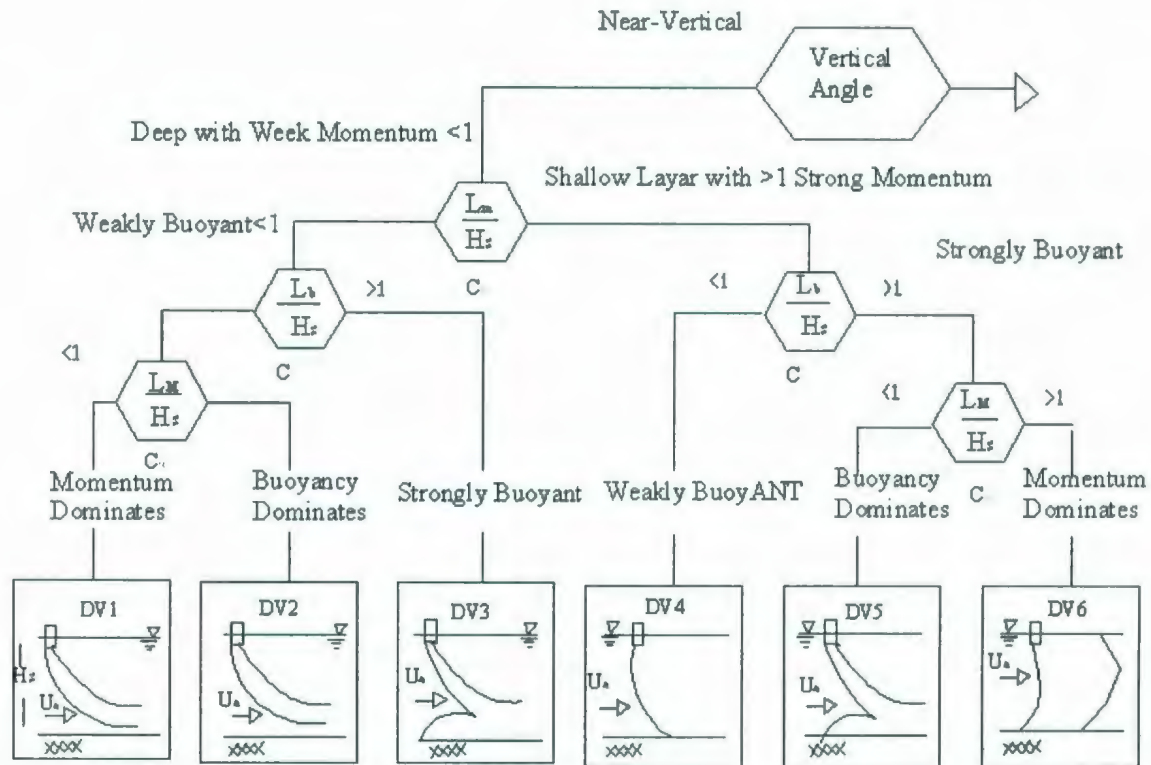


Figure 2.6. CORMIX Diagram for Surface Discharges (Doneker and Jurka,2001)

Compared to other mixing zone software, CORMIX is a user friendly; it guides the user through the modeling process and interpret output predictions. In an assessment study for brine discharges from a desalination plant (Doneker and Jirka, 2002) have used CorJet integral model and recommended using 30° to 45° port angle above the horizontal instead the conventional 60° angle. Bleninger and Jirka (2004) have coupled CORMIX near-field model with Delft3D Eulerian far-field model for coastal and estuary modeling. They have selected CORMIX because it can accommodate a wide range of discharge conditions and predicts different flow configurations.

2.1.4.2. Far-Field Mixing Zone Model

Unlike the near-field models, which are mainly controlled by the jet momentum and buoyancy, far-field models are used to model the water quality dominated by ambient conditions. Bleninger and Jirka (2004) have mentioned some of the commercially known far-field models which can be coupled with near-field models. These models include Delft3D (Delft Hydraulics), ECOM (Hydroqual), Mike 3 (Danish Hydraulic Institute), POM (Princeton University), and Telemac-3D (HR Wallingford). For coastal applications, Bleninger and Jirka (2004) have recommended Delft3D for far-field modeling. Since the far-field modeling requires additional far-field oceanographic data, it was not included in this work.

2.2. Outfall disposal Regulations

2.2.1. Outfall Design

According to the Government of Newfoundland and Labrador Outfall Disposal Regulations (Section 5.2.15), the objective of the outfall is to introduce the effluent stream into the receiving water in a manner to achieve efficient mixing with receiving water. The outfall must be located, designed, constructed and maintained for efficient mixing of the effluent discharges with receiving water. Wind speed and direction, tidal currents, other relevant oceanographic measurements, positive and negative buoyant plumes shall also be considered in the outfall design. An Outfall shall not impact on fish plants, shellfish beds, and aquaculture areas, recreational areas, and sensitive areas. The length and depth relation of the outfall was also specified (Table 2.2).

Table 2.2. Depth and Length relationship of Outfall Design (Section 5.2.15)

Dept. of Natural Resources, Government of Newfoundland & Labrador

Discharge Rate (Q) Liters/Day		Depth and length of the outfall (m)		
		Shellfish, intakes	Recreational	Others
Q ≤ 50,000	Depth	Study Required	5	3
	Length		50	30
50,000 < Q ≤ 350,000	Depth	Study Required	6	5
	Length		75	50
350,000 < Q ≤ 2,500,000	Depth	Study Required	Study Required	Study
	Length			Required
Q > 2,500,000	Depth	Study Required	Study Required	Study
	Length			Required

*Length refers to the distance from the low water mark to the point of discharge or the first diffuser nozzle.

* Depth refers to the distance between the low normal spring tide level to the top of the outfall.

In Section 5.2.15.3 of the receiving water quality objectives, the regulations state that the typical level of treatment required for any new treatment plant is secondary treatment with disinfection. However, treatment level will be evaluated on case-by-case basis.

2.2.2. Dilution Ratio and Mixing Zone Regulations

Reference to section 5.2.15.3.2.1 of the regulations, dilution ratios should be based upon 7 consecutive day average low stream flow occurring once in 20 years (7Q20) and the peak hourly effluent discharge rate. Section 5.2.15.3.2.2 has indicated that the mixing

zone should be as small as possible to minimize impact on the marine environment. Mixing zone size shall be established on case-by-case bases, but for marine bodies of water, it shall not exceed a radius of 100 m or 25 % of the width of the body of water, whichever is less.

At the boundaries or the outer limits of the mixing zone, beneficial water uses should be achieved. No conditions within the mixing zone should be permitted that:

1. are rapidly lethal to aquatic life;
2. cause irreversible responses or effects;
3. result in bioconcentration of toxic materials to the organism or its consumer; or
4. attract an organism to the mixing zone.

2.3. *In-Situ* Environmental Monitoring

In-situ monitoring is performed through miniature sensors or analytical systems. A sensor is defined as a device developed to measure a single or a few species and composed of an electrode (metal) or optode (fiber optic) combined with one or several diffusion/reaction chambers separated from the sample medium by a membrane (Buffle and Horvai, 2000). Analytical systems are more complicated than sensors; they are used to measure compounds by combining one or more sensors and reagents for chemical transformation or separation of the analyte. Analytical systems usually include pumps, injection valves, reaction chambers, and sensors. There is a big demand for the development of *in-situ* sensors and analytical systems for environmental monitoring applications.

2.3.1. Sensor Selection Criteria

As any other field instrumentation device, important criteria shall be considered when selecting an *in-situ* sensor or analytical system for environmental monitoring. These criteria include:

Reliability: Reliability is defined as the ability of a product to perform well without failure during its life cycle. For field applications, robustness of the sensor shall be high, especially for measurement at a depth in which no visual contact is possible and repairs are difficult. The most common reliability problems associated with *in-situ* sensors are pressure and temperature variations, which may affect the integrity of the sensor.

Sensitivity: Sensitivity of a sensor is evaluated based on the wide range of concentrations it can detect. For major components such as O₂, CO₂, alkalinity, NO₃⁻ and phosphate, the *in-situ* device shall be able to detect concentration in the range of 10⁻² to 10⁻⁶ mol/L and 10⁻⁶ to 10⁻¹⁵ mol/L for minor or trace compounds including organic pollutants and most of the periodic table elements (Buffle and Horvai, 2000). It is recommended to select a sensor that detects contaminants at levels less than the regulatory limits and responds to extremely high concentrations.

Response Time: The sensor response time is the time required for a sensor to detect process, and record a signal. This time may vary from a fraction of a second to hours. However, for environmental monitoring, it is always preferable to accumulate large amount of data within a short period of time. Usually, sensors have a faster response time than analyzers because they are simpler and do not require chemical reactions. The response time of a sensor often depends on the type of parameter to be measured and its concentration (Kraft et al., 2003).

Power consumption: A sensor's power consumption can limit the duration of the monitoring mission. The higher the consumption, the less monitoring time is achieved. Rechargeable lithium-ion batteries are commonly used for AUV applications. Vestgard and Hensen (2001) have extended the mission of HUGIN 300 AUV for seabed mapping to hours using a 40 kWh aluminum oxygen fuel cell.

Stability: Stability of measurements is related to the ability of the sensor to resist drifts due to pressure and temperature variations. Most of the *in-situ* monitoring sensors have numerous sensitive components that could be affected by environmental conditions. Environmental conditions such as temperature, pressure and PH are the main factors affecting the stability of *in-situ* sensors (Alai et al., 2005).

Speciation Capabilities: *In-situ* analyzers are designed to measure simultaneously different parameters or compounds, while sensors often measure only one selected species (Buffle and Horvai, 1998). The elevated ionic strength, high content of dissolved substances, and presence of marine organic matters make seawater a difficult matrix for chemical analysis (Kraft et al., 2003).

None Perturbing: Perturbation occurs when the sensor size and shape disturb the test medium. Therefore, with a smaller sensor size less perturbation occurs. In general, the size of a sensor is smaller than an analyzer.

Sensor Noise: Noise is a common problem associated with *in-situ* monitoring. When the sensor signal indicates a change, but actually no change has occurred, it's considered as a false positive noise. When the source signal does not indicate a change, but actually a change has occurred, it's considered a false negative noise. There could be various

reasons for such failures including electronic issues, matrix effects, sensor misplacement, wrong installation, and sensor malfunction (Alai et al., 2005).

Weight & Size: Weight and size are important features of a sensor, particularly for AUV applications. Since the payload of the AUV is limited and can affect the vehicle buoyancy in the water column, it is recommended to select a lighter weight and smaller size sensor.

Life Expectancy: The life expectancy of a sensor represents the time that a sensor is expected to operate under normal conditions. Preventive maintenance programs can extend the life time of a sensor. It is recommended to use a sensor or analytical system on regular bases to keep it in good working condition.

Operation: In most cases, sensors are used by personnel with limited knowledge in electronics, therefore they should be simple to operate and easy to troubleshoot.

2.3.2. *In-Situ* Water Quality Sensor and Analyzers

The objective of this review was to select appropriate sensors for the proposed environmental monitoring experiment. Three *in-situ* sensors and two analytical systems were reviewed in this work. The parameters of consideration were conductivity, temperature and depth (CTD), oxygen, chlorophyll *a*, nutrients and hydrocarbons.

2.3.2.1. CTD

CTD is a commonly used oceanographic instrument for measuring salinity, temperature and depth. By measuring conductivity, salinity measurement can be determined. Since an electrical current passes more easily through water with a higher salt content, salinity

concentration can be determined (Figure 2.7). Aravamudhan et al. (2005) explains this as based on the fact that more salt is added to water, hydration of the salt ions takes place and becomes more difficult for the ions to orient themselves in the direction of the electric field. This change corresponds to a change in the sensors' capacitor. Therefore, when the conductivity of water is determined, the amount of salt in the water can be determined. Salinity is measured in psu (practical salinity unit). Fujinawa et al. (1980) demonstrated from their experiment that CTDs can provide sufficient accuracy of 0.03% for salinity and 0.01 °C for temperature while cruising at up to 4 knots. For temperature, Platinum Resistance Thermometer (PRT) and thermistors are the most widely used temperature sensing elements. The PRT works on the principle of resistance through a fine platinum wire. They are known to be stable over a long period of time and their resistance is listed either 50 or 100 ohms at 0 °C.

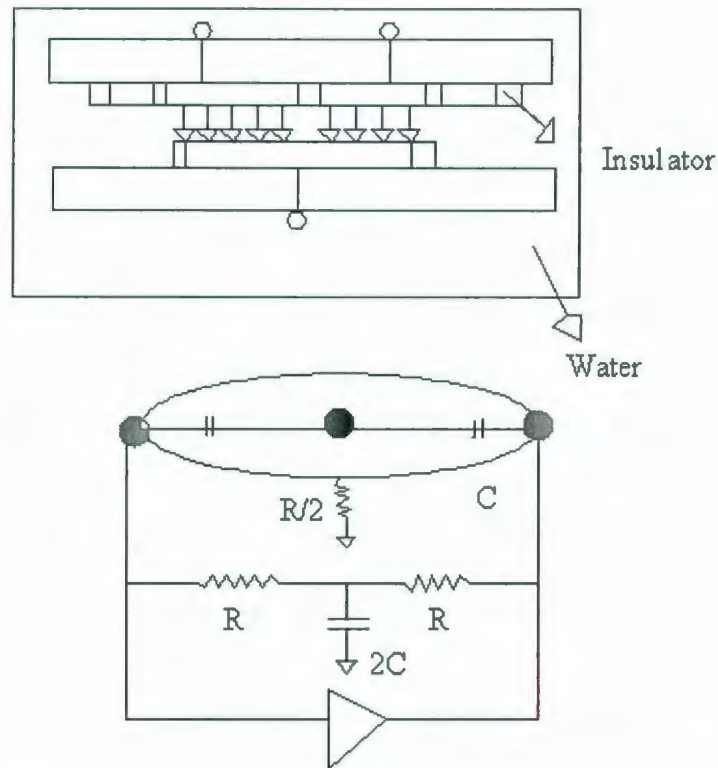


Figure 2.7. Parallel Plate Arrangement for Conductivity Measurement (Aravamudhan et al., 2005)

Two types of PRT sensors are commonly used, the first one is ceramic coated and the other is glass ceramic coated. Ceramic PRTs are good for temperatures ranging from -200 to 750 °C. The glass coated ceramic PRTs are good over a range of -100 to 500 °C.

The pressure sensor design is based on a flexible membrane as the coil element for the sensing pressure. The deflection of the membrane due to pressure is converted into electrical output through a piezoresistor component, which is sensitive to diaphragm deflection (Aravamudhan et al., 2005). The piezoresistive micro-electro mechanical (MEMS) pressure sensor can operate up to 1000 meter depth (Mohan et al., 2004). It consists of a thin silicon diaphragm with small regions diffused with p-type or n-type elements that act as a piezoresistor (Figure 2.8). The pressure values at such depths would

typically be in the range of 3000 psi, and the temperature conditions would vary from -5 to 60 °C (Mohan et al., 2004).

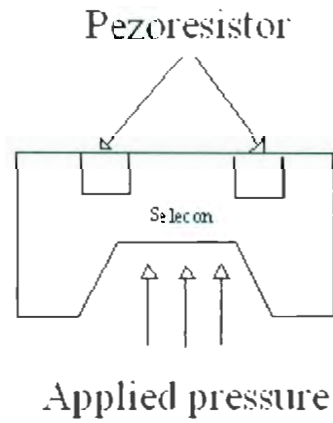


Figure 2.8. Piezoresistive Sensor (a) Side View (b) Top View (Mohan et al., 2004)

Zhaoying (2004) compared the performance of three commonly used CTDs in oceanographic studies, the Sea-Bird Electronics (SBE911), the Falmouth Scientific Inc (ICTD), and the InterOcean Systems Inc (513D) (Table 2.3).

Table 2.3. Comparison of Commonly Used CTD Sensors (Zhaoying, 2004).

Sensor		SBE-911	ICTD	513D
Temperature	Range (°C)	-5 to 35	-2 to 35	-5 to 45
	Accuracy(°C)	± 0.001	± 0.001	± 0.02
	Response (s)	65ms	20ms	1400ms
Conductivity	Range(ms/cm)	0 to 70	0 to 70	0 to 65
	Accuracy(ms/cm)	± 0.00	± 0.002	± 0.02
	Response (s)	65ms	50ms	20ms
Pressure	Range(MPa)	± 0 to 6800	± 0 to 6000	± 0 to 6000
	Accuracy(MPa)	± 0.015%	± 0.01%	0.15%
	Response (s)	35ms	30ms	

2.3.2.2. Dissolved Oxygen

Monitoring Dissolved Oxygen (DO) can directly indicate the quality of a water column. The most common *in-situ* DO measurements are conducted through the amperometric and optical based sensors.

2.3.2.2.1. Electrochemical Technique

Electrochemical microsensors have been developed for several applications including medical, industrial and environmental monitoring. For *in-situ* monitoring, the Clark type has been recommended and widely used over other techniques (Wu et al., 2005). Many improvements to the original design of the Clark type have been made since the

publication of a pioneering patent in 1959 by Leland C Clark (Lembit and Compton, 1996). Fraher et al. (1998) described the system as it consists of a platinum disk cathode, a working electrode embedded in a cylindrical insulator, and a ring shaped silver anode located around the lower end of the insulator (Figure 2.9). The electrode and the insulator are placed inside a rod made of glass that contains an electrolyte (KCl 3M). The oxygen permeable membrane is fixed at the bottom of the outer glass rod with an O-ring. Various membranes have been used, the most common ones are collodion, polystyrene, silicon, acrylic polymers, cellulose acetate and DPX resin gold plated cathode. The sensor measures dissolved oxygen indirectly through an electrochemical reaction.

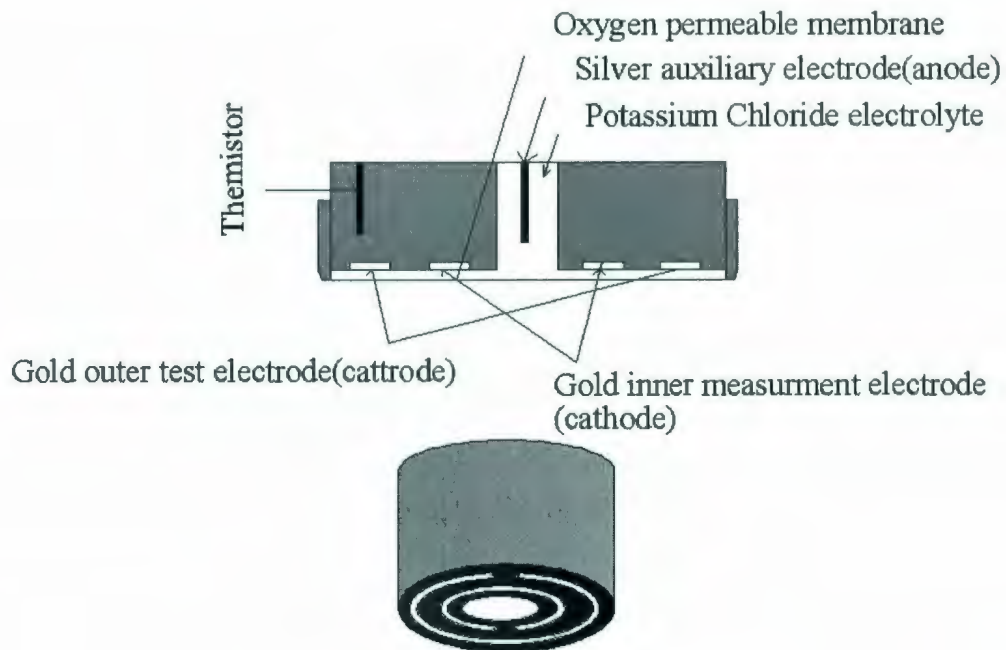


Figure 2.9. Cross Section of Clark Type DO Sensor (Farhar et al., 1998)

Buffle and Horvai (2000) have described the working principle of the sensor is based on the fact that its tip contains a cathode (positive electrode) and anode (negative electrode) that are connected electrically by a saturated electrolyte solution (KCl), all covered by a permeable membrane. Oxygen molecules dissolved in the water pass through the membrane and are chemically reduced within the sensor generating an electrical current that is proportional to the oxygen concentration in the water. The current is then converted to the oxygen concentration that is either displaced on the meter or stored as data for later retrieval. Compared with other microoptodes, the Clark type has a faster response time (Tengberg et al., 2006). A well designed Clark-type oxygen sensor can have a 90% response time (t_{90}) of around 0.1 second (Glud et al., 2001). In general, microelectrodes suffer from interference with other ions, particularly Ca^{+2} and Mg^{+2} (Kohls et al., 2000). Johnson et al. (2004) reported, for continuous monitoring application, the Clark type requires frequent calibration due to environmental changes. Permeability and the thickness of the membrane can determine the sensitivity of the sensor. Buffle and Horvai (2000) expressed this relationship as R/δ , where R is the electrode radius and δ is the diffusion layer thickness. Membrane contamination could be a limiting factor for the Clark type, particularly in a highly polluted water column. Contamination of the membrane causes a change in the sensor's sensitivity, which requires external recalibration (Johnson et al., 2004). Another limitation is when the electrolyte consumes all the available oxygen, making it not practical for long term measurements (Hendrikse et al., 1998).

In several AUV monitoring experiments, the Clark type DO sensor has been selected due to its fast response time. A solar operated AUV was fitted with a fast response galvanic

oxygen micro-sensor (AMT Analysenmesstechnik GmbH, Rostock, Germany). Criminns et al. (2005) have reported that the sensor provided a response time of a few milliseconds while profiling at a depth of 100 m. Tervalon et al. (2002) have integrated Seabird SBE 43 Clark type DO sensor with AUV for ice profiling mission in the Arctic. In another mission, the Seabird oxygen sensor, based on a modified Clark polarographic membrane, was used on the Sea Glider AUV (Rudnick et al., 2004). Adams (2005) has used a Clark type sensor for environmental monitoring of effluent plumes in coastal Newfoundland.

2.3.2.2.2. Fiber Optic Technique

Optodes technology has been known for many years, but it is relatively new to aquatic research. Tengberg et al. (2006) have described the optical fiber sensor as consisting of an optical silica fiber with an outer diameter of 140 μm tapered to a final diameter of 30 μm by heating. The fiber dip is coated with the indicator matrix. An additional layer of black silicon is coated onto the sensor to shield out ambient and backscattering light during measurements. The backward light is collected by the same fiber to the measuring device containing a miniaturized photodiode (Figure 2.10).

The working principle is based on the ability of a selected parameter to act as dynamic luminescence quenchers. In the case of oxygen, if the ruthenium-complex is illuminated with a blue/green Light Emitting Diode (LED) at a wave length of 450 μm , it will be excited and emit a red luminescent light with an intensity of 690 μm (Tengberg et al., 2006). The fluorescence intensity is used as the information carrier and it is proportional to the oxygen concentration.

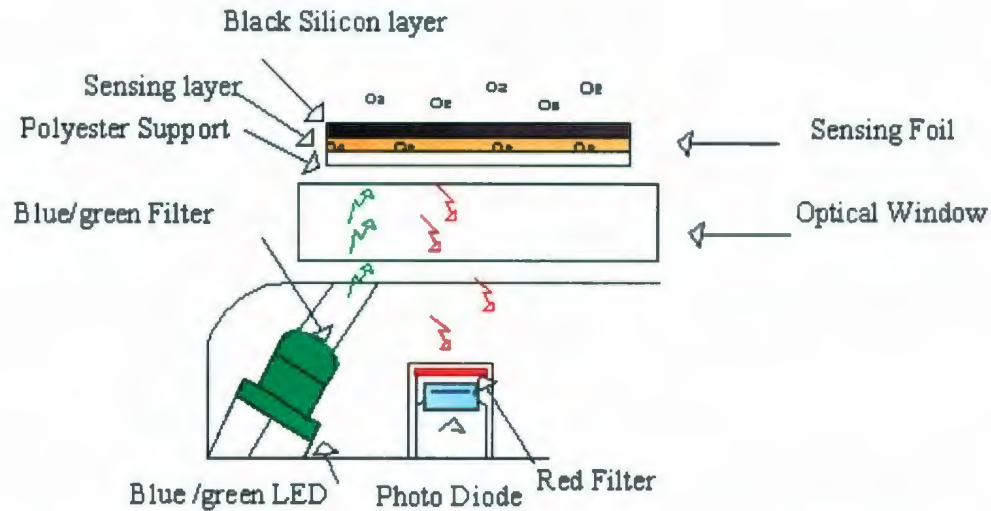


Figure 2.10. Schematic Diagram of DO Optical Sensor (Tengberg et al., 2006)

In eleven different laboratory and field experiments, Tengberg et al. (2006) have reported that a fiber optic based oxygen sensor is more suitable than other methods due to its high accuracy ($\pm 2\mu\text{M}$); long-term stability; lack of pressure hysteresis; lower fouling and cross sensitivity. Oxygen optical sensors are not affected by interference such as Ca^{+2} and Mg^{+2} like microelectrodes and there are no metallic components generating electrical fields (Kohls et al., 2000). In addition, optical oxygen sensors are suitable for long deployment periods because no oxygen is consumed during measurements, unlike electrochemical based sensors (Koneke et al., 1999). But when it comes to response time, electrochemical sensors are unmatched. However, the use of oxygen optodes in the oceanographic community is relatively new and the assessment of its performance is still an active laboratory research (Rudnick et al., 2004).

2.3.2.3. Chlorophyll *a* Fiber Optic Technique

Chlorophyll *a* is the pigment that allows plants including algae to convert sunlight into organic compounds in the process of photosynthesis as illustrated below



Chlorophyll *a* is the predominant type found in algae and cyanobacteria (blue-green algae), and its abundance is a good indicator of the amount of algae present in the waters. Excessive quantities of chlorophyll *a* can indicate a presence of algae blooms.

Monitoring chlorophyll *a* level is a direct way of tracking algal growth. Water column containing high chlorophyll *a* levels are typically high in nutrient levels, particularly phosphorous and nitrogen. High levels of nitrogen and phosphorous can be indicators of man-made pollution, such as a poorly operated wastewater treatment plant, leakage from a sewer system or fertilizer runoff. There are various techniques for measuring chlorophyll *a* concentrations, including High Performance Liquid Chromatography (HPLC), spectrometry and fluorometry. All these methods are published in the standard methods for the examination of water and wastewater. However, for *in-situ* applications, the fiber optic technique is the only dominating technique.

One of the characteristics of chlorophyll *a* is that it fluoresces when irradiated with light of a particular wavelength and emits light of higher wavelength (lower energy). The ability of chlorophyll *a* to fluoresce is the basic operating principle of all *in-situ* fluorometers. A Light Emitting Diode (LED) is used as a light source, and it has a peak wavelength of approximately 470 nm. The LED with such a wavelength produces radiation in the blue region of the visible spectrum. When the blue light hits the

chlorophyll *a* cell, it will emit a light within 650-700 nm region of the spectrum. The emitted light is then absorbed by another fiber optic and directed to a photodetector through a filter. The purpose of the filter is to prevent any backscattered excitation light to reach the photodetector. Wesson et al. (1999) have described the components and the working principle of a fluorometer (Figure 2.11) as: (1) a clock is used to switch a light emitting diode having wavelength around 490 nm, (2) the LED passes through a blue optical filter (3) and illuminate the volume of water containing fluorescent sodium dye (4). The dye is excited at this wavelength and fluoresces near 575 nm. Emitted light passes through a green optical filter (5) and into a miniature photomultiplier tube (PMT) (6). The green optical filter prevents the LED to enter and allows only the excited light from the sample to pass. An electronic band pass filter (7) is used to reduce the very high frequency noise. The signal is then fed through an electronic synchronous chopper (8) synchronized to clock frequency. Finally, the signal is filtered (9) before showing any signal.

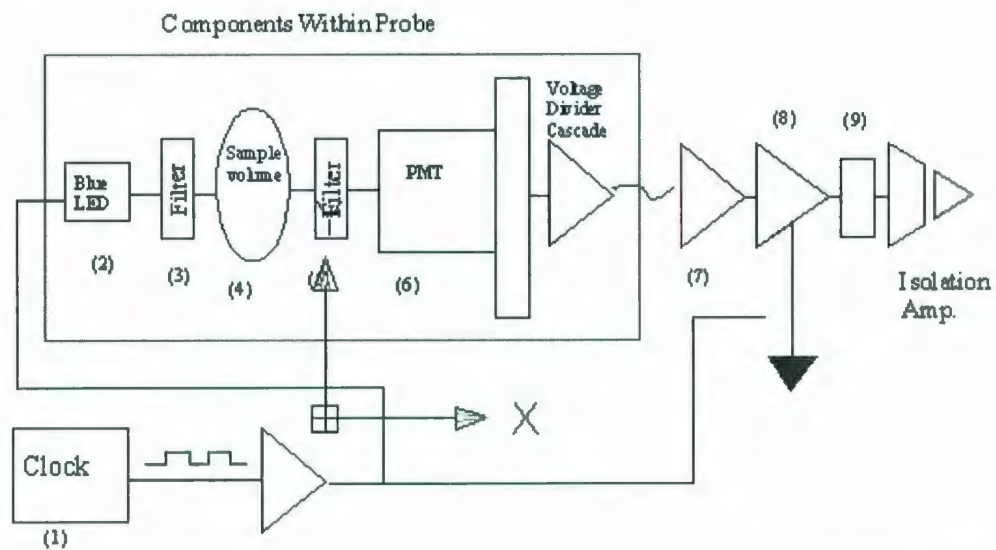


Figure 2.11. Schematic Diagram of Chlorophyll *a* FO Sensor (Wenson et al., 1998)

The advantage of fiber optic sensors is that the power consumption is low, particularly for long term deployment. The power consumption of a chlorophyll *a* fiber optic sensor manufactured by WET Labs makes the device well suited for measuring ocean dye patches, where size and power consumption are limiting factors (Wesson and Sauners, 1990). For long term deployments, biofouling problem may affect measurements of the fiber optic sensor. Antifouling agents can be used to minimize this problem, but may affect the optical properties of the sensor (De'Sa et al., 1997).

Another common problem associated with fluorometers is the effect of stray light and bioluminescent bacteria *vibrio fischeri* which might be registered as fluoresce (Wesson and Sauners, 1990). Also, environmental stresses on the sensor may cause fiber degradation, biofouling, strobe, and electronic drift (Wesson and Sauners, 1990).

Chlorophyll *a* has been monitored using AUVs in many fresh and marine water environments. Siccardi et al. (1997) used a multiple input fiber optic LED fluorometer on the AUV to estimate the seabed vegetation. Carder et al. (2001) have mounted a chlorophyll *a* fluorescence sensor with the AUV for environmental monitoring. Ishikawa et al. (2005) have mounted a fluorescence chlorophyll *a* sensor (AQFL-1000MG Aquamatic) on the AUV for image analysis and detection of freshwater red tide.

2.3.2.4. Turbidity

Many methods exist for measuring the concentration of suspended sediments in the marine environment. The traditional turbidity sampling technique is conducted through an instantaneous bottle sampling or through a continuous pump sampling. These methods are considered intrusive, labor intensive and expensive. Another problem with intrusive

sampling is that it's difficult to maintain the sediment aggregate found *in-situ*. Aggregates that exist in suspension may be broken up while sampling or new aggregates may form after settling (Creed et al., 2000). The three common *in-situ* monitoring techniques are the Optical Backscattering Sensor (OBS), the Acoustic Backscattering Sensor (ABS), and the Laser Diffraction Sensor (LDS).

2.3.2.4.1. Optical Backscattering Sensor

Turbidity is a general indicator of the optical clarity of water and is defined as the amount of light scattered from particles in the solution. In practice, a light beam is directed into a water sample and a photo detector measures the light scattered at a 90° angle. While other scatter angles are possible, the 90° measurement angle has become the standard for turbidity measurement. In working principle, the lens in front of the light source directs a beam of light at a 45° angle into the sample, while another lens in front of the photodetector collects the 90° scattered light and directs it to the detector. The signal generated by the detector is then recorded (Figure 2.12).

The Nephelometric Turbidity Unit (NTU) is a standard unit used for measuring turbidity. Depending on the application, some sensors can measure turbidity values ranging from 0 to 1,000 NTU, while others are capable of measuring up to 4,000 NTU (Rasmussen et al., 2002). Optical backscatter sensors have advantages of being relatively inexpensive, rugged, relatively unobtrusive and easy to operate (Battisto, 2000). The Potential limitation of the OBS is its sensitivity to suspended particle grain size such as silt and clay (Battisto, 2000). Biofouling problems may also occur during long-term deployment and affect the sensitivity of the sensor.

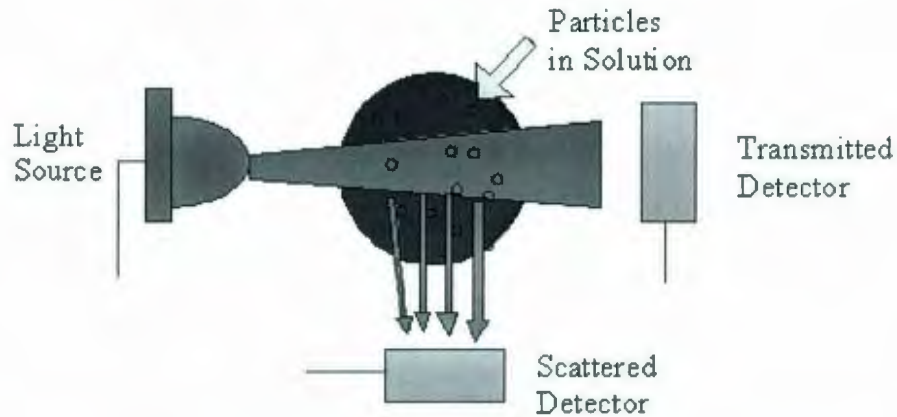


Figure 2.12. Schematic Diagram of Conventional OBS Turbidity Sensor

Several AUV monitoring missions were conducted using OBS sensors. An optical backscatter sensor was mounted on Remote Environmental Monitoring Units (REMUS) with other scientific payload sensors (Alen, 1997). A long-term ecosystem mission for coastal observation has employed an optical backscattering sensor to measure turbidity in the water column (Schofield et al., 2002). A combination of backscattering and a fluorescence sensor was integrated on the Glider AUV for an ocean research program (Rudnick et al., 2004).

2.3.2.4.2. Acoustic Backscatter Sensor

The Acoustic Backscatter Sensor (ABS) measures suspended sediment concentration through the echo sounding technique. The transducer emits a very short pulse ($\sim 10 \mu\text{s}$) at a high frequency ($\sim 1\text{-}5 \text{ MHz}$), and the acoustic energy is scattered off the suspended sediments back to the transducer (Figure 2.13). The concentration and size of the suspended sediments are related to the magnitude of the backscattered signal and the

range of the sediment associated with the time delay between transmission and reception of the signal (Battisto, 2000).

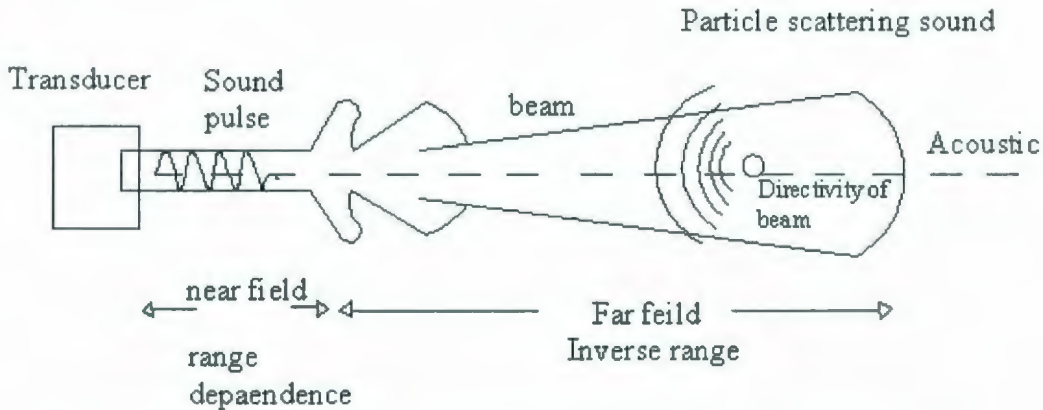


Figure 2.13. Schematic Diagram of ABS Turbidity Sensor (Thome et al., 1991)

The ABS technique has a relatively long signal path length, which makes the signal highly affected by adsorption and air bubbles (Battisto, 2000). Gartner (2002) reported that this technique suffers from the same limitation as any single frequency sensor, as it does not differentiate between changes in size distribution and concentration.

2.3.2.4.3. Laser Diffraction

The laser diffraction turbidity measurement technique is considered as the most recent technique for turbidity measurement. Sequoia Scientific has described the process as when a parallel laser light wave strikes a particle, part of the wave enters the particle and the other part is blocked by it. The wave entering the particle senses the particle composition. This part is scattered into a wide range of angles, in which very little of which appears in the original light wave direction. Laser diffraction technique has many advantages over other techniques, as it can precisely measure scattering light at a 32°

angel. As for its limitations, this technique is new and has not been widely tested and is considered more expensive compared to other techniques. The LISST costs around \$ 10,000, limiting its application only to larger monitoring projects (Campbell et al., 2004). Sibenac et al. (2002) have reported using the LISST for measuring particle size distribution on the Odyssey AUV for routine deep water monitoring operations.

2.3.2.5. Nutrient Sensors

Excessive nutrient levels in the water column often resulting depletion and disturbance of ecosystem. Gray et al. (2005) have reported, considering the high spatial and temporal variability of nutrients in the water column, there is a need for developing *in-situ* measurement techniques with a rapid response and the ability to collect long-term data. The most common techniques used for measuring nutrients are: the potentiometric method; the flow injection analysis; and the UV Absorption spectrometry analysis.

2.3.2.5.1. Potentiometric Technique

Potentiometric analyses are based on measuring the potential difference of an electrochemical cell in the absence of the current. An Ion Selective Electrode (ISE) is a commonly known potentiometric technique used to measure the ion concentrations of a sample. These electrodes measure a wide range of anions and cations. For an *in-situ* environmental monitoring application, the ion-selective membrane is the main component of all potentiometric sensors. It establishes the selectivity of the sensor's response to various interfering ions present in the sample. The sensing platform of the membrane consists of an ion carrier (ionophore) entrapped within a liquid polymeric

membrane. The membrane offers interaction with numerous species, but the main interaction governing the selectivity of the sensor is between the analyte interference and the ionophore. Once an ionophore that offers the preferred selectivity has been developed and the polymer components that are ionophore compatible have been optimized, the production of functional ISE becomes easy and rapid (Buffle and Horvai, 2000). The potentiometric technique is still a typical research tool mainly used for microbiological studies. Buffle and Horvai (2000) have reported that ISEs are more fragile, noise sensitive, and difficult to prepare, therefore, they are not considered instruments of choice or routine water analysis. Figure 2.14 demonstrates a schematic diagram of a typical ISE.

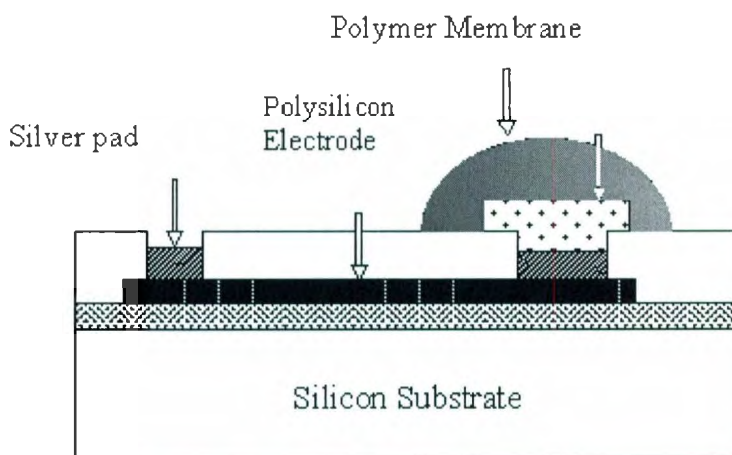


Figure 2.14. Schematic Diagram of a Typical ISE (Malinowska et al., 1995)

2.3.2.5.2. Flow Injection Analyzer

For some *in-situ* applications where interference between analytes and seawater ions is difficult to discriminate, the Flow Injection Analyzer (FIA) is considered a better alternative to the ISE. It was developed to automate many of the steps performed in a typical laboratory analysis. Unlike the Continuous Flow Analyzer (CFA), where air

bubbles are used to segment the flow of the sample, the FIA technique is based on an unsegmented stream of an inert carrier in which a defined sample volume is determined (Birot et al., 1994). The analyzer consists of five major components, the rotation valves, motor driven syringe, colorimeter, reagent housing and electronic controlling unit. Buffle and Horvai (2000) have demonstrated the principal of nitrate determination using FIA in three steps: (1) Nitrate (NO_3^-) is reduced to nitrite (NO_2^-) by buffering the sample to neutral PH and pumping the sample buffer mixture through copperized cadmium column. (2) The nitrite reacts with sulfanilamide in acid to form a diazonium ion. (3) The diazonium ion then reacts with ethylenediamine to form brightly colored azo dye molecules, which can be quantified using spectrometric technique. Worsfold (2006) has demonstrated this process in Figure 2.15.

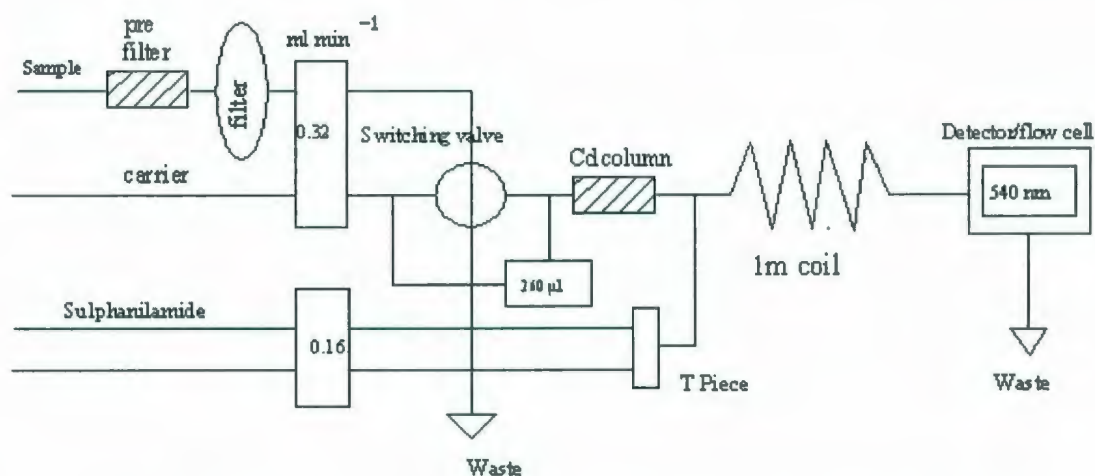


Figure 2.15 FIA Process Diagram for Determining Nitrate (Worsfold, 2006)

The FIA technique has demonstrated good capabilities for monitoring dissolved compounds in the aquatic environment more than any other method. Jannasch et al.

(1994) have reported that FIA can be calibrated *in-situ* using standards with known nitrate concentrations, it's mechanically simple, rugged, and does not consume much power. FIA components have also been designed to work under high hydrostatic pressure (Biro et al., 1994). Worsfold (2006) has reported that FIA operates in an enclosed environment reducing contamination and is compatible with most detection systems. Tover et al. (2002) have demonstrated from several experiments the applicability of FIAs to analyze both synthetic and real seawater samples. However, this method still has some limitations. The accuracy of the nitrate determination based on the reduction of nitrate to nitrite on copperised cadmium has been found to be highly dependent on the reduction of nitrite if present in the sample (Novic et al., 1994). Another common problem associated with FIA is filtration, particularly in a highly turbid environment. There is a pressing need for research into inert, high performance filtration or particle separation devices that are compatible with flow analysis systems, which can be deployed for extended periods of time in different environments (Gray et al., 2005). Worsfold (2006) has reported that FIAs are not recommended for long term deployment due to their continuous consumption of reagents. As other wet chemical techniques, the response time of FIAs is slow (minutes). The concentration of NO_3/NO_2 in submicromolar range is determined at approximately 15 minute intervals. Wet chemistry techniques are still problematic for AUVs monitoring applications, because of long analysis times (Griffiths et al., 2001). These types of chemical sensors are not suitable for fast measuring platforms such as CTD towed platforms or AUVs due to its slow response time (Prien and Hydes, 2003). Wet Labs, Inc and sub *champak Systems Inc.* have readily integrated the analyzer with oceanographic CTDs and other underwater sensors for vertical and horizontal profiling.

The sensor has a size of 63.5 by 12.7 cm, weighting 12 lbs in the air and has a depth range of 200 m. Hanson (2007) has used the four channel subChem autonomous profiling nutrient analyzer (nitrate, nitrite, phosphate, ammonia) systems to investigate the role of nutrient gradients in episodic formation, maintenance and decay of thin plankton layers in coastal water using Remote Environmental Monitoring Units (REMUS).

2.3.2.5.3. UV Absorption Analyzer

The Ultra Violate (UV) absorption technique has been used for many years by water authorities as a standard technique for nitrate monitoring. The UV analysis is based on the principle that different molecules have different absorption spectra. Many chemicals absorb light in the UV, where each has a unique absorption spectrum. The concentration of these chemicals can be determined by measuring the spectrum of a water body in the UV and then deconvolving the spectra to yield the concentration of each component. Two aquatic research facilities have developed this technique for *in-situ* monitoring applications. The Monterey Bay Aquarium Research Institute (MBARI) has developed an *in-situ* UV spectrophotometer (ISUS) for high resolution and long-term monitoring of nitrate, bromide and disulfide (Johnson and Coletti, 2002). The sensor is composed of four key components: (1) the UV source, (2) an optically coupled sensing probe, (3) a high resolution spectrometer and, (4) a low power instrument controller with a large amount of data storage. ISUS can operate while submerged at 2000 m depth. Johnson and Coletti (2002) reported that the instrument was deployed in the Pacific for a period of 6 months with no apparent degradation in performance. Wijesekera (2003) has deployed ISUS on an AUV mission to detect biophysical information and nitrate concentrations.

Tervalon et al. (2003) integrated the ISUS with an AUV for Arctic monitoring mission. The fast response time (1 sec) has made it suitable for use on a towed vehicle (Prien et al., 2003).

The National Oceanography Center in Southampton has also developed an *in-situ* UV spectrometer analyzer (SUV6). The system can measure a number of wavelengths in the region of 220 nm to determine the concentration of dissolved nitrate, sea salt and dissolved organics (Finch et al., 1998). The instrument uses a xenon flash lamp light source, fused silica windows and lenses, a sample cavity, a grating spectrometer and an UV enhanced silicon photodiode detector (Figure 2.16). The sensor was tested on a number of platforms such as SeaSoar and Autosub AUV and has demonstrated good results in spite of the temperature drifting problem (Prien et al., 2003).

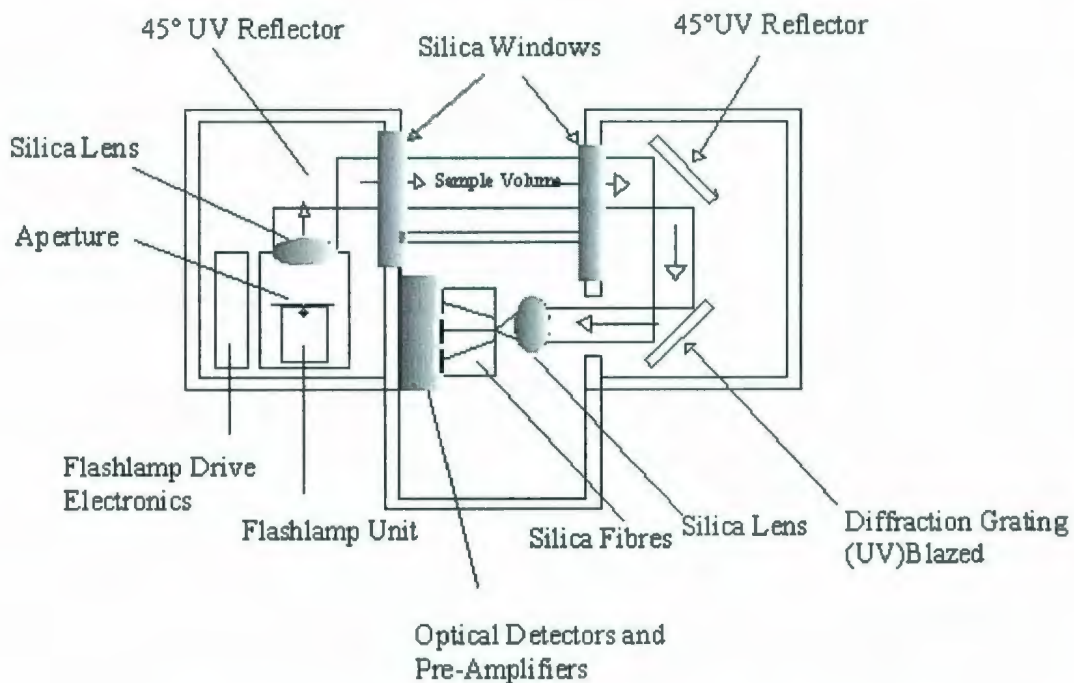


Figure 2.16 Schematic Diagram of Mark I UV Sensor (Finch et al., 1998)

2.3.2.6. Hydrocarbons

There is a pressure from regulators to continuously monitor hydrocarbon contamination resulting from offshore oil and gas operations. The major sources of these pollutants are offshore rigs and oil tankers. Traditionally, land based laboratory analysis can be performed using Fourier Transform Infrared (FTIR), Gas Chromatography (GC), and Mass Spectrometry (MS). In many situations, a more effective monitoring tool is needed to assess the degree of contaminations as it occurs. Kraft et al. (2003) have reported that the ionic strength of seawater, the high content of dissolved substances, and the presence of marine humus resulting from organic matter such as cellular debris, humic acids, and metabolic products are some of the problems encountered during *in-situ* hydrocarbon monitoring. Several *in-situ* techniques have recently been developed for hydrocarbon monitoring. The most prominent techniques are fiber optics and flow injection analysis.

2.3.2.6.1. Fiber Optic Sensor

Two optical approaches are commonly used for determining hydrocarbons. The first is the Mid-Infrared (MIR) spectral range and the second is the UV/VIS spectral range. MIR radiation of a laser diode coupled into a light guide coated with a special polymer has been used for aromatic and aliphatic monitoring, while the UV Fluorometer has been developed to measure various hydrocarbon compounds. Kraft et al. (2003) have reported detecting 1,2-dichlorobenzene, tetrachloroethylene, 1,2-xylene, 1,3-xylene, 1,4-xylene, 1,2-dichlorobenzene and 1,2-dichlorobenzene at low concentrations using Mid-Infrared Sensor.

Mizaikoff (1999) has integrated the Fourier Transform Infrared spectroscopy (FTIR) sensor for seawater monitoring applications. The sensor consists of three main components: the sensor head; the optical components; and the electronic components. The sensor head is composed of polycrystalline silver halide fibers coil coated with an appropriate polymer layer used as an active transducer for determining organic compounds in water. The optical component consists of parabolic mirrors used to focus the IR beam onto the sensor head.

Beyer et al. (2003) reported that traditional MIR is an effective monitoring technique used for verification of environmental pollutants. They noted that the technique can detect a variety of chlorinated hydrocarbons operating in the mid-infrared spectral range of 8 – 2.5 μm based on Attenuated Total Reflection (ATR) measurements. The detection occurs through the characteristic absorptions technique (Figure 2.17). Kraft et al. (2003) and (Mizaikoff, 1999) have well described this technique for hydrocarbon monitoring. Woolsey et al. (2001) proposed a remote, multi-sensor station for a monitoring project near the sea floor within hydrate stability zone in northern Gulf of Mexico using MIR sensor for long term detection of hydrocarbons.

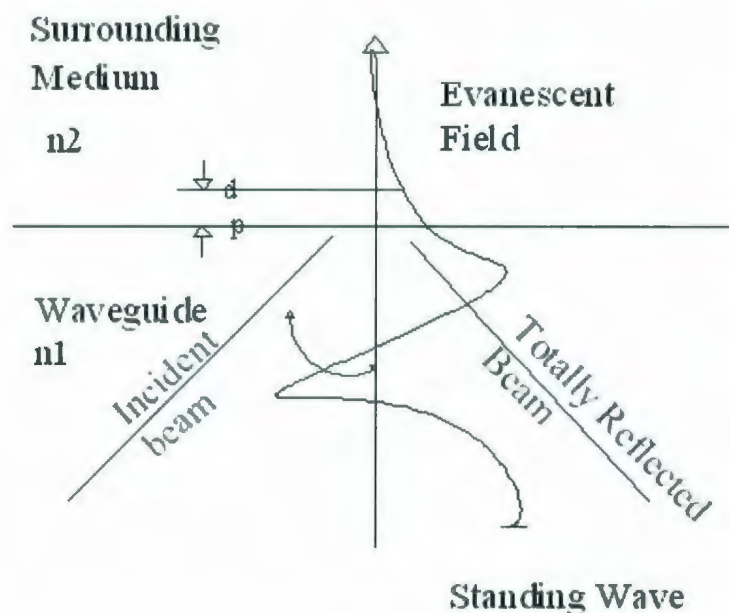


Figure 2.17. A Standing Wave and Evanescent Field Established Near Reflecting Interfaces (Kraft et al., 2003)

Kraft et al. (2003) reported that the sensor can simultaneously detect Volatile Organic Compounds (VOCs) in both freshwater and seawater below 100 ppb concentration, provide qualitative and quantitative information, withstand an underwater pressure of 500 m, and work under temperature ranging from 3 °C to 20 °C. However, Mizaikoff (1999) reported for quantitative multi component analysis in seawater, the sensor has shown low sensitivity to parameters such as salinity, turbidity and chemically interfering substances. Furthermore, the response time is still a limiting factor for using this technique. For real-time profiling operations, such as plume tracing, response time shall be below 1 min, which has not been reached currently with FTIR technique, having a response time ranging from 5 to 10 minutes (Kraft et al., 2003).

As for the UV technique, Chelsea has developed an Ultraviolet (UV) Fluorimeter named “UV AQUA Traka”. The sensor was designed to monitor hydrocarbon concentrations at a 360 nm wavelength. The company has reported that the sensor can be used on a towed vehicle and withstand pressure up to 6000 m depth, while profiling at a response time of 4Hz (can be extended to 10Hz). Controls Systems and Solution has also designed a methane sensor for offshore monitoring operations. The system can detect the presence of hydrocarbons/methane in gaseous or liquid forms. The company has reported that the sensor can monitor pipelines leaks, Christmas trees and subsea installations, and can be integrated with ROV and AUV platforms.

2.3.2.6.2. Flow Injection Analyzer

Considering the need for an *in-situ* underwater hydrocarbon monitoring device, an Underwater Mass Spectrometer (UMS) was developed for this application. In general, the MS is considered the most multipurpose chemical analyzer. It can analyze compounds ranging from small molecules to large biomolecules with high sensitivity. Also it can be used to monitor CO₂, nutrients, radioactive isotopes, metals, and other chemicals. One of its newly developed applications is *in-situ* monitoring of man-made and non man-made hydrocarbon seepage (McMurry et al., 2005).

The Center for Ocean Technology at University of South Florida has developed an UMS for AUV monitoring application. Short et al. (1999) reported that three challenges were encountered during the design of the system. These challenges are: the sample introduction through flow injection system; the vacuum maintenance under high pressure;

and the power consumption. The system consists of three main components (Figure 2.18): the flow-injection pressure vessel; the quadrupole-mass-spectrometer with the membrane introduction mass spectrometer; and roughing-pump pressure vessel

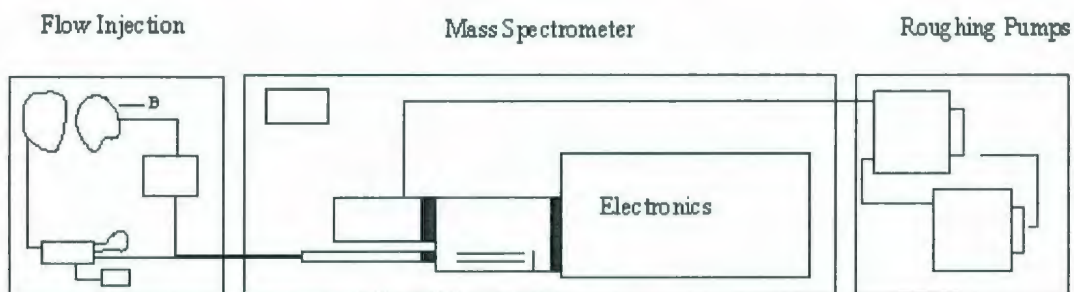


Figure 2.18. Schematic Diagram of UMS (Short et al., 1999)

All mass spectrometers have several similar features. Analytes must be transported from their normal state (solid or liquid) into the vacuum through a sample interface. After entering the vacuum system, ionized analytes are then dispersed according to their mass-to charge ratio (m/z) by combination of electrical and magnetic fields. The ion signal is recorded as a function of m/z using a high-gain electron multiplier or Faraday-cup detector. Measured intensities in the mass spectrum can often be related to the concentration of the analyte in the original sample or possibly used for identification of an unknown compound in a complex mixture. A number of field experiments demonstrated capabilities of UMS, particularly for VOCs detection and quantification. Pennell et al. (2003) have mounted the UMS on an AUV for a plume tracking study. She reported that the system has successfully detected dimethyl sulphide chemical tracer. The UMS can detect and quantify various types of VOCs including benzene, toluene and trichloroethene. Short et al. (1999) have reported that UMS has detected toluene at a

concentration of 1 ppb. However, there are still many challenges to improve the performance of UMS for long term deployment in deep water. These challenges can be summarized as the hydrostatic pressure at deep water, vacuum system management, the power consumption and the background noise as a result of residual gas in the ionization chamber (McMurry et al., 2005). Short et al. (1999) reported that the biggest obstacle is the complexity and format of the associated electronics.

Chapter 3. Experiment

3.1. Objective

The objective of this experiment was to monitor the coastal area affected by the Spaniard's Bay outfall by integrating *in-situ* sensors with the AUV. The generated spatial and temporal data was used to characterize the plume behavior and assess the water quality around the outfall location.

3.2. Study Area

Most of the ocean discharges in Newfoundland are generated from municipal sewage outfall and the fishery industries. Adams (2005) conducted an experiment studying effluent discharges from a fish plant. She indicated in her study that fish industries and sewage outfalls are the main sources of coastal pollution in Newfoundland. Coastal pollution has negative socioeconomic and environmental consequences. Treatment plants minimize the impact of these outfalls on the marine environment, but their construction, operation and maintenance costs, particularly from small scattered communities, could be a burden on tax payers and federal government. In this work a new monitoring technique was developed to investigate the effect of a small sewage outfall on the coastal marine environment and validate CORMIX near-field hydrodynamic model.

3.3. Site Selection

Two important criteria were considered in selecting the appropriate site to conduct the experiment; the first criteria was, to locate a coastal outfall discharging either an industrial

or a sewage effluent in a quantity that may pose an impact on the marine environment; the second criteria was, the selected outfall site shall be safe for the crew members conducting the experiment and the AUV. Initially, two sites were proposed to conduct this experiment. The first was located in Foxtrap and the second in Spaniard's Bay. Both sites have sewage outfalls discharging to marine environment and located along the Conception Bay South of Newfoundland (CBS). Considering the AUV safety, deployment and recovery operations, Spaniard's Bay was recommended over the other site (Figure 3.1).



Figure 3.1. Aerial Map of Spaniard's Bay Outfall

Spaniard's Bay outfall was installed in 1988 to handle municipal wastewater from both Spaniard's Bay and the town of Tilton. According to the town manager, the outfall serves a population of about 1600 people. It extends to 100 m length and about 6 m depth (Figure 3.2). A small preliminary sewage treatment plant was constructed along with the outfall and operated for a short period of time. Eventually, it was closed due to frequent maintenance problems. Since then, the raw sewage waste has been disposed directly into the ocean. During the time of conducting the experiment, floating raw sewage waste was obvious at water surface. Birds were frequently observed feeding on the outfall floating waste.

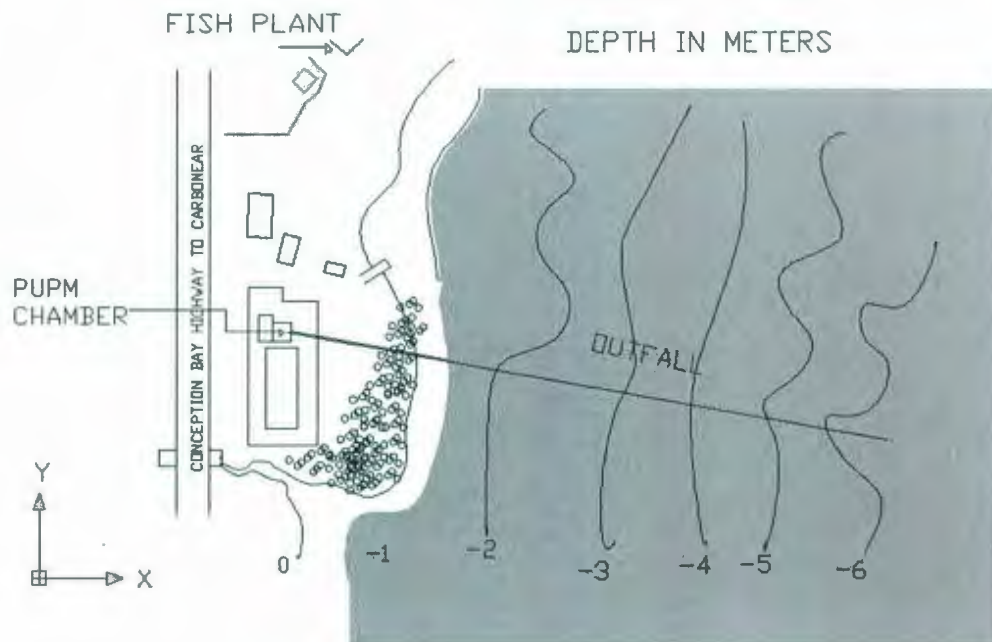


Figure 3.2. Spaniard's Bay Outfall Layout

3.4. Previous Work

Sharp (1989) carried out a monitoring study on Spaniard's Bay outfall for the Department of Environment and Natural Resources. The study showed that the faecal and total coliform counts were low and below the published standard. The sampling results of November 29, 1986, showed that the total coliform at surface and center of the boil was 1,600 and on January 29, 1987, the result was 56,000, where the EEC limit for bathing beaches is 100,000 (Sharp, 1989). Gowda (1992) has conducted a field and experimental study using a novel shape mixing tube. The study showed that a better performance can be achieved at a low Froude number, which is defined as the ratio of the inertial to gravity forces in the flow, and the improvement of overall dilution with a slot mixing tube was limited compared to a circular mixing tube. Mukhtasor (1998) has developed and applied design procedures using a probabilistic method to calculate initial dilution and bacterial concentration at a location of interest. Comparison among the various probabilistic and deterministic methods showed that all methods provided similar results for initial dilution.

3.5. Instrumentation

Salinity, temperate, chlorophyll *a*, turbidity and DO were identified as important parameters for monitoring a sewage outfall effluent. Due to the limited resources and time constraint, it was not possible to measure other important parameters, such as nutrients using an underwater analytical system. The selection of *in-situ* sensors was based on the literature review described in Chapter 2.

3.5.1. CTD

The CTD sensor was designed and manufactured by Applied Microsystems. This instrument was previously used by other graduate students for a similar application. Adams (2005) used the sensor in her experiment for an effluent monitoring study. Niu (2007) also used the sensor in a hydrodynamic model validation study. Both experiments have shown reliability and a fast response time of the sensor. The sensor has a response time of 25 milliseconds in a 1.0 m/s flowing environment. In July 2007, the sensor was sent to Applied Microsystems for maintenance and calibration.

3.5.2. Chlorophyll

The Turner Designs CYCLOPS-7 Chlorophyll *a* sensor was selected for this experiment (Figure 3.3). The sensor has a single channel detector that can be used for freshwater and seawater applications. It can detect chlorophyll *a* pigments by fluorescence. It can be integrated with the CTD to obtain its power and deliver an output voltage to the system data logger, which is proportional to the chlorophyll *a* concentration. For better sensitivity, the sensor can be set to measure concentrations at three different gain settings, X1, X10 and X100. As the gain increases, the sensitivity increases and the concentration range decreases. According to the Turner Designs manual, X10 provides the appropriate sensitivity for ocean monitoring applications.



Figure 3.3 Cyclops 7 Chlorophyll *a* Sensor (Turner Design)

3.5.3. Turbidity

The Turner Designs turbidity sensor was selected for this experiment. The sensor looks similar to and works under the same principle as chlorophyll *a* sensor. The turbidity Cyclops7 sensor provides a fast and accurate way to determine *in-situ* measurements. For higher sensitivity, the sensor has three gain settings: X1 for 0 - 3000 NTU; X10 for 0 – 1000 NTU; and X100 for 0 – 100 NTU concentrations.

3.5.4. Dissolved Oxygen

The Idronaut Dissolved Oxygen (DO) sensor was used in this experiment to monitor DO percent saturation. Adams (2005) has integrated this sensor with the CTD in her experiment. It has a scan rate of 1 Hz with a range of 0 to 15 mg/l and accuracy of 0.2 mg/l (Adams, 2005). This polarographic sensor reports its measurement in percent saturation. In May 2007, the sensor was sent to Applied Microsystems for testing and calibration.

3.5.5. Current Meters

Two current meters were used in this experiment for measuring the current velocity and direction. In the first experiment, the RCM 9 LW was used and in the second experiment, the S-4 was used as the only current meter available at that time. According to at Oceans Ltd, both current meters have high accuracy and were recommended for our application.

RCM 9 LW - Aanderaa Instruments, Inc

The current meter (Figure 3.4) was used during the May 2007 experiment. It has the following specification:

- Depth Rating 300 meters
- For use in fresh and seawater
- Range: 0 to 300cm/s
- Resolution: 0.3cm/s
- Absolute Accuracy: $\pm 0.15\text{m/s}$
- Relative Accuracy: $\pm 1\%$ of reading
- Statistical Precision: 0.45cm/s (standard deviation)

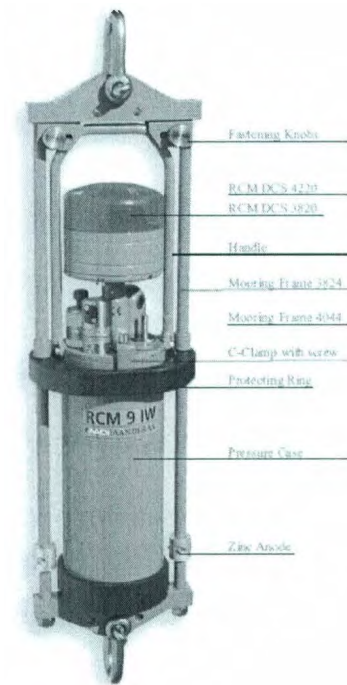


Figure 3.4 RCM 9 LW Current Meter (Aanderaa Instruments, Inc)

S-4 – InterOceans

This current meter (Figure 3.5) was used during the July 2007 experiment. It has the following specifications:

- Range: 0-350 cm/sec (standard)
- Accuracy: 2% of reading +/- 1 cm/sec
- Sampling rate: 2 Hz
- Resolution: 2 Hz 0.03 to 0.35 cm/sec depending on range
- Noise: less than the resolution for averages of 1 minute or longer

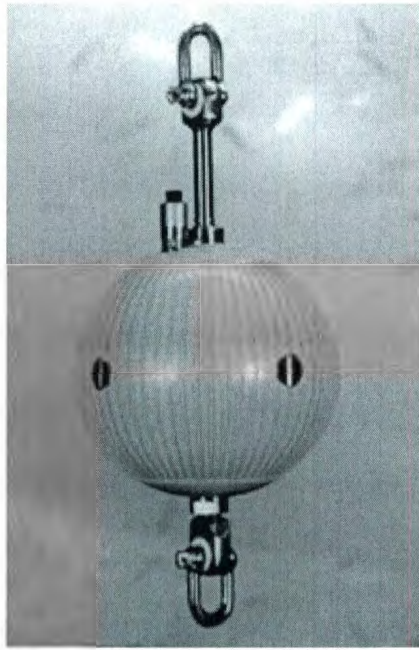


Figure 3.5. S-4 Current Meter (InterOceans)

3.5.6. GPS

A Handheld Garmin Geographical Positioning System (GPSMAP® 60C) was used to collect geographical coordinates at the same locations while towing the sensor platform (Figure 3.6). This device can be used for marine navigation, it is rugged, waterproof, and has a battery life span of 30 hours. The system collects spatial coordinates continuously at a point per second interval with approximate 15 feet accuracy. The unit is supported with the Map Source software, which can be synchronized with the GPS for downloading and viewing spatial data.



Figure 3.6. Handheld GPS (Garmin)

3.6. Apparatus

3.6.1. MUN Explorer

As described in chapter 1, AUVs are autonomous robots that travel underwater. They can be piloted or can perform pre-programmed missions for several hours depending on their battery capacity. Most of the previously conducted experiments were on the hydrodynamics aspects and their maneuvering capabilities.

Considering the importance of this technology, Memorial University of Newfoundland acquired an AUV named “Explorer” in 2006 for oceanographic and environmental monitoring research (Figure 3.7). The vehicle specifications are elaborated in Table 3.1.



Figure 3.7. MUN Explorer at Spaniard's Bay Wharf

Table 3.1. MUN Explorer AUV Specifications

MUN Explorer	
Parameter	Specifications
Length	4.5 m long
Diameter	0.69 m
Dry Weight	700 kg
Displacement	710 kg
Payload Capacity	150 kg
Cruising Speed	1.5m/s
Speed range	0.5 to 2.5 m/s
Maximum Depth	3000 m
Battery Capacity	Long endurance (>100 km)

3.6.2. Boats

A fishing boat and a zodiac rubber boat were used to deploy and recover the current meter and tow the sensor at different depths (Figure 3.8).



Figure 3.8. Fishing Boat used for the Deployment of Current Meter

3.6.3. Sensor Towing Platform

A special towing platform was designed and fabricated for the sensor towing experiment (Figure 3.9). The platform was designed to safeguard the sensors from hitting seabed rocks, minimizes current drifting effects, and easily deploy at different depths. The platform length is 0.5, width 0.5, and depth 0.3 m. It was fabricated from steel to minimize current drifting effects. Two wooden side wings were fixed on both sides of the platform to prevent rotation while monitoring.

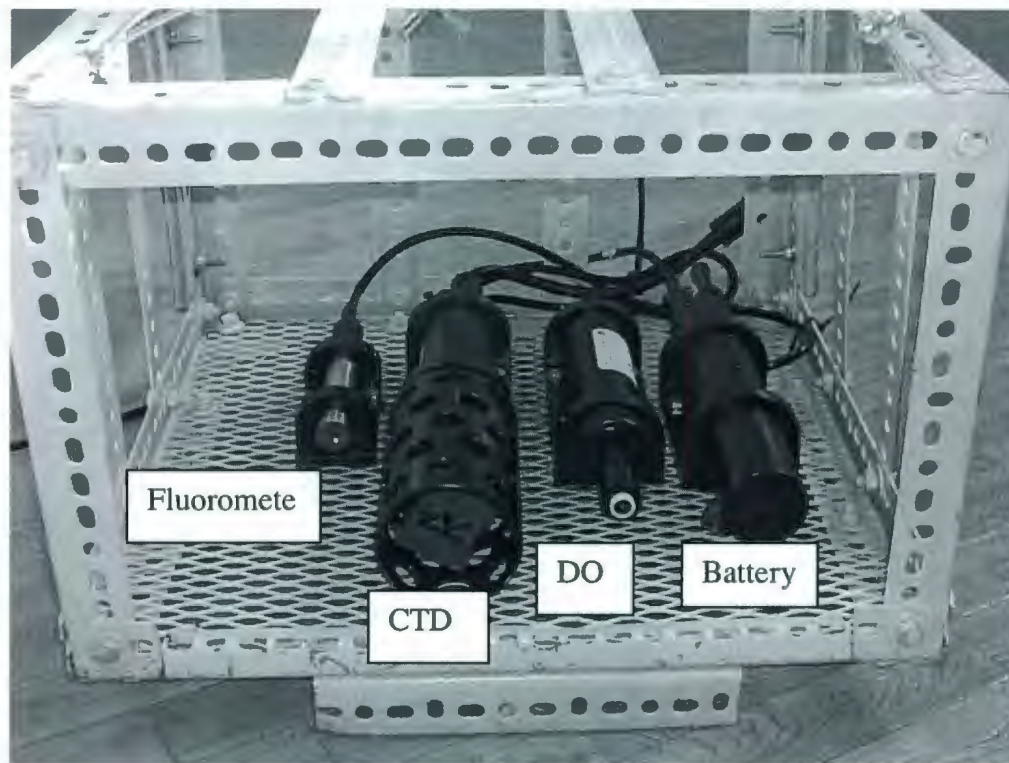


Figure 3.9. Sensor Towing Platform

3.7. Experimental Design.

Initially, it was proposed to use the AUV for the outfall monitoring experiment. Since this was the first time to conduct an experiment after integrating the AUV with the CTD, it was important to have a backup plan in case of any problem or if it was deemed not safe to use the AUV. The sensor towing platform was proposed as an alternative plan.

3.7.1. Site Survey

A site survey was carried out on May 10, 2007. The intention of this survey was to identify a suitable location to deploy and recover the AUV. The Spaniard's Bay fire department volunteered a fire truck to rinse the vehicle out after recovery. An electric generator was required to run the ground facilities at the wharf.

3.7.2. Sensor Calibration

Chlorophyll *a*

According to the Turner Design, the Chlorophyll *a* Cyclops-7 was set up for the following approximate ranges;

X100 0 to 5 μ g/L(max)

X10 0 to 50 μ g/L(max)

X1 0 to 500 μ g/L(max)

As recommended by the Turner design, X10 gain setting is the most appropriate setting for a marine monitoring application. They have also mentioned that Rhodamine WT dye can be used to calibrate the sensor. A laboratory experiment was conducted to convert the voltage output to mg/l concentration. Figure 3.10 demonstrates the calibration curve using Rhodamine WT dye obtained from the experiment.

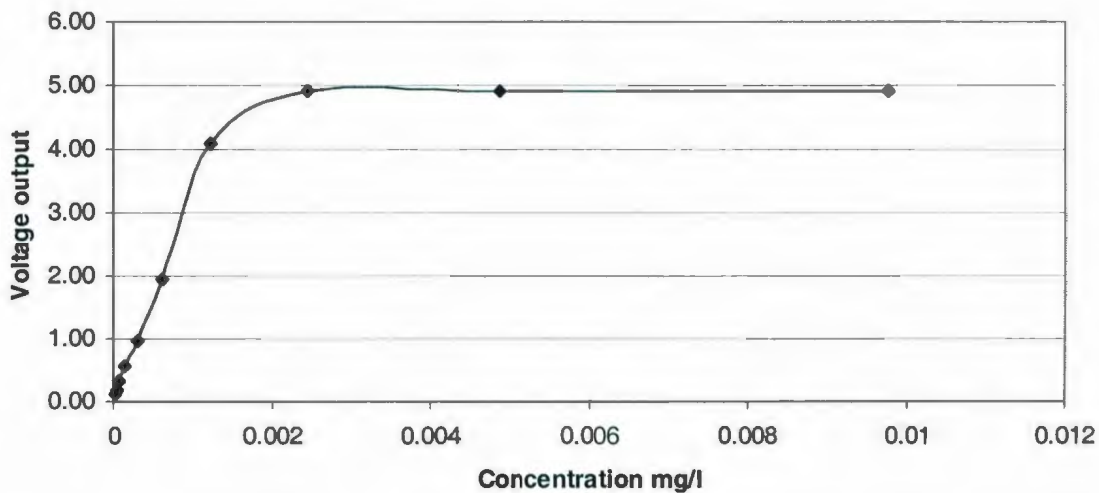


Figure 3.10. Chlorophyll *a* Calibration Curve

Turbidity

The Turbidity Cyclops-7 sensor has the following ranges:

X100 0 to 100 NTU

X10 0 to 1000 NTU

X1 0 to 3000 NTU

1000 NTU formazin based turbidity standards were ordered from GF Chemicals. For moderately turbid waters, X10 range was recommended because it offers the best resolution and range for our application. The calibration curve was obtained from the lab experiment in order to convert the voltage output to a Nephelometric Turbidity Unit (NTU) (Figure 3.11).

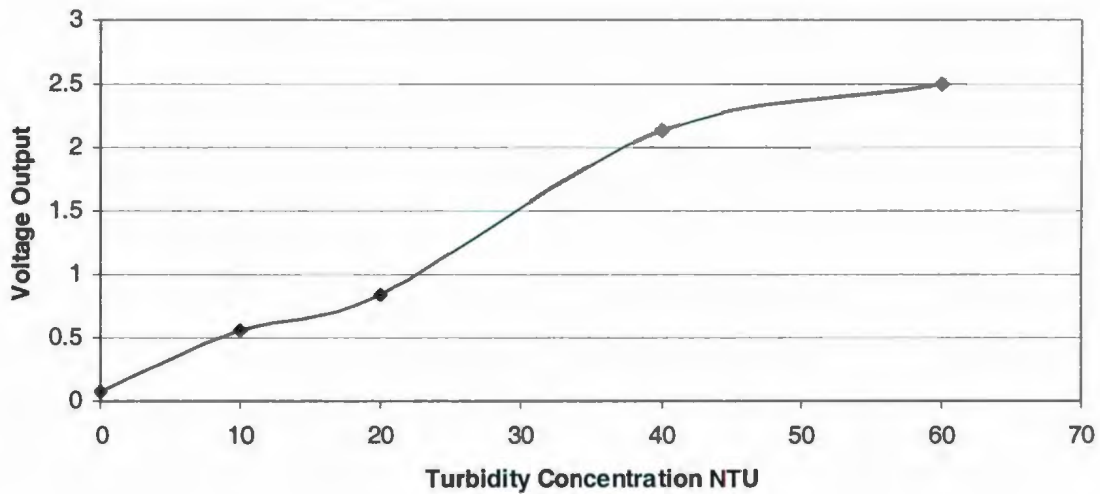


Figure 3.11. Turbidity Calibration Curve

3.7.3. AUV Sampling Plan

Initially, a two day monitoring mission was planned to collect real-time water quality data around the outfall using AUV. The sampling plan was designed to collect a large amount of information from the water column. The safe monitoring depth was set at 3 meters from the seabed. It was proposed to monitor 5 depth layers of the water column at 1 m depth intervals. Figure 3.12 demonstrates the horizontal trajectory of each depth layer. In order to generate higher resolution maps, the collection frequency was designed at 10 hertz/sec.

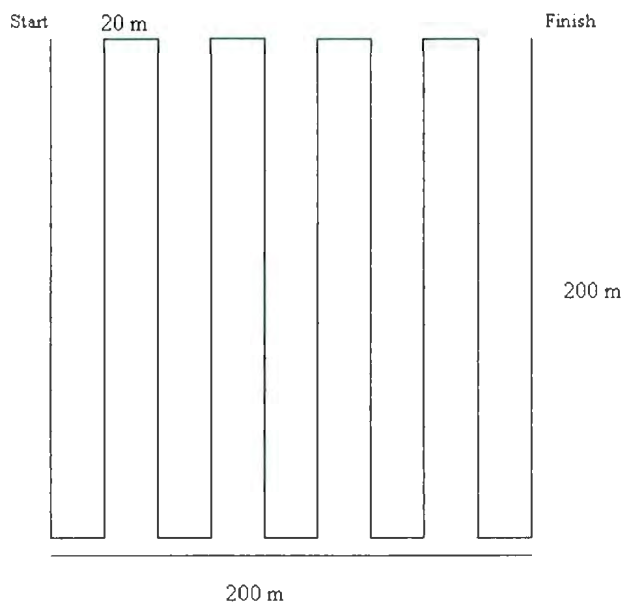


Figure 3.12. Proposed Horizontal Trajectory

Since the CTD can only accommodate two sensors at the same time, turbidity and Chlorophyll *a* fluorometers were alternated on each day. Table 3.2 presents the proposed monitoring plan for the two day AUV mission.

Table 3.2. Proposed AUV Environmental Monitoring Plan

Mission	Date	Depth m	Parameter	Estimated time min
1	May 16,2007	1	CTD + Chlorophyll <i>a</i>	30
1	May 16,2007	2	CTD + Chlorophyll <i>a</i>	30
1	May 16,2007	3	CTD + Chlorophyll <i>a</i>	30
1	May 16,2007	4	CTD + Chlorophyll <i>a</i>	30
1	May 16,2007	5	CTD + Chlorophyll <i>a</i>	30
2	May 18,2007	1	CTD + Turbidity	30
2	May 18,2007	2	CTD + Turbidity	30
2	May 18,2007	3	CTD + Turbidity	30
2	May 18,2007	4	CTD + Turbidity	30
2	May 18,2007	5	CTD + Turbidity	30
Total				300

3.7.4. Alternative Sensor Towing Plan

As mentioned earlier in this Chapter, the sensor towing experiment was proposed to collect data at locations not safe for the AUV.

3.8. AUV Monitoring Experiments

Two environmental monitoring missions were conducted on May 16 and 18, 2007. In these missions, the CTD, chlorophyll *a* and turbidity fluorometers were integrated with

the AUV computer system to achieve real-time spatial and temporal information simultaneously. The vehicle is equipped with 2 positioning systems. At surface, the Geographical Positioning System (GPS) collects spatial data, and when the vehicle dives, an Acoustic Positioning System (APS) collects spatial data underwater. The collection frequency was set at 10 Hz/s. The RCM 9 LW current meter was deployed at 5 m depth and about 72 m from the outfall diffuser to collect speed and current direction data.

3.8.1. AUV Experiment 1

In this experiment, the CTD was integrated with the chlorophyll *a* fluorometer. The InterOceans current meter was deployed at 6 meters depth and about 100 m downstream of the outfall diffuser location. The proposed mission was programmed and downloaded to the AUV computer system. Initially, the AUV was tested on a pilot mode and at various depths. During the test, a technical fault occurred at about 16 m depth, which meant that the experiment had to be abandoned on this day. However, some data were recovered before the fault occurred. Figure 3.13 demonstrates the trajectory of this pilot test.

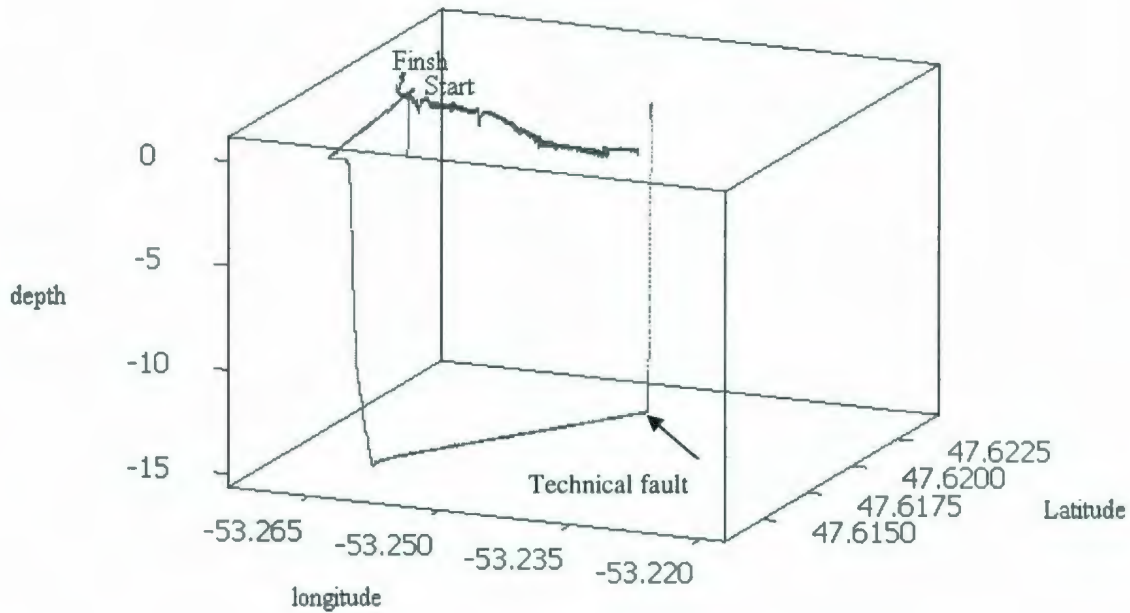


Figure 3.13. AUV Experiment 1 Trajectory

3.8.2. AUV Experiment 2

In this experiment, the CTD was integrated with the turbidity sensor. After diagnosing and repairing the fault that occurred in experiment 1, it was suggested by the technical crew to conduct a few pilot tests before setting the vehicle on mission mode. The current meter was deployed at the same location of experiment 1. While piloting the AUV, its propeller was accidentally tangled into a lobster trap. The vehicle was rescued and towed back to the wharf (Figure 3.14) for damage assessment. The technical crew determined that the tangled rope caused extensive damage to the propeller motor. This damage could not be repaired on site. However, data were recovered from the data logger. Figure 3.15 illustrates the pilot test trajectory before the accident occurred.



Figure 3.14. Experiment 2 AUV Rescue

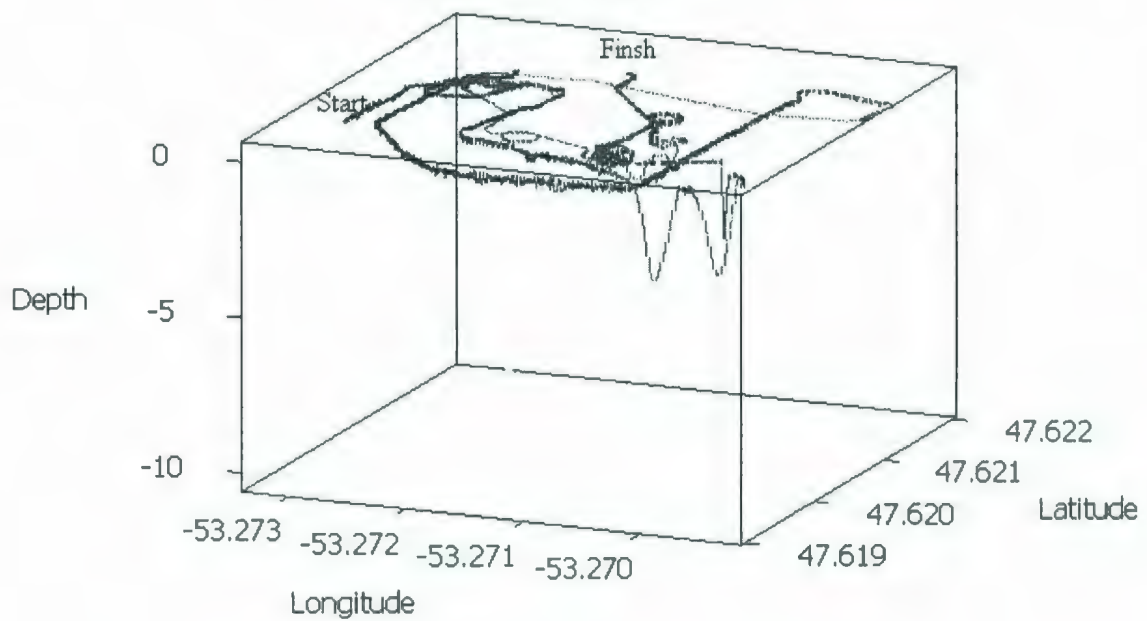


Figure 3.15. Experiment 2 AUV Trajectory

3.9. Sensor Towing Experiments

After analyzing the environmental data obtained from experiments 1 and 2, it was determined that the data was not sufficient to characterize the water quality and trace the effluent plume. In order to fulfill the study goals and objectives, it was important to conduct additional experiments by towing a sensor platform around the outfall location. In this experiment a handheld GPS device was used to collect longitudinal and latitudinal spatial data simultaneously while towing the sensor platform.

3.9.1. Water Column Monitoring Plan

It was proposed in this experiment to accumulate a large quantity of environmental information covering the near-field and the far-field mixing zones. To achieve that, the environmental monitoring boundaries were set at 100 m length by 100 m width by 3 m depth. To obtain three dimensional (3-D) information of the water column, 6 depth layers were proposed for each experiment (Figure 3.16).

In order to verify that the proposed boundaries are exceeding the near-field mixing zone, an initial simulation was performed using the CORMIX model. Considering that the effluent flow rate is $0.051 \text{ m}^3/\text{s}$, the discharge depth is 5 m (Mukhtasor, 1998), and current speed is 2.67 cm/s as obtained from the May experiment, the model has predicted that the near-field mixing zone is less than 12 m. Based on the proposed monitoring boundaries, the time of each layer was estimated at about 30 minutes at an average speed of 2 m/s.

After analyzing the AUV experimental data, it was speculated that the large amount of noisy data was associated with the high collection frequency set for the CTD. Therefore,

a lower collection frequency of 1 hz/sec was proposed in this experiment. It was also determined that 2 days of monitoring would be required to complete this experiment.

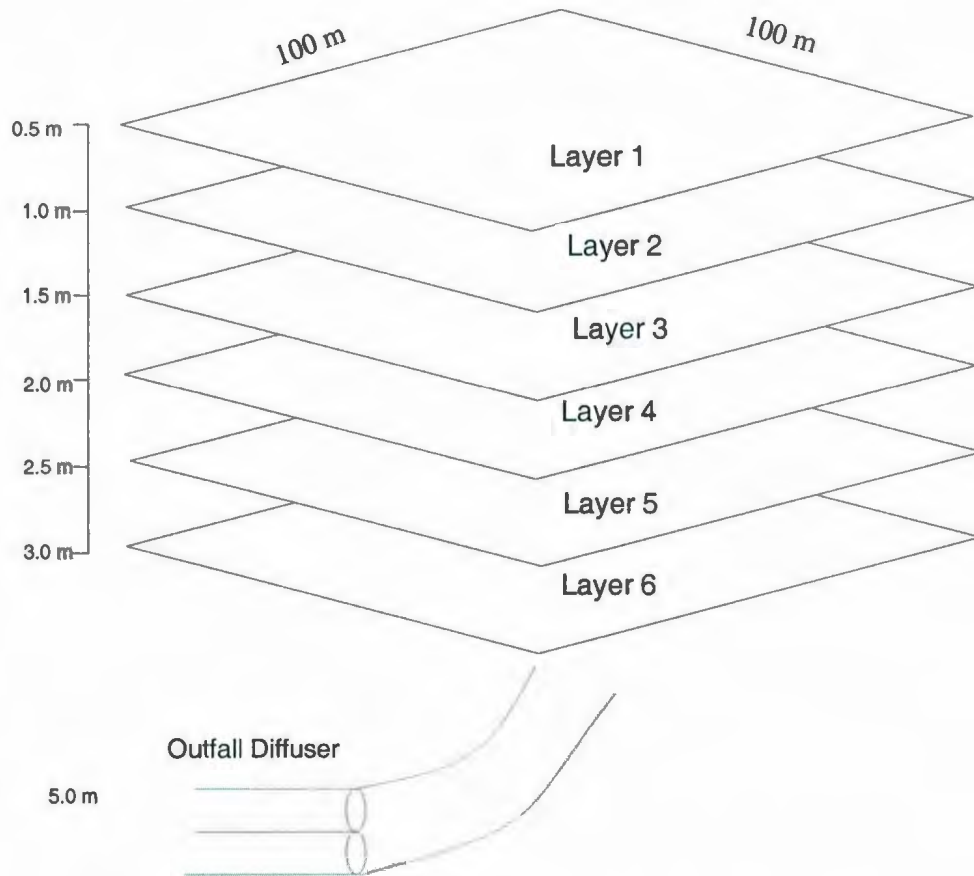


Figure 3.16. Towed Sensor Environmental Monitoring Experiment Design

In the first experiment, it was decided to integrate both CTD and DO with the turbidity fluorometer in the first day and with the chlorophyll *a* fluorometer in the second day. Table 3.3 presents the design parameters of the sensor towing experiment.

Table 3.3. Sensor Towing Design Parameters

No	Design Parameter	Length
1	Length	100 m
2	Width	100 m
3	Area	1.0 square km
4	Time	25-35 minutes
5	Average Speed	≈2 meter per second
6	Average data points collection	2000 -2200

3.9.2. Towed Sensor Experiment 1

The first sensor towing experiment was successfully conducted on July 18, 2007. The S-4 current meter was deployed at 5 meters depth and about 70 m downstream of the outfall diffuser location (Figure 3.17).

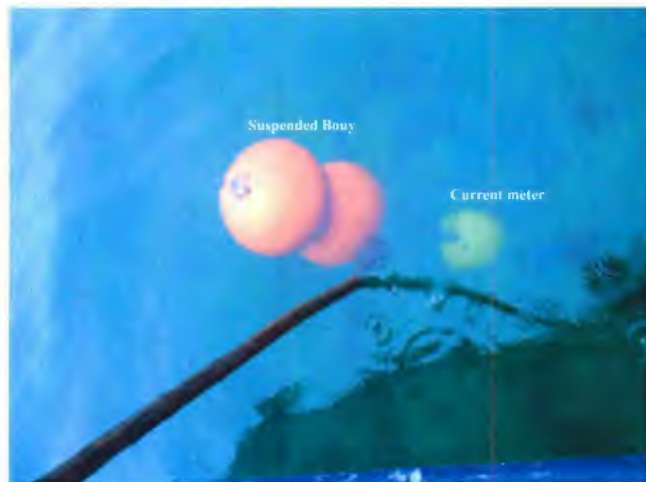


Figure 3.17 Current Meter Deployment - Looking Down

The experiment began at 10:39 am and ended at 4:20 pm. The DO and turbidity sensors were integrated with the CTD sensor. As proposed, six depth layers were monitored. The handheld GPS collected the geographical coordinates at the same location and simultaneously with the sensor platform. The platform depth was controlled by a mechanical pulley attached to the fishing boat (Figure 3.18). The obtained data are summarized in Table 3.4.

Table 3.4. Experiment 1 Data Summary

Layer	Data points	Proposed	Depth m	Length	Time	Ave speed
		Depth m	Mean - Std. Dev	Km	min	Km/h
1	2207	0.5	0.54 - 0.15	1.19	37:20	1.93
2	2490	1.0	1.1 - 0.18	1.33	41:50	1.93
3	1685	1.5	1.54 - 0.19	0.93	28:00	2.0
4	2327	2.0	2.0 - 0.21	1.30	39:10	2.0
5	2102	2.5	2.5 - 0.29	1.16	35:00	2.0
6	2458	3.0	2.81 - 0.48	1.31	41:00	1.93
Total	13269			7.22	222:20	1.965



Figure 3.18. Left the Boat Mechanical Poly and Right is the Towed Sensor Platform

3.9.3. Towed Sensor Experiment 2

The second experiment was successfully conducted on July 20, 2008. The current meter was deployed at the same location of experiment 1. The experiment started at 10:35 am and finished at 5:23 pm. The DO and chlorophyll *a* sensors were integrated with the CTD sensor. Figure 3.19 demonstrates a typical GPS trajectory and location of the current meter and outfall diffuser. Table 3.5 presents a data summary of this experiment.

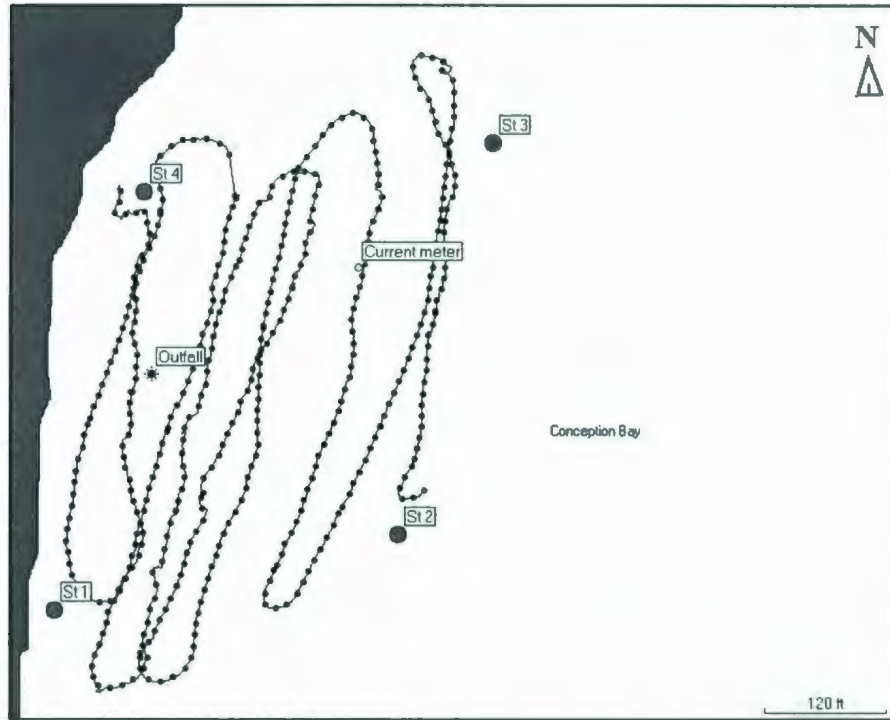


Figure 3.19. Experiment 2 Horizontal Trajectory at 0.5 m depth

Table 3.5. Experiment 2 Data Summary

Cast	Data points	Proposed Depth m	Actual depth m Mean - Std. Dev	Length km	Time min	Ave speed km/h
1	2499	0.5	0.59 - 0.10	1.35	42:05	1.93
2	3353	1.0	0.86 - 0.08	1.86	56:00	2.0
3	2567	1.5	1.40 - 0.18	1.38	43:18	1.93
4	2252	2.0	1.89 - 0.19	1.25	37:53	2.0
5	2184	2.5	2.24 - 0.27	1.17	36:41	1.93
6	2056	3.0	2.78 - 0.39	1.01	34:26	1.77
Total	14911			8.02	250:23	1.926667

Chapter 4. Results

4.1. Outfall Modeling

As described in Chapter 2, length scale models are commonly used to predict the near-field mixing zone. One objective of this study is to compare near-field dilution of two commonly used outfall diffusers. The existing staged diffuser design and the T-Shape riser design was modeled using CORMIX 2 and RSB model, respectively. By comparing these two designs with the same modeling concept, it is possible to evaluate the performance of each design under the same ambient and discharge conditions.

4.1.1. Outfall Effluent

Sharp (1989) conducted a flow rate study of Spaniard's Bay outfall and projected the flow for 2006 as 4,426 m³/d. It is speculated that no significant change in socioeconomic activities and population growth has occurred since then. According to the Spaniard's Bay town manager, the population in 2007 was about 1800. Since the outfall consists of a typical raw sewage effluent, the density was assumed to be close to fresh water (999 kg/m³) and salinity as 1 psu. The effluent turbidity values were obtained by suspending the turbidity fluorometer as close as possible to the center of the effluent jet. Figure 4.1 demonstrates the turbidity measurements obtained from this experiment. Few isolated high turbidity values were obtained due to the presence of large sized effluent waste. For the modeling application, a mean value of 15.49 NTU was used as a representative turbidity sample.

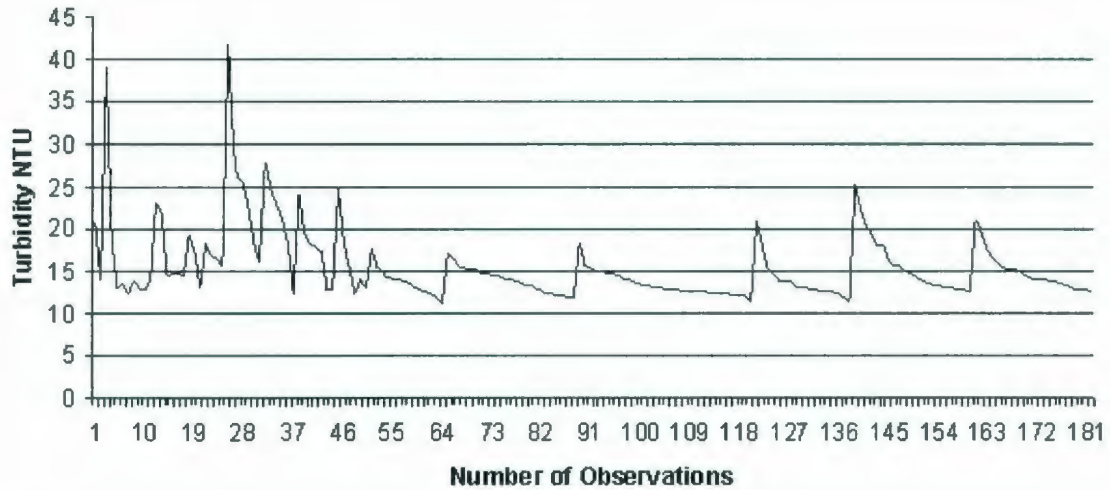


Figure 4.1. Spaniard's Bay Outfall Effluent Turbidity Sampling Plot, July 20, 2007

4.1.2. Diffuser Geometry

The outfall consists of a 200 mm diameter pipe discharging through two 100 mm diameter nozzles and extending 100 m offshore in a water depth of about 6 m (Sharp, 1989). The two nozzles (ports) were designed to discharge in a horizontal downstream direction (Figure 4.1). In the original design, it was reported that the depth of the discharge ports was about 5 m from the surface of the water.

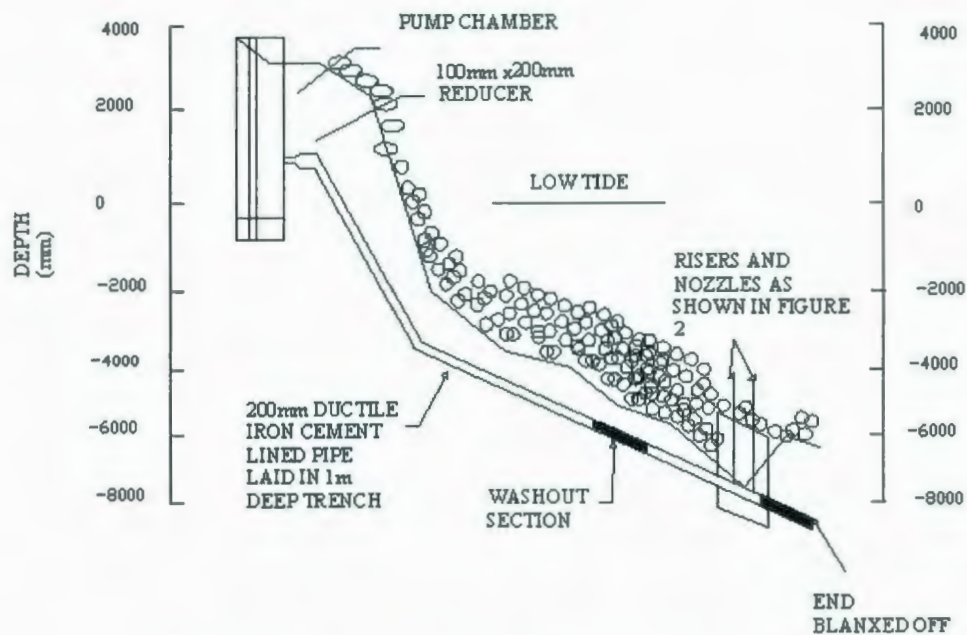


Figure 4.2. Spaniards Bay Outfall Design (Sharp, 1989)

Unfortunately, the original outfall design (Sharp, 1989) did not include the full scale diffuser geometry (Figure 4.3). The Government of Newfoundland and Labrador Water Resources Department was contacted to provide the complete design, but no additional information was available. The diffuser length was assumed based on field observations. Since only one single boil was observed at the surface, this indicated that the risers were closely spaced and tended to merge below the surface. As a conservative number, the distance between the two risers was assumed to be 5 m and the diffuser length to be 6 m (Figure 4.3). For the multiport discharge modeling, the CORMIX requires a minimum number of four ports. To overcome this problem, each single port riser was divided into two identical adjacent ports. In this case the effluent will tend to merge immediately and behave as a single port (Figure 4.4).

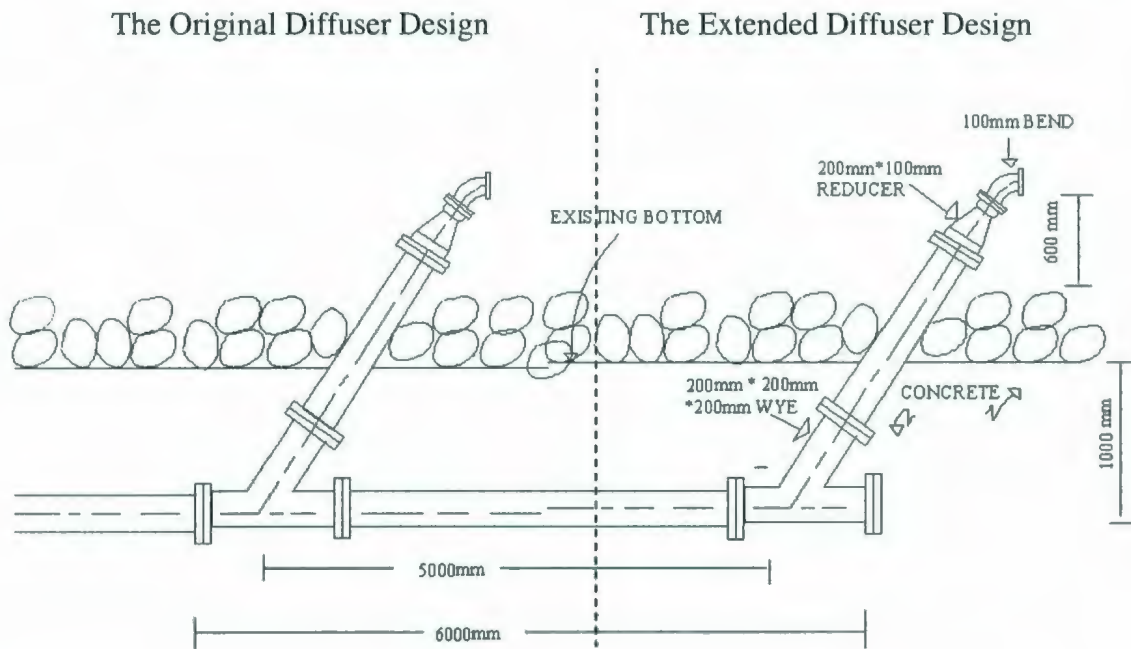


Figure 4.3. Spaniards Bay Outfall Diffuser Design (Sharp, 1989)

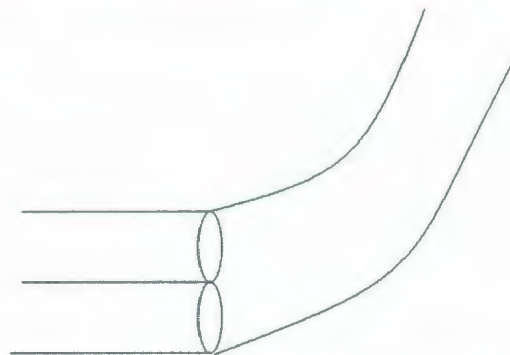


Figure 4.4. Outfall Diffuser Port Geometry

4.1.3. Ambient Conditions

4.1.3.1. Current

As mentioned in Chapter 3, due to an internal current meter fault, no data was retrieved from July experiment. Therefore, the collected data in May experiment was used as the

only available source. Figure 4.5 shows the current rose diagram from the May 16 and 18 current data recorded between 10:00 am to 4:00 pm. The dominating current speed was observed to be ≤ 5 cm/s, the minimum was 0.28 cm/s, the maximum was 21.36 cm/s and the mean was 2.67 cm/s, with a standard deviation of 2.410.28 cm/s. For the modeling application, the mean velocity was used.

Based on the Environment Canada hourly weather station located in Long Pond, which is along the Conception Bay South and about 25 km from Spaniard's Bay, on May 18 the average wind speed between 10:30 am and 4:30 pm was recorded as 21.42 km/hr. While on July 20 the average wind speed was recorded as 26.28 km/hr at the same time.

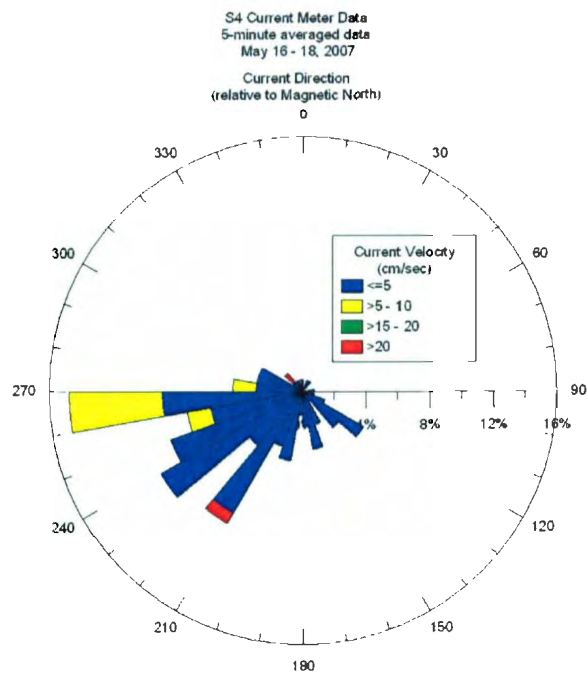


Figure 4.5. Current Rose Diagram - May 16-18, 2007

0.5 m depth, the salinity was observed as 30.33 psu (PSS-78), the temperature was 7.73 °C, and density was 1023.650 kg/m³. At 4 m depth, the salinity was observed as 31.34 psu, the temperature was 6.94 °C, and density was 24.557 kg/ m³ (Figure 4.7). As a practical guide, if the vertical variation in density is less than 0.1kg/m³ then it can be neglected and considered uniform (CORMIX Manual). Since the difference between the upper and lower layers was 0.9 kg/ m³, then the ambient density was considered as non-uniform.

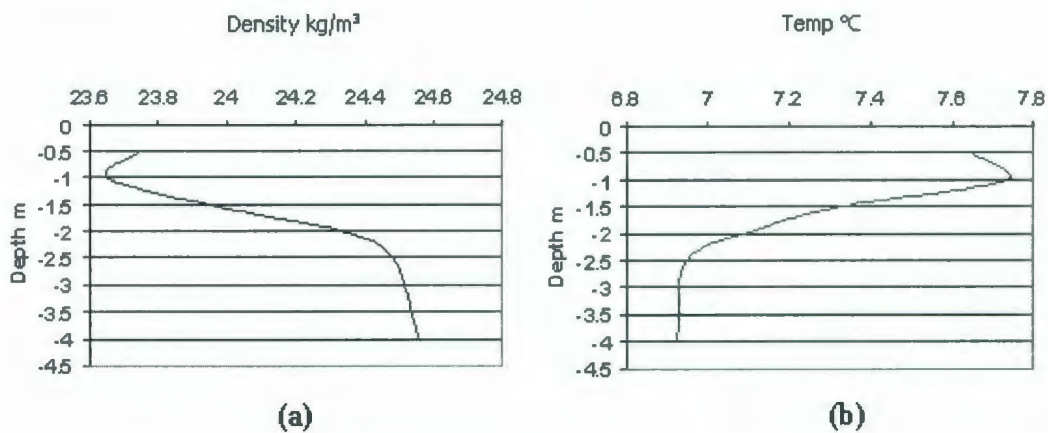


Figure 4.7. Spaniard's Bay Density (a) and Temperature (b) Profile. July 20, 2007.

4.1.4. Model Inputs

Based on effluent characteristics, outfall geometry, and ambient conditions described above, the model inputs were summarized in Table 4.1.

Table 4.1. Spaniard's Bay Outfall Model Input Summary

Effluent Characteristics	
Effluent flow rate	0.0514 m ³ /s
Density	999 kg/ m ³
Salinity	1 psu
Mean turbidity	15,49 NTU
Outfall Characteristics	
Outfall Length	100 m
Outfall diameter	0.2 m
Diffuser Length	6 m
Total number of risers	2
Spacing between risers	5 m
Riser height	0.6 m
Total number of ports for each riser	2
Riser diameter	0.07 m
Port vertical angle	0 ° (horizontal discharge)
Port orientation	0 ° (staged diffuser)
Horizontal angle	270°(perpendicular to the ambient direction)
Port direction	Same direction
Ambient Conditions	
Average current Velocity	0.0267 m/s
Average current direction	225 ° (SW)
Average water depth	6 m (above the diffuser)
High water slag	11:00am - 12:00 pm
Low water slag	5:00 pm - 6:00 pm
Upper layer density	1023.65 kg/m ³ (0.5 m)
Bottom layer density	1024.55 kg/m ³ (4 m)
Average wind speed	7.22 m/s

4.1.4.1. CORMIX Model

As a result of feeding the input data to the CORMIX model and running it, flow description and numerical prediction files were generated. The following is a summary of flow description file:

- Since the effluent density is less than the surrounding ambient water density at the discharge level, the effluent is positively buoyant and will tend to rise to the surface.
- The effluent will experience instability with full vertical mixing in the near-field, which may have a benthic impact of high pollutant concentration.
- The plume becomes vertically fully mixed within near-field, but may re-stratify later in the far-field.
- The plume in the unbounded section contacts nearest bank at 96.47 m downstream.

The numerical file demonstrated that the near-field mixing zone ends at 11.58 m with a 35.6 dilution ratio corresponding to a 0.43 NTU turbidity concentration (Table 4.2).

Table 4.2. CORMIX Near-Field Dilution Summary

	X (m)	Y (m)	Z (m)	S	C- NTU	BV (m)	BH (m)
Start of Near-field	0	-2.50	4.40	18.9	0.82	4.40	0.58
End of Near-field	11.58	-17.96	4.40	35.6	0.43	0.71	11.45

where X is the plume downstream length, Y is the plume width from the centerline, and Z is the plume height. S is the dilution rate, C is the turbidity concentration, BV is the top-hat thickness measured vertically in X-direction, and BH is the top-hat half-width measured horizontally in Y-direction. Figure 4.8 demonstrates the near-field dilution ratio and Figure 4.9 is a 3-D near-field turbidity concentration graph.

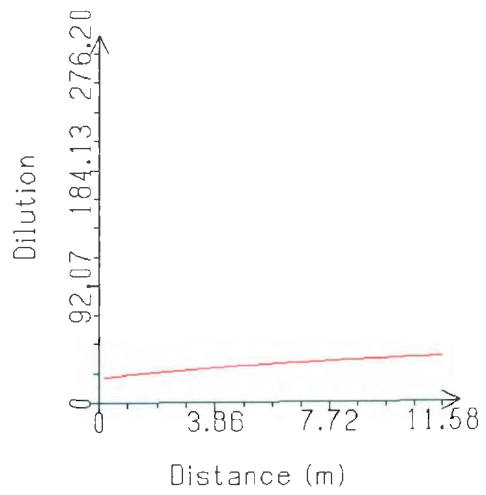


Figure 4.8. CORMIX Near-field Dilution

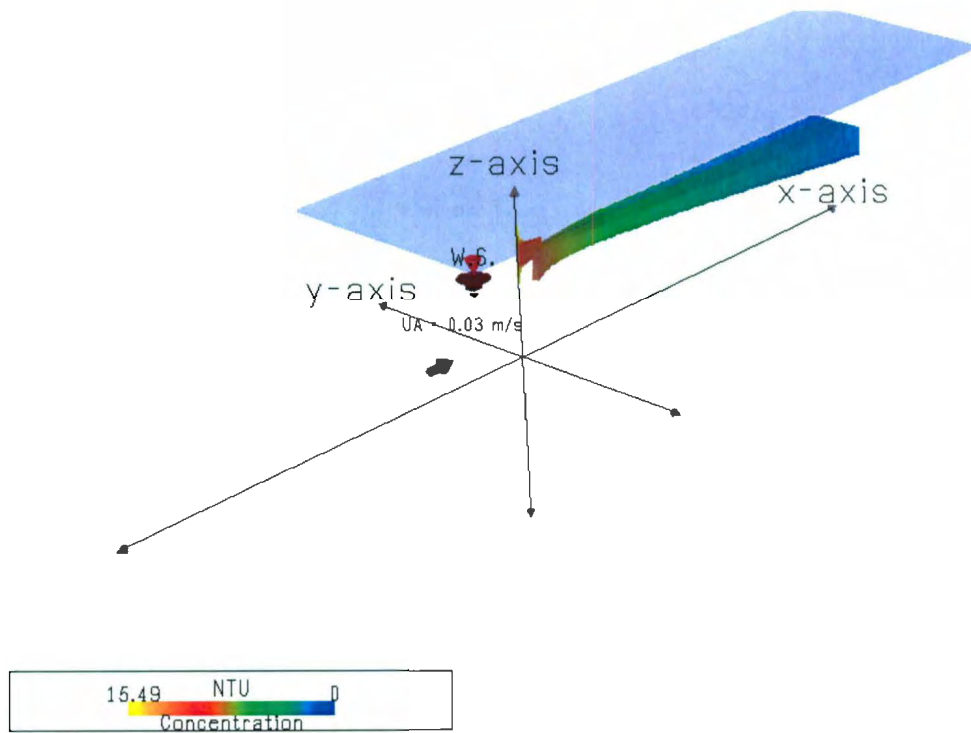


Figure 4.9. CORMIX 3-D Turbidity Concentration Graph

4.1.4.2. RSB Model

In this model, the same discharge characteristics and ambient conditions fed to the CORMIX model were considered. However, in this model the existing staged diffuser design was compared with the T-Shape riser design (Figure 4.10).

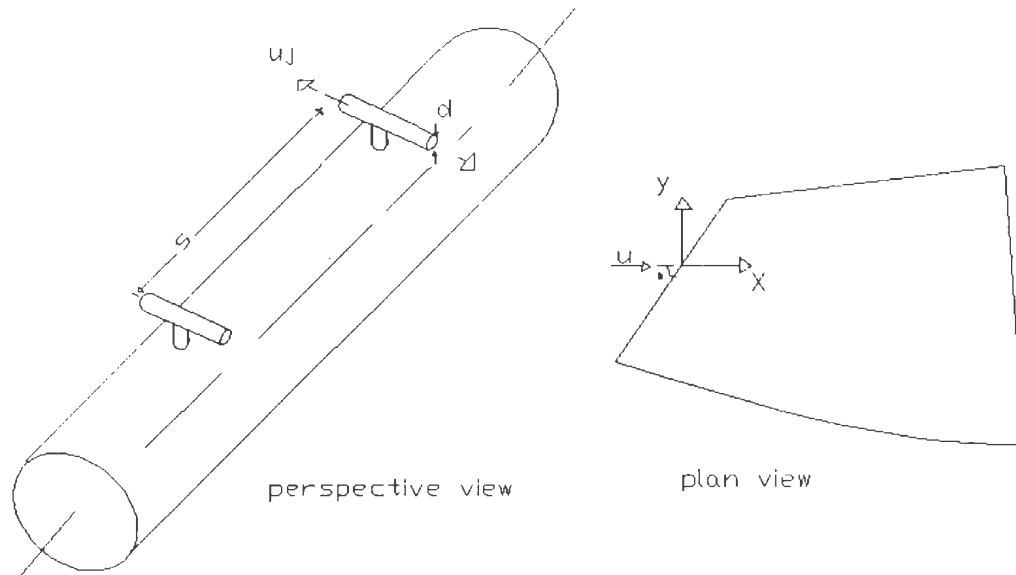


Figure 4.10. Alternative T-Shape Risers Diffuser Geometry

where d is the port diameter, s is the riser's spacing, n is the total number of ports, u_j is the port exit velocity.

Considering linear density stratification, the buoyancy frequency can be calculated by (Daviero and Roberts, 2006):

$$N = \sqrt{\left(\frac{-g}{\rho_a}\right)\left(\frac{d\rho_a}{dz}\right)} \quad (4.1)$$

where g is the gravity force, $d\rho_a/dz$ is the stratification difference at the discharge depth, and ρ_a is the ambient density.

By substituting equation. 4.1, the buoyancy frequency becomes:

$$N = \sqrt{\left(\frac{-9.81m/s}{1023.65kg/m^3}\right)\left(\frac{10.23.65kg/m^3 - 1024.55kg/m^3}{5m}\right)}$$

$$N = 0.0415s^{-1}$$

Considering that the effluent density variation is small compared to the absolute ambient density (the Boussinesq approximation), Tian et al. (2004-a) calculated the modified acceleration due to gravity using:

$$g'_o = g \frac{\rho_a - \rho_o}{\rho_a} \quad (4.2)$$

where ρ_o is the effluent density.

By substituting the column density field data,

$$g'_o = 9.81m/s \frac{1023.65kg/m^3 - 999kg/m^3}{1023.65kg/m^3}$$

$$g'_o = 0.236m/s^2$$

The discharge per unit diffuser length is calculated using (Tian et al., 2004-a).

$$Q_T = qL \quad (4.3)$$

where Q_T is the total discharge, q is the discharge per unit length, and L is the diffuser length.

Considering the effluent discharge is $0.514 m^3/s$ and the diffuser length is 6 m, the discharge per unit length becomes:

$$q = 0.00856m^2 / s$$

Daviero and Roberts, (2006) computed the buoyancy flux per unit length in a stratified stationary environment using:

$$b = g_0 q \tag{4.4}$$

$$b = 0.00202m^3 / s^3$$

Daviero and Roberts (2006) calculated the length scale for a linearly stratified ambient using:

$$l_b = \frac{b^{1/3}}{N} \tag{4.5}$$

$$l_b = 3.0m$$

Tian et al. (2006) conducted an experiment under a stratified and flowing environment. As a result, they concluded that the near-field dilution is effected by the port spacing when $s/l_b < 2$, where the near-field dilution can be predicted using:

$$\frac{S_n q N}{b^{2/3}} = 1.23 F^{1/6} \tag{4.6}$$

when $s/l_b \geq 6$, the authors predicted the near-field dilution using:

$$\frac{S_n q N}{b^{2/3}} = 1.66 (s/l_b)^{-1/3} F^{1/9} \tag{4.7}$$

As for a stationary environment when $s/l_b < 2$, they predicted the near-field using:

$$\frac{S_n q N}{b^{2/3}} = C1 \tag{4.8}$$

For the Spaniard's Bay outfall, the diffuser port spacing length scale was determined as:

$$s/l_b = 5/3.0 = 1.6$$

Since $s/l_b < 2$, then equation 4.6 applies.

Davis (1999) used the Froude number to express the effect of the flowing current (equation 4.9).

$$F = U^3 / b \quad (4.9)$$

Substituting the mean current velocity obtained from the current meter as 0.0267 m/s

$$F = 0.00942$$

Therefore, the near-field dilution was found:

$$Sn = \frac{(0.00202m^3/s^3)^{2/3}(0.00942)^{1/6}}{0.00856m^2/s \times 0.0415/s}$$

$$Sn = 22.038$$

When $s/l_b < 2$, the near-field length is obtained using equation 4.10 (Tian et al., 2006).

$$X_n / l_b = 8.0F^{1/3} \quad (4.10)$$

$$X_n = 5.06m$$

For weak currents ($F < 0.1$), Tian et al. (2006) suggested using equation 4.11 for computing the waste field centerline.

$$Z_n / l_b = 1.7 \quad (4.11)$$

$$Z_n = 5.1m$$

Therefore, when using the RSB model for the T-shape riser design, the near-field boundary (X_n) was predicted at 5.6 m with 22.03 dilution ratio and 5.1m centerline height (Z_n).

4.2. Data Management

As described in Chapter 3, large sets of raw data were generated from the AUV and sensor towing experiments. Often these raw data convey very little information because of the associated sensor noise with it. Initially, it was important to statistically analyze and validate the accuracy of these data. Therefore, some statistical analysis techniques were applied to investigate when and where large variations have occurred. These variation or outliers could be true due to actual environmental changes caused by the outfall effluents or false as a result of sensor errors.

Four data sets were generated from the environmental monitoring experiments. Two sets were obtained from AUV experiments and the other two from towed sensor experiments. Figure 4.11 demonstrates a procedure developed to analyze the raw and extract useful information.

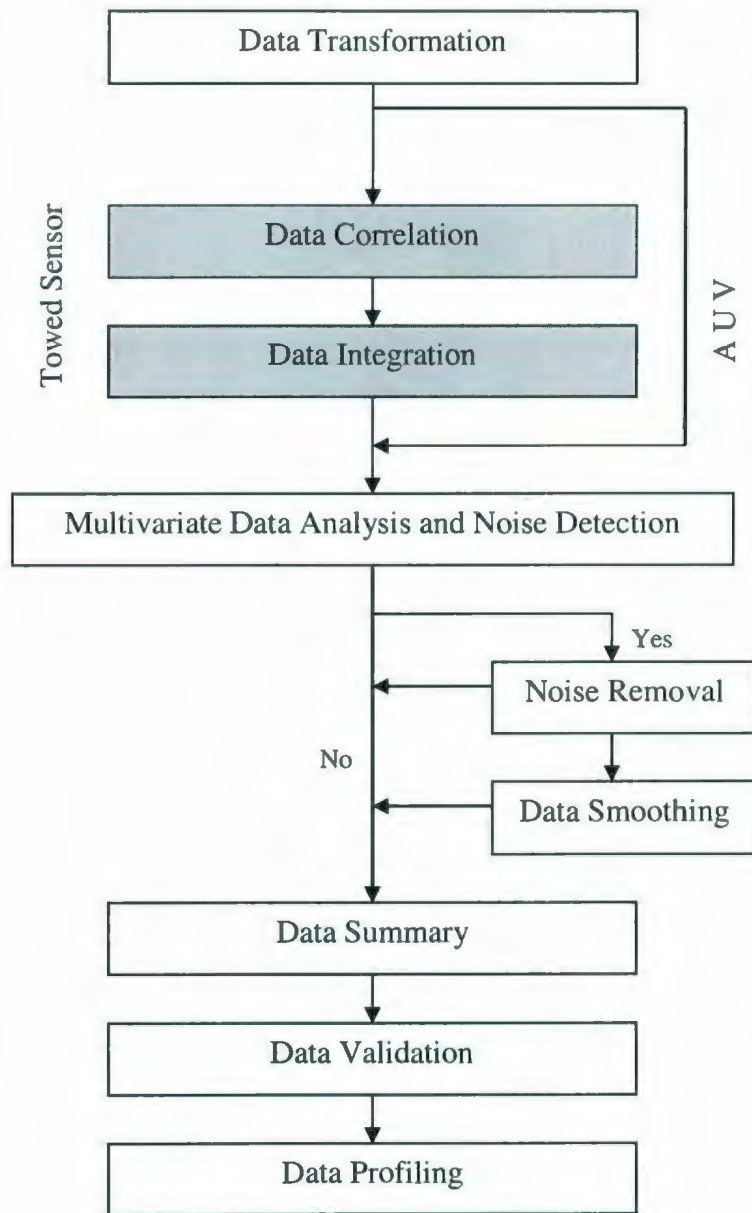


Figure 4.11. *In-Situ* Data Management and Analysis Diagram

4.2.1. Data Transformation

The raw data obtained from the data logger and GPS were transferred from comma delaminated format (cvs) to Excel workbook (xls) format.

4.2.2. Data Correlation

The GPS spatial data were correlated with environmental monitoring data acquired from the CTD. The correlation was based on the synchronized timing of the GPS and the CTD performed at the beginning of each experiment.

4.2.3. Data Integration

The six horizontal depth layers were integrated in ascending order. Such integration was used for determining when and where variations occurred in the water column.

4.2.4. Multivariate Data Analysis

A multivariate data analysis technique was applied to characterize the time series data of all experiments. This was done by plotting the relevant data in one chart for identifying when and where noise occurred.

Sensor noise is a common problem associated with *in-situ* monitoring activities. Often the nature and origin of noise is unknown. Brerton (2002) reported two types of noise associated with *in-situ* environmental monitoring, a stationary and a correlated noise. The stationary noise occurs at each successive point in time and does not depend on the noise at the previous point. There are two forms of stationary noise, the homoskedastic and the hetroskedastic noise. When the mean and standard deviation remain constant over the entire data series, it is considered as homoskedastic. As for the hetroskedastic noise, it is dependent on the size of the measurement, which is often proportional to its intensity. However, this noise is still represented by the normal probability distribution. The

correlated or non-stationary noise occurs when the level of noise in each sample of a time series depends on that of the preceding one.

By integrating AUV experiment 1 data (Figure 4.12), unrealistic salinity variations ranging from 0 to 30 psu were observed. Also, similar variations were observed for temperature and chlorophyll *a* concentrations. By comparing chlorophyll *a*, temperature and depth variations, it was observed that at 15 m depth these variations did not adjust back to their surface observations (2 – 4 °C for temperature and 0 to 0.2 ppb for chlorophyll *a*), which indicates measurement errors. At the surface, the noise was attributed to surface waves and currents. It was observed that when the AUV was moving against the current, the tendency of the vehicle is to resist the current and rise up to the surface, where sensors are exposed to the ambient air causing noisy signals. After 1528 seconds, a technical fault occurred and generated noisy data. All noisy data were screened out and eliminated from this experiment. Experiment 2 raw data demonstrates noisy salinity observations at the surface due to wave and current issues (Figure 4.13).

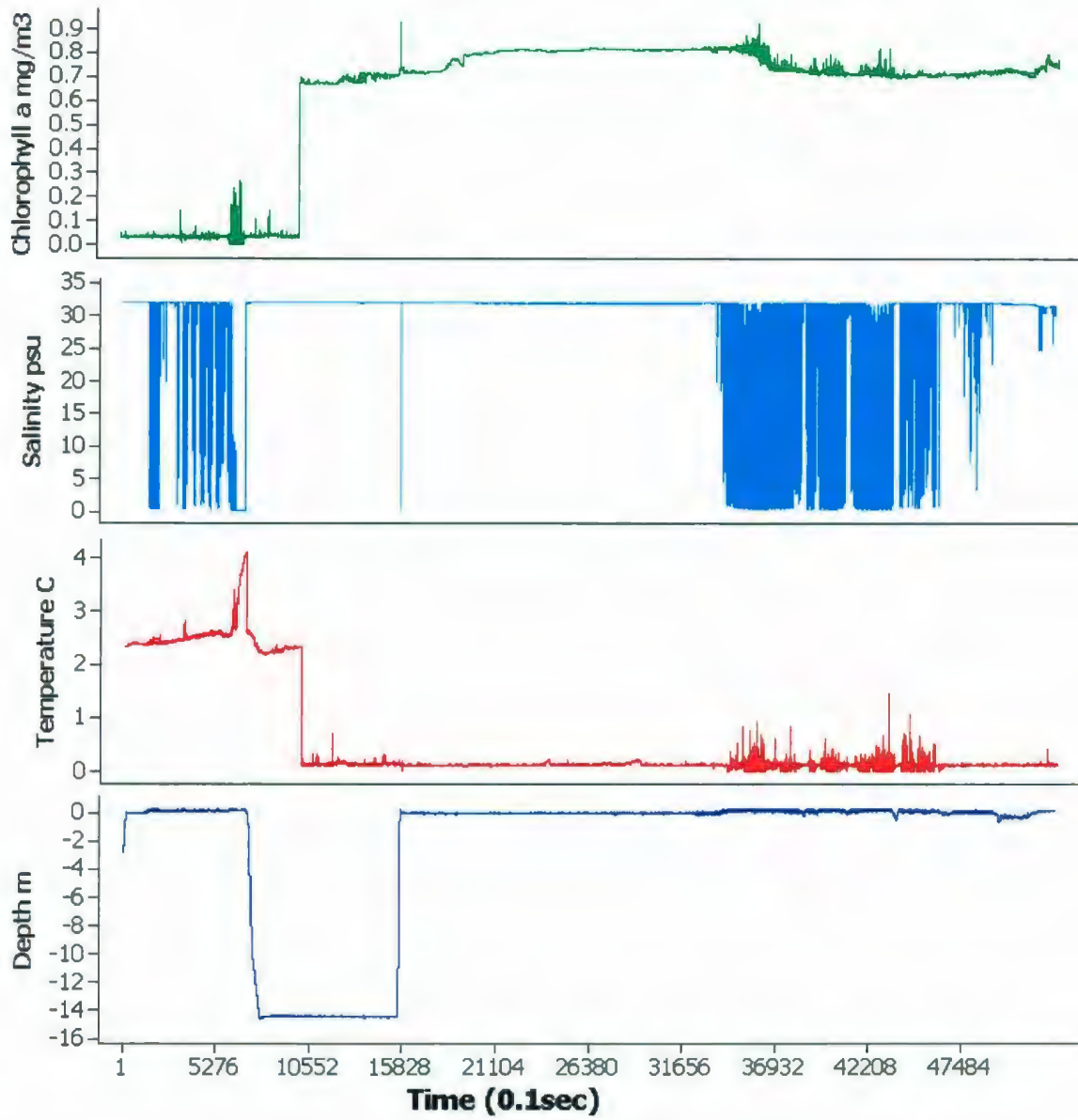


Figure 4.12. AUV Experiment 1 Raw Data Analysis

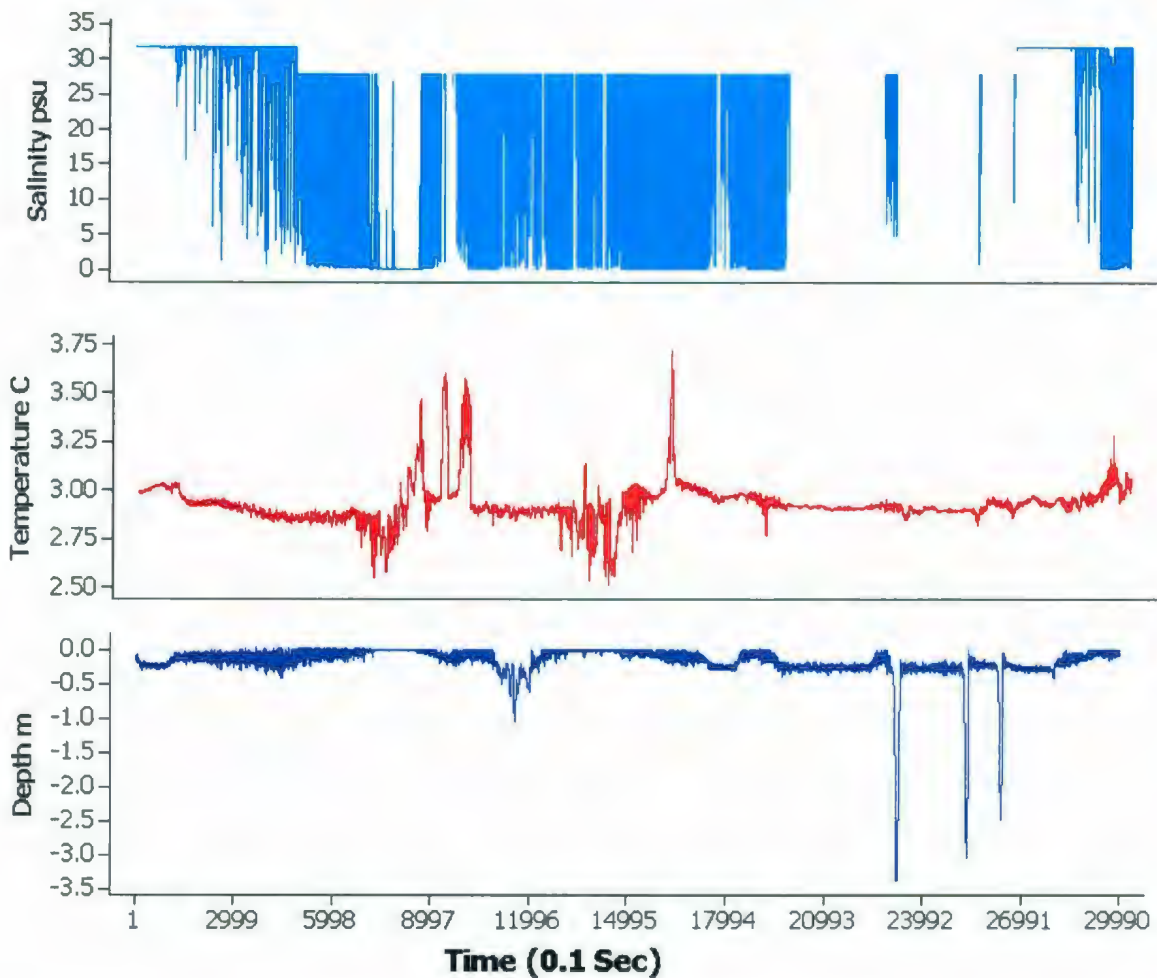


Figure 4.13. AUV Experiment 2 Raw Data Analysis

The sensor towing experiments (Figures 4.14 and 4.15) demonstrate more realistic results and fewer variations compared to AUV experiments. The only variation observed was when the sensor platform was deployed at the beginning of each mission and recovered back at the end. These data were eliminated by deleting the first and the last 10 seconds of each horizontal layer allowing the sensor to rest at the desired depth.

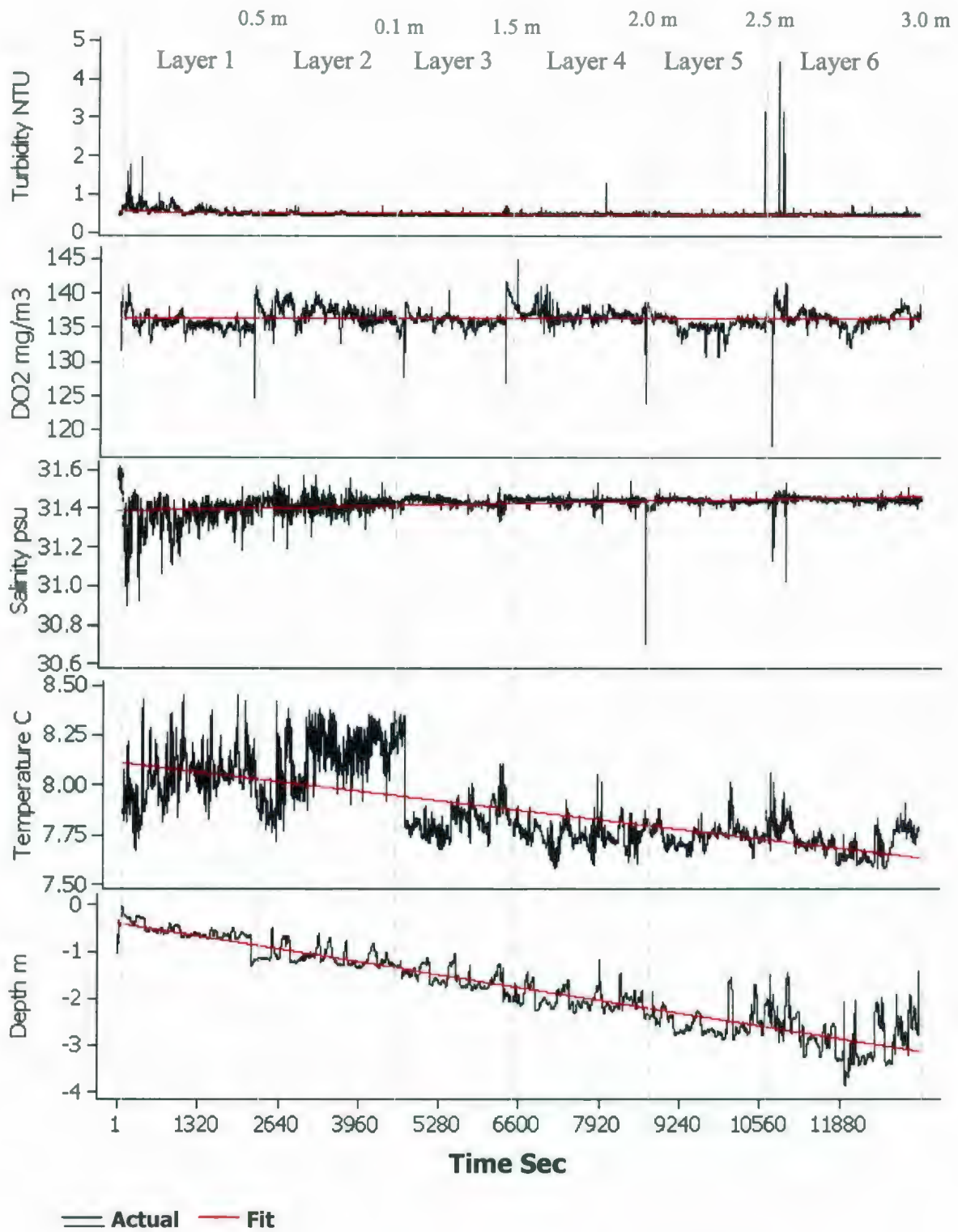


Figure 4.14. Sensor Towing Experiment 1 Raw Data Analysis

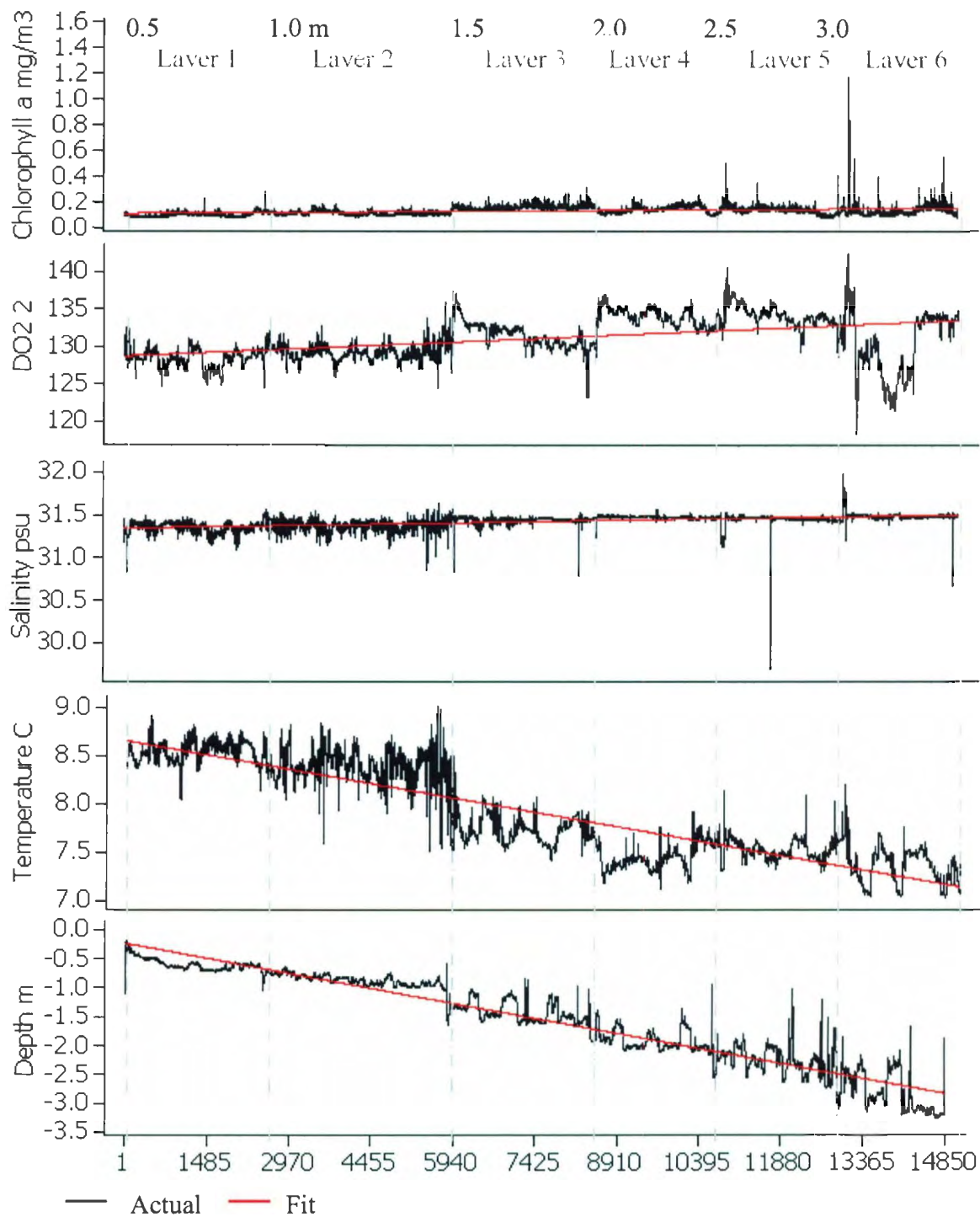


Figure 4.15. Sensor Towing Experiment 2 Raw Data Analysis

4.2.5. Smoothing

Smoothing is a statistical technique used when the time series data is associated with noisy signals. The moving average method was applied to smooth out fluctuations of time series data using the trend line method (Fleming, 2000). This is accomplished by taking the rolling averages of the data over a number (n) of consecutive periods. It is important to avoid over-smoothing the data by choosing too large a value of n. The moving-average trend values have to be “centered” against the mid-point of the average period. Table 4.3 demonstrates an example of a three point moving average of salinity observations. The Minitab statistical software was used to calculate the moving average of time series data. Figure 4.16 graph shows the smoothed salinity data (fits) of experiment 2 after eliminating the depth related noise. It was possible to visualize and characterize the trend after smoothing the salinity observations.

Table 4.3. Moving Average Smoothing Technique

Time series	Salinity	Three point moving average
1179329786	31.377	= (31.377+31.768+31.762)/3 = 31.635
1179329786	31.768	= (31.768+31.762+31.803)/3= 31.777
1179329786	31.762	= (31.762+29.803+27.805) /3= 29.79
1179329786	29.803	
1179329786	27.805	

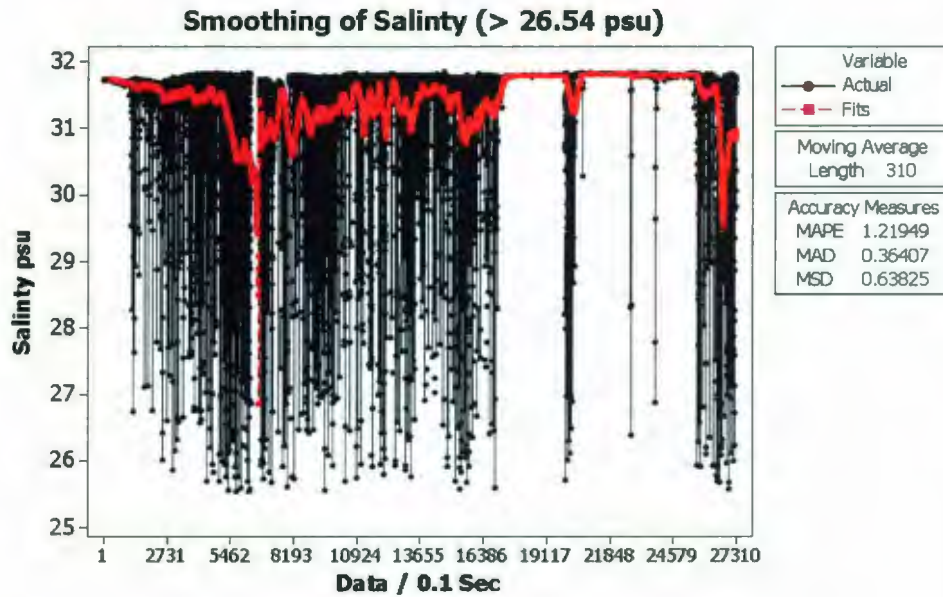


Figure 4.16. AUV Experiment 2 Salinity Smoothing Technique

4.2.6. Data Validation

The towed sensor data was validated by correlating temperature and salinity observations with depth. Figures 4.14 and 4.15 show temperature observations decreased with depth, while density observations increased with depth. These observations reveal summer thermal and density stratification, where the surface water layer has a higher temperature and lower density than bottom layer. Such observations have provided confidence for further analysis.

4.3. Environmental Monitoring and Plume Tracking

One of the challenges of environmental monitoring is water quality assessment and plume tracking in a dynamic and complex system, such as the ocean. Traditional sampling and analysis can be very expensive, tedious, and represent a few discrete points in the water column. With the rapidly developing *in-situ* sensors and GPS technology,

more comprehensive assessments can be performed by characterizing large quantity of spatial and temporal data simultaneously. This monitoring technique can determine when and where changes occur in the water column. Therefore, it was applied to assess the impact of raw sewage outfall on a coastal water quality. The *in-situ* data were statistically analyzed using Minitab software and mapped using Surfer 8.

4.3.1. AUV Experiment 1

The AUV data obtained from experiment 1 was used to characterize temperature, salinity, and chlorophyll *a* concentrations at different depths. The temperature varied from 2.2 to 2.6 °C. The vertical trajectory (Figure 4.17a) demonstrates that from 0 to 2 m depth the temperature was around 2.6°C, from 2 to 10 m the temperature was close to 2.5°C, from 10 to 12 m a slight increase of 0.1°C was observed, and from 12 to 15m the temperature varied between 2.2 and 2.3°C. Figure 4.17b demonstrates a weak salinity stratified water column, where, from 0 to 8 m the salinity values were around 31.9 psu, and from 8 to 15 m the salinity was around 32 psu.

Chlorophyll *a* concentrations varied from 0.02 to 0.14 ppb. Figure 4.17c demonstrates higher concentrations at the bottom layers. Such observation reveals that ambient light penetrated the water column at such depth, due to the fact that phytoplankton communities rely on sunlight for their production. Penetration of light to such a depth also indicates a clear, non-turbid water column.

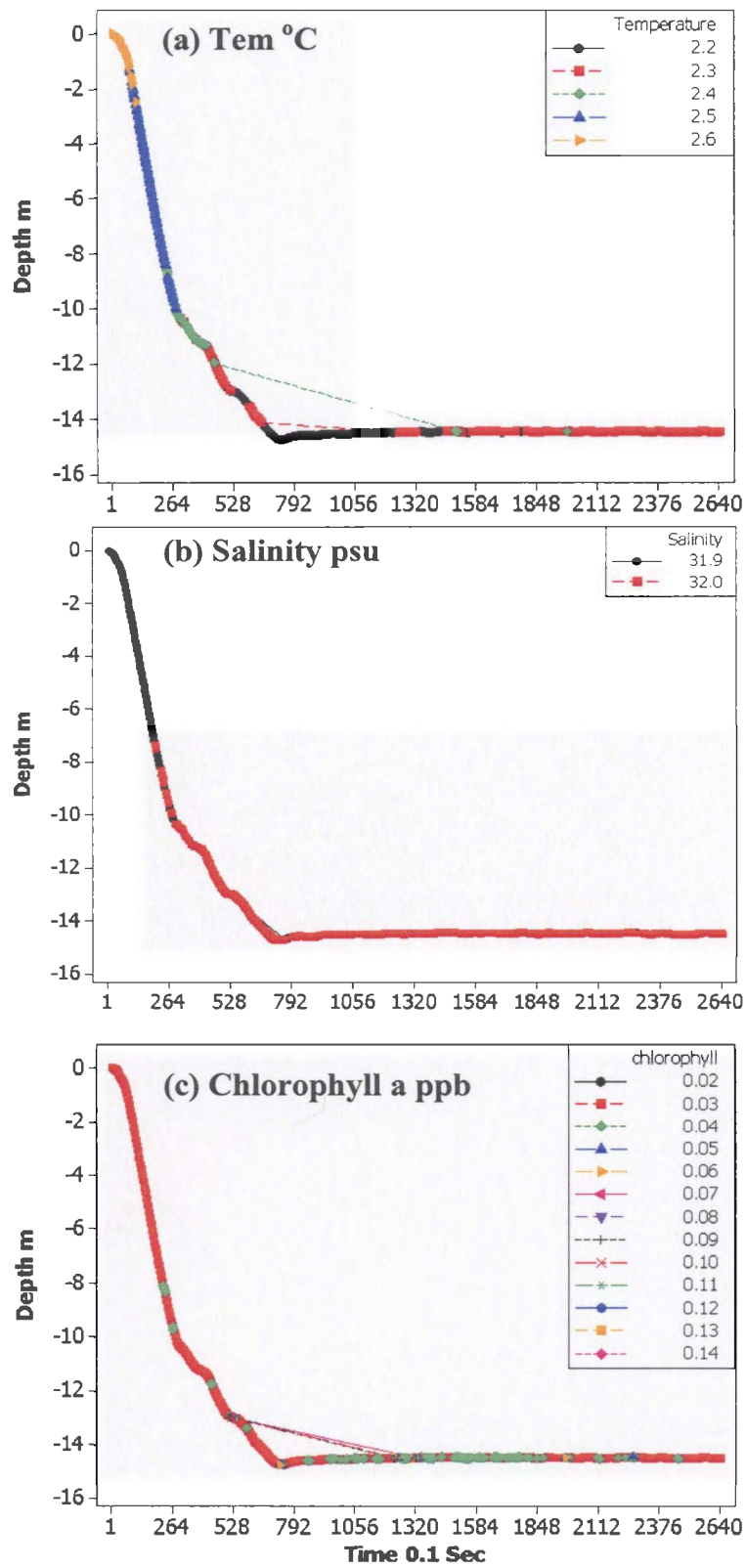


Figure 4.17. AUV Experiment 1 Vertical Profiling at the Center of the Bay

4.3.2. AUV Experiment 2

In this experiment the AUV was piloted at the surface and the middle of the bay. The salinity and temperature plots (Figure 4.18) demonstrate that the minimum temperature was 2.50 °C, the maximum was 3.71 °C, and the mean was 2.93°C. The minimum salinity value was 31.27 psu, the maximum was 31.69 psu, and the mean was 31.48 psu.

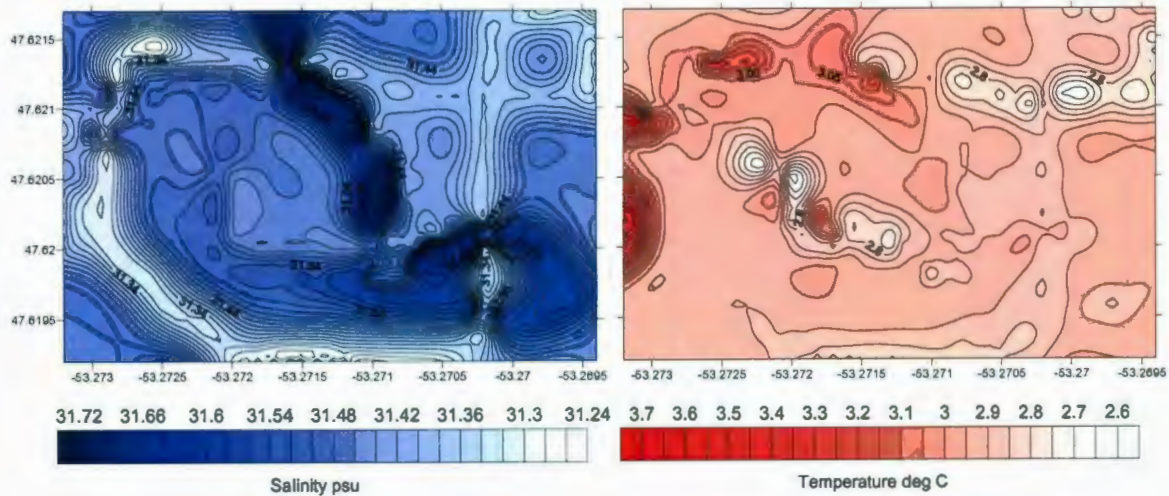


Figure 4.18. AUV Experiment 2 Surface Contour Maps

4.3.3. Sensor Towing Experiment 1

Six depth layers were monitored covering an approximate area of 11,910 m². In order to characterize spatial variations of each layer, the contour map was divided into nine geographical grids (Figure 4.19). The outfall is located in the western grid.

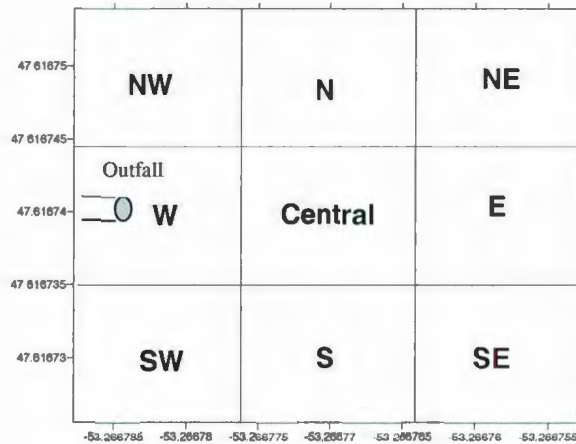


Figure 4.19. Geographical Distribution Grids

4.3.3.1. Salinity

Figure 4.20 demonstrates a slight positive salinity correlation with depth, where the correlation coefficient $R^2 = 0.23$. With the exception of a few low salinity observations obtained around the outfall area, the graph indicates a weakly stratified water column.

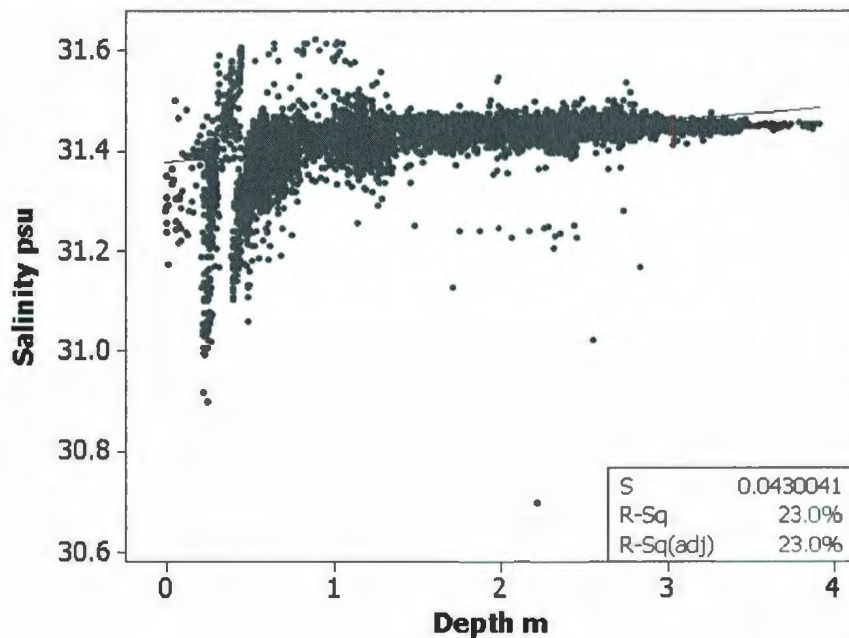


Figure 4.20. Sensor Towing Experiment 1 Salinity - Depth Correlation

The longitudinal salinity distribution plots (Figure 4.21) demonstrate more salinity variations and less concentration in the upper layers compared to the lower layers. The mean values from the top to the bottom layers were 31.38, 31.42, 31.43, 31.44, 31.44, and 31.45 psu, corresponding to standard deviations of 0.087, 0.028, 0.018, 0.012, 0.014, and 0.016 psu, respectively. Such observations reveal that the buoyant effluent plume rose to the surface layer before being advected by the ambient current in a downstream direction. It is evident from the upper two layers that salinity variations were decreasing in a downstream direction. With the exception of a few upstream low salinity values observed in layer 6 caused by the outfall effluent, the small standard deviations of the lower 3 layers indicate homogenized salinity layers, which means that the lower layers were not affected by outfall effluent. Salinity contour maps (Figure 4.22) demonstrate that salinity variations decrease with depth, where the lowest salinity concentrations were identified in the surface layers and around the diffuser location extending to an eastern and northeastern direction. These observations conclude that the effluent plume was advected downstream by the current.

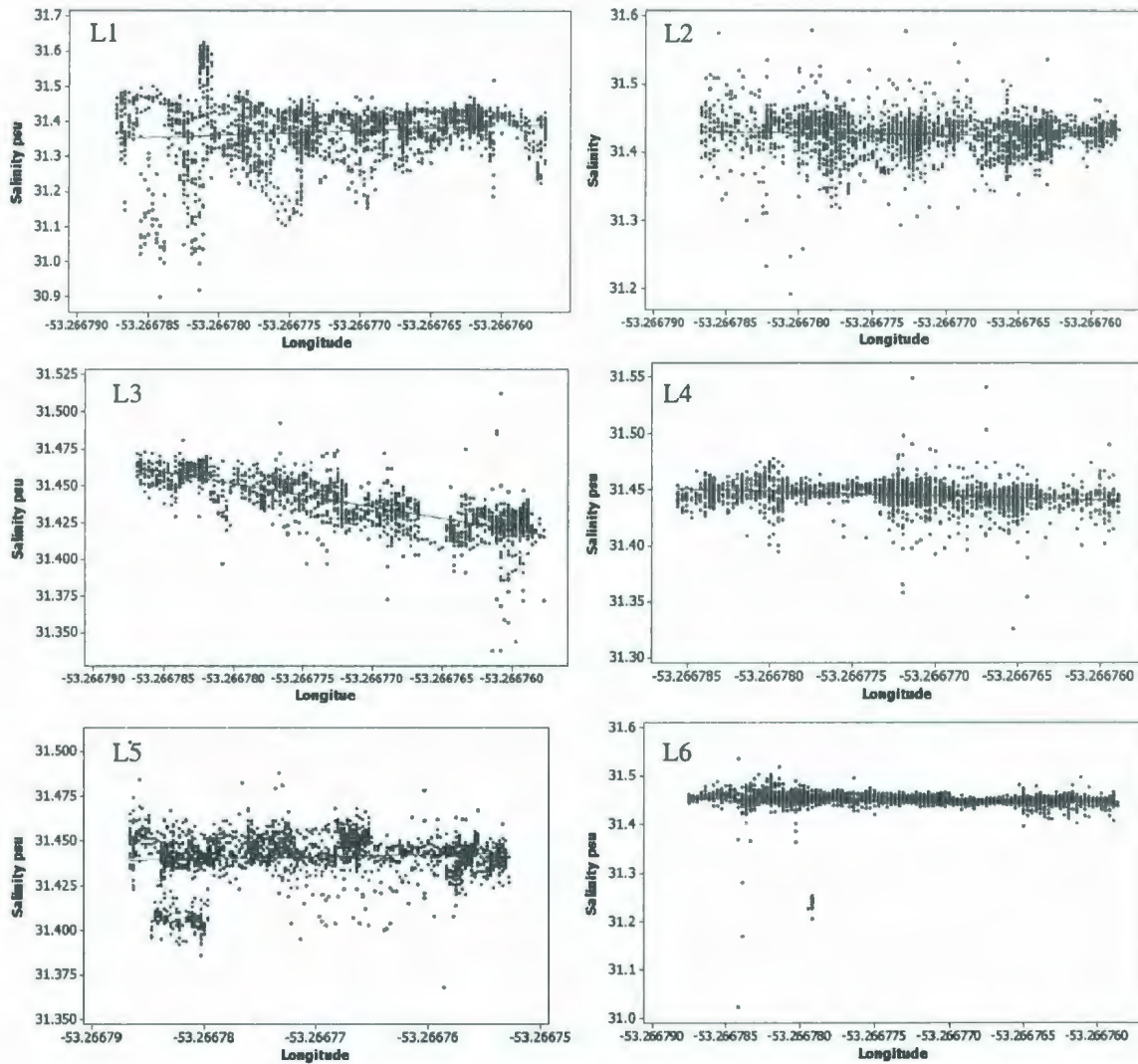


Figure 4.21. Sensor Towing Experiment 1 Downstream Salinity Distribution Plots

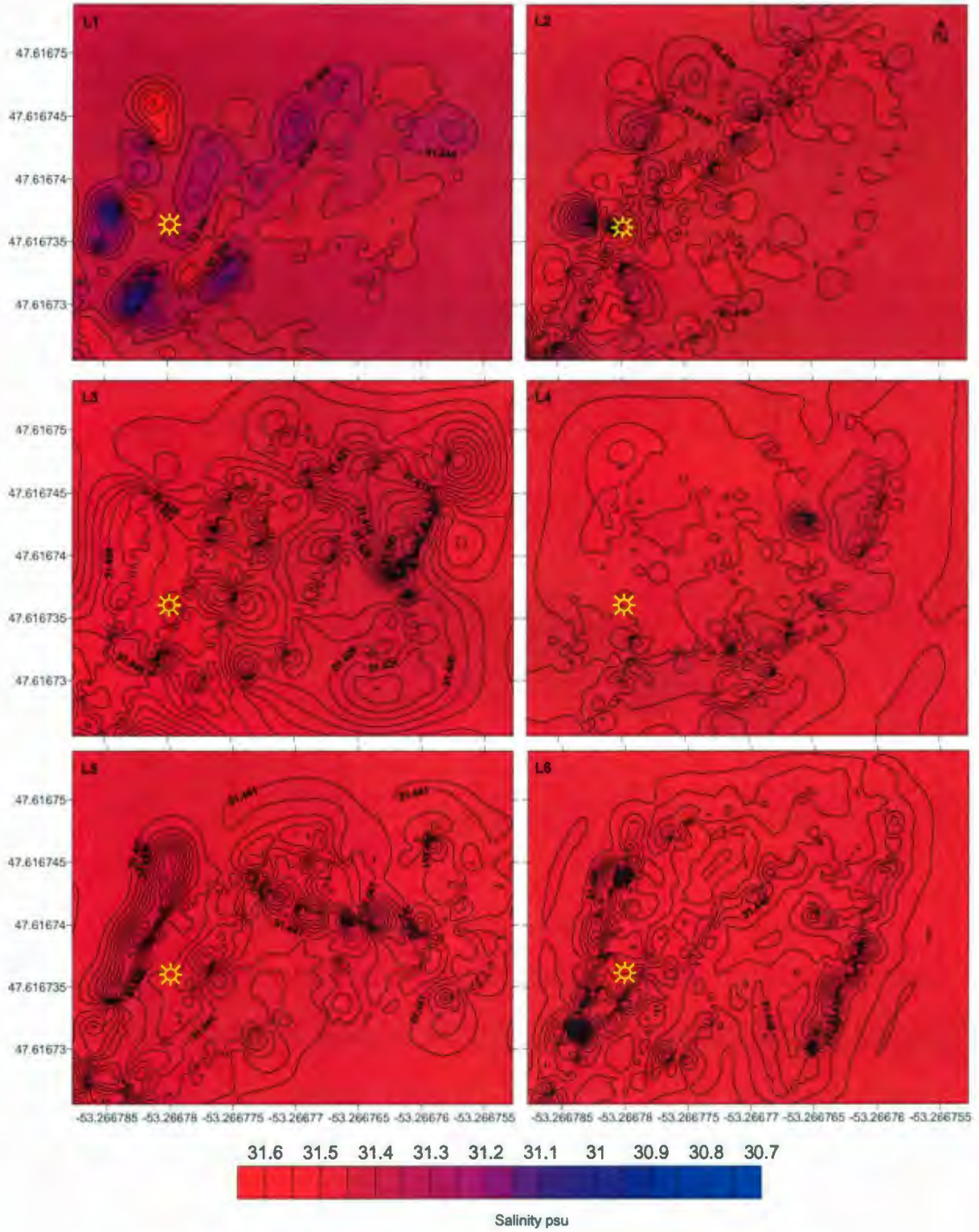


Figure 4.22. Sensor Towing Experiment 1 Water Column Salinity Contour Maps

4.3.3.2. Temperature

Figure 4.23 shows a strong negative temperature correlation with depth, where $R^2 = 0.57$. This observation indicates a thermally stratified coastal zone. The temperature observations varied from 8.45 °C at 0.53 m to 7.0 °C at 2.83 m depth with a mean value of 7.86 °C and 0.19 °C standard deviation.

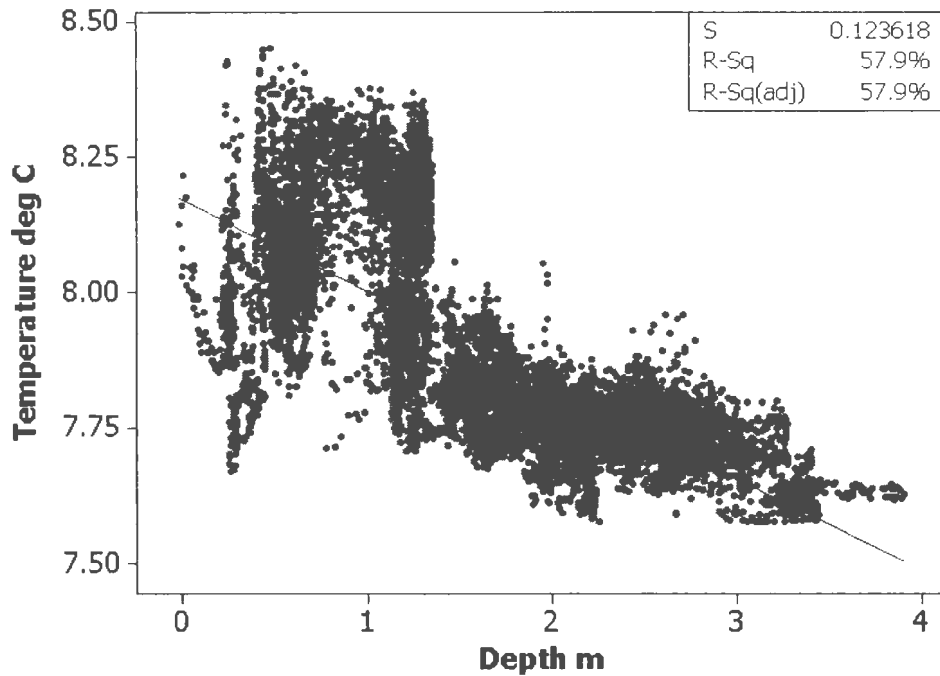


Figure 4.23. Sensor Towing Experiment 1 Temperature - Depth Correlation Plot

The highest temperature values were identified in the upper layers. It was observed from the longitudinal distribution graph that the upper surface layers (L1, L2, and L3) are positively correlated with distance, where $R^2 = 0.29$, 0.21 , and 0.3 , respectively (Figure 4.24). Layers 4 and 5 did not demonstrate any longitudinal correlation, while layer 6 demonstrated a negative correlation. These observations indicate a temperature increase in a downstream direction. Figure 4.25 shows the highest temperature variations are present in the surface layers.

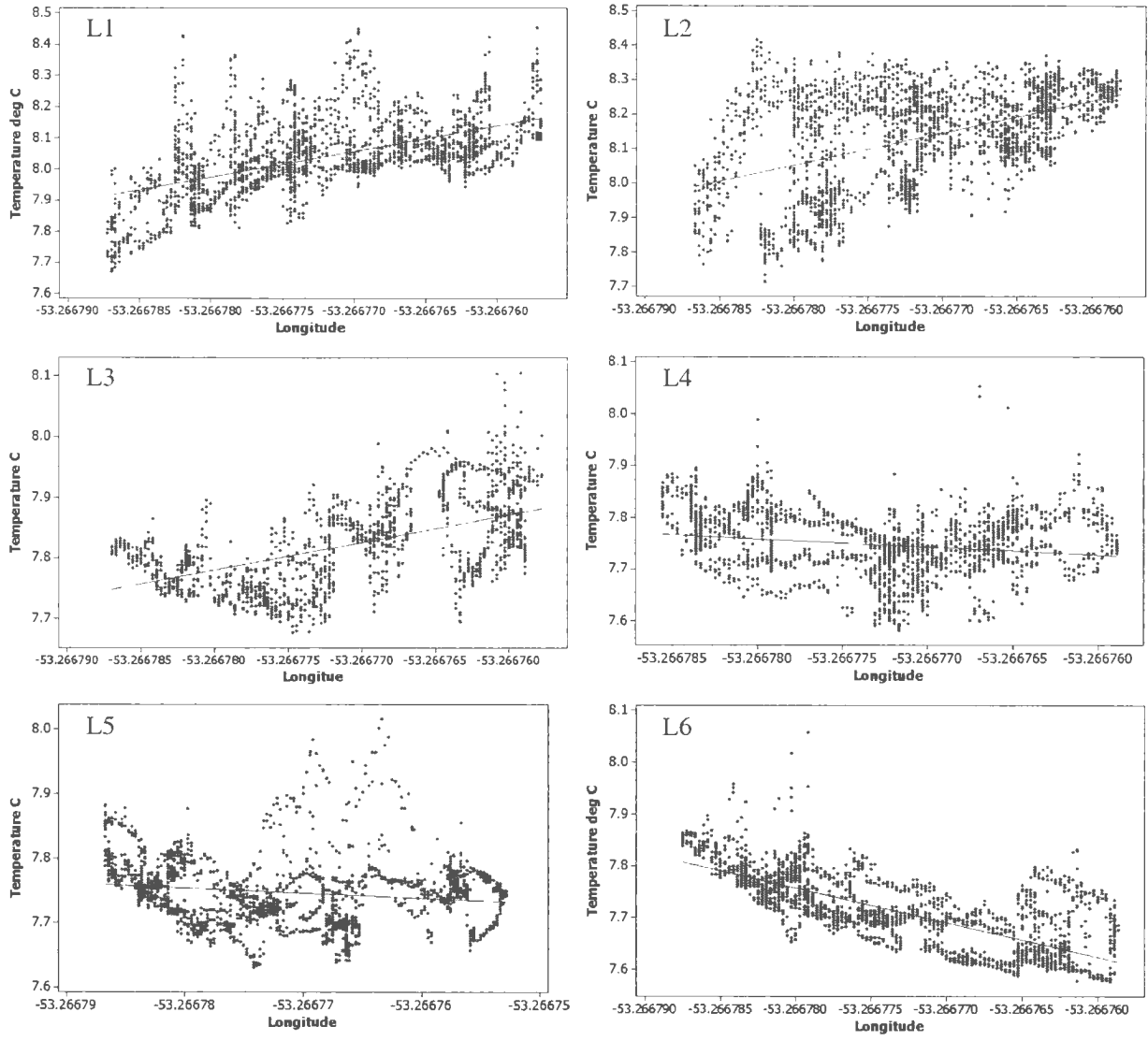


Figure 4.24. Sensor Towing Experiment 1 Downstream Temp Distribution Plots

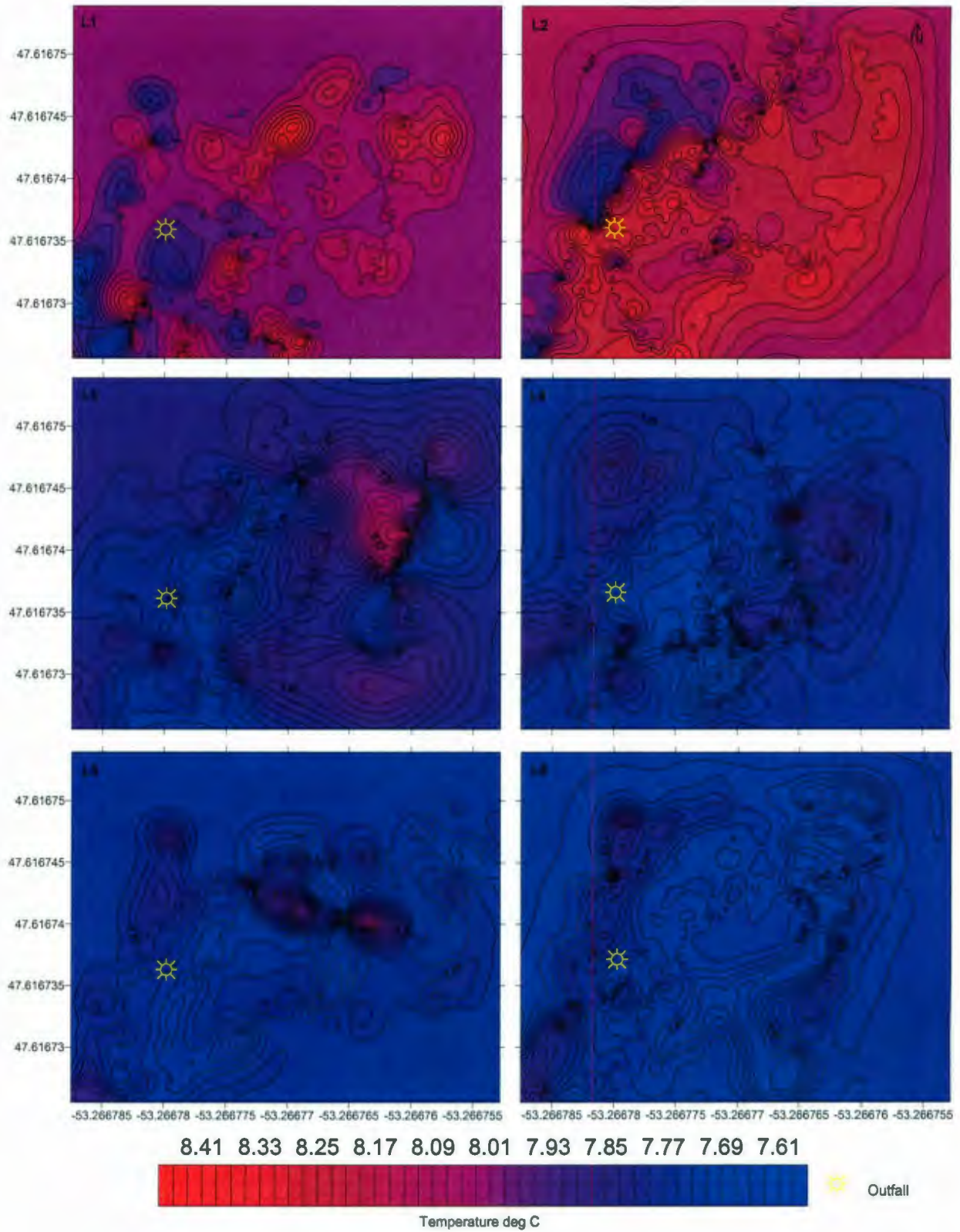


Figure 4.25. Sensor Towing Experiment 1 Water Column Contour Maps

4.3.3.3. Dissolved Oxygen

No DO correlation was observed with depth, where $R^2 = 0.08$ (Figure 4.26). The lowest DO saturation was observed in layer 5 (130.8% saturation) and the highest in layer 4 (145% saturation). The overall mean was 136.37% saturation and standard deviation was 1.27.

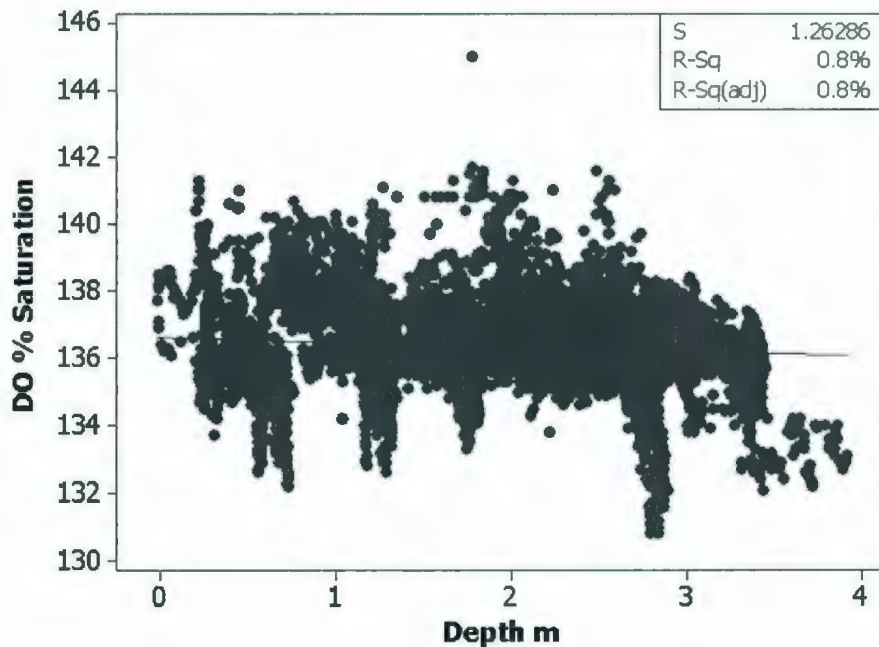


Figure 4.26. Sensor Towing Experiment 1DO-Depth Correlation Plot

The mean percent saturation from the top to the bottom layers were 135.74, 136.99, 136.08, 135.61, 137.09, and 136.47. All of the longitudinal DO plots demonstrate negative downstream correlation (Figure 4.27). This indicates that the biodegradation process was taking place with time. Due to the positive buoyancy force and downstream advection of the effluent, the biodegradation process of the organic matter was occurring at the surface layer and was exponential with time. Figure 4.28 demonstrates the highest

DO concentrations were observed around the outfall area and decreased in a downstream direction.

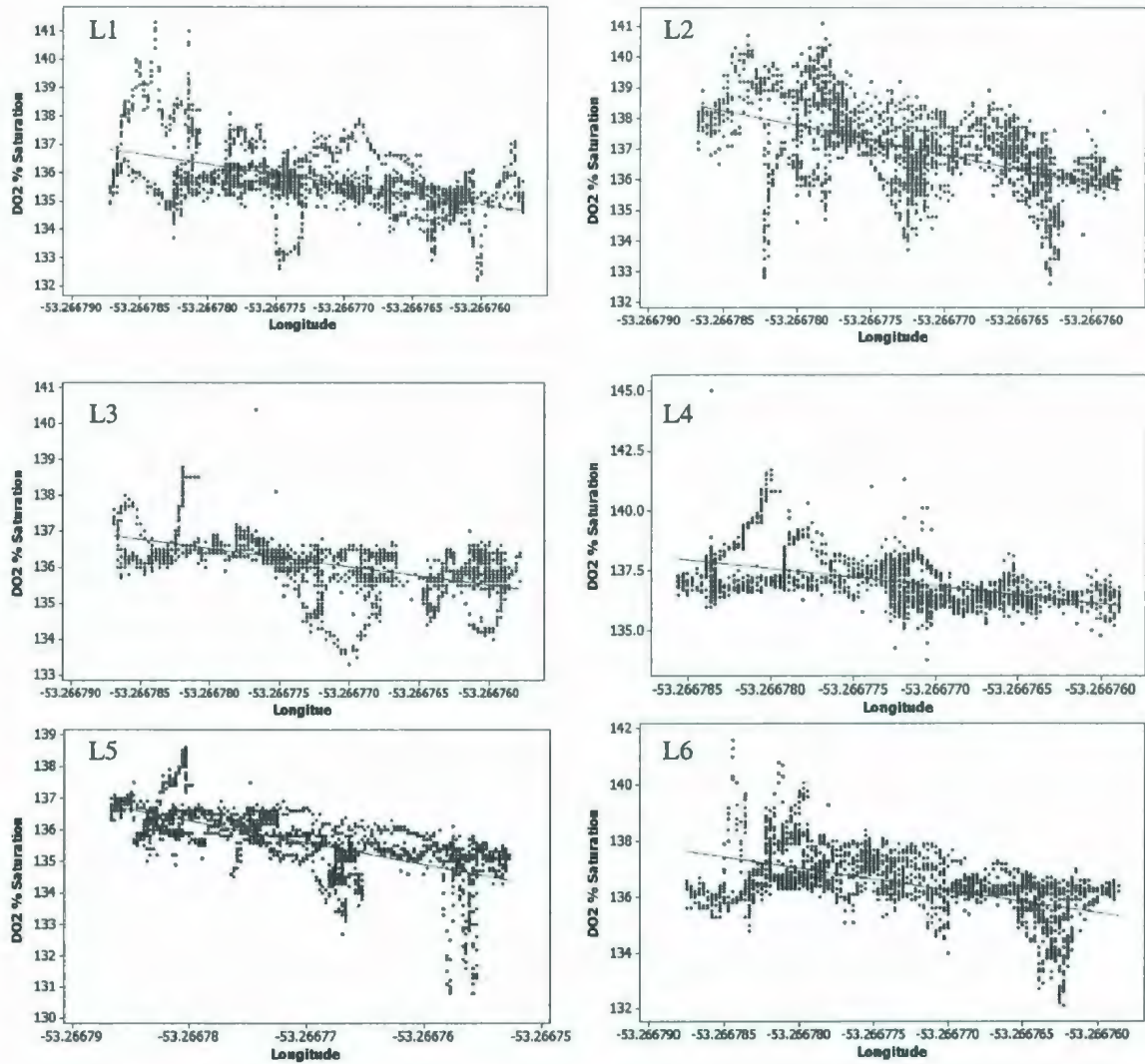


Figure 4.27. Sensor Towing Experiment 1 Downstream DO Distribution Plots

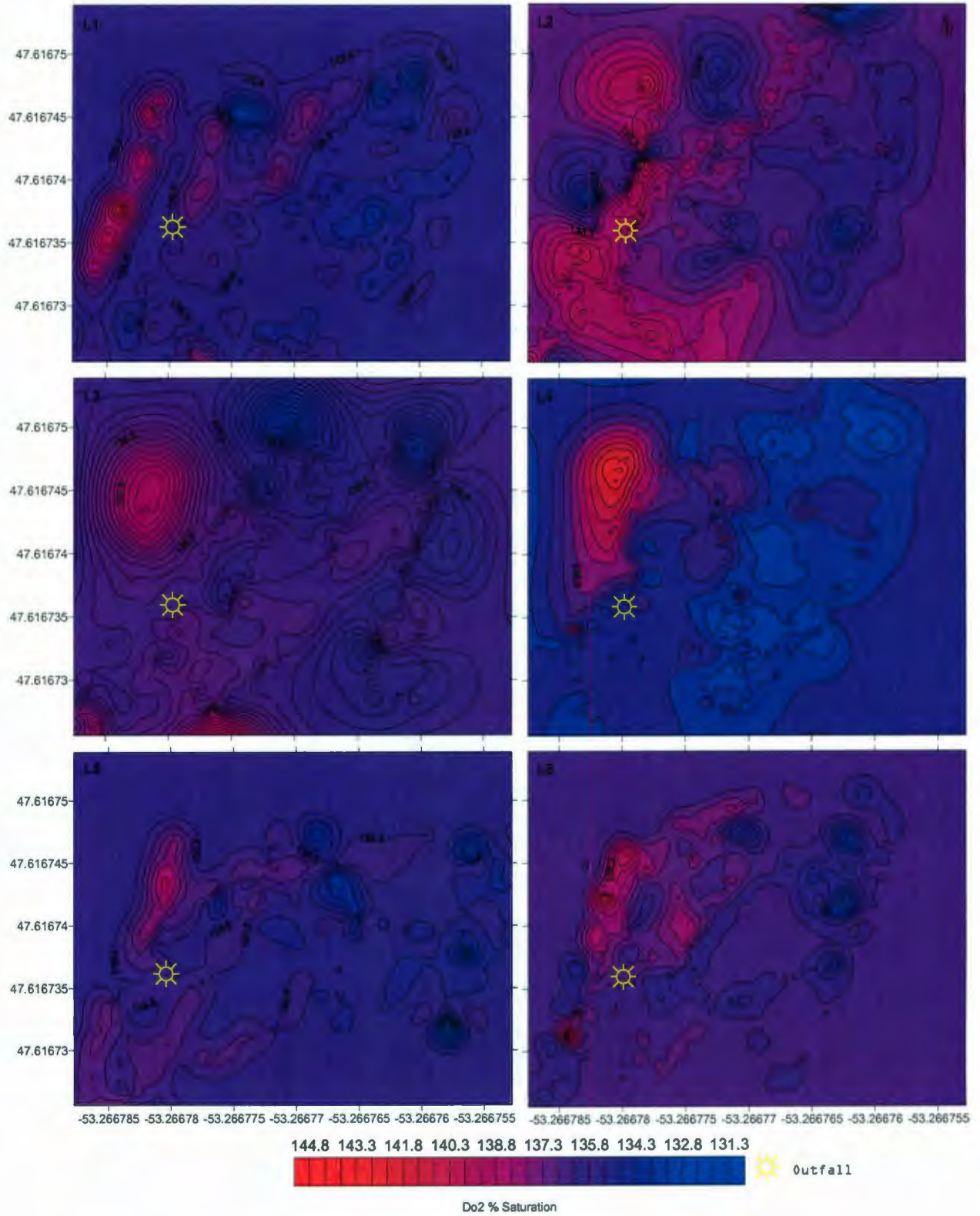


Figure 4.28. Sensor Towing Experiment 1 Water Column DO Contour Maps

4.3.3.4. Turbidity

The lowest turbidity value was observed as 0.4 NTU and the highest was 4.49 NTU at the bottom layer. The mean observations starting from the top to bottom layers were 0.54, 0.44, 0.43, 0.43, 0.44, and 0.45 NTU and the maximum were 1.93, 0.66, 0.61, 0.68, 1.27, 1.27, and 4.49 NTU, corresponding to 0.11, 0.02, 0.01, 0.01, 0.02, and 0.11 standard deviation. It was also observed that the highest and lowest standard deviations were identified in the top and bottom layers. By eliminating few isolated outliers due to large size effluent chunks, a negative turbidity correlation can be observed with depth, where $R^2 = 0.18$ (Figure 4.29).

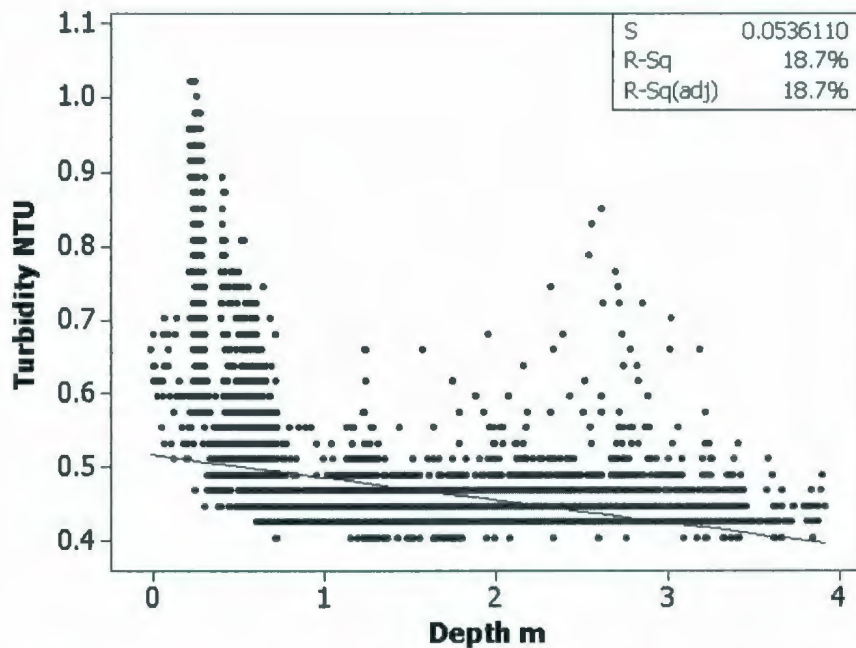


Figure 4.29. Sensor Towing Experiment 1 Turbidity - Depth Correlation Plot

Such observations reveal that due to the positive buoyancy force, the turbid effluent rose up to the surface layer. This can be justified as the raw sewage effluent, which usually has a similar density of fresh water was dispersed at the surface and then advected by the

surface current. The longitudinal turbidity distribution plots demonstrate that the highest turbidity variations were identified in the surface layer. While moving in a downstream direction, these variations were gradually decreased (Figure 4.30). The highest observations were identified upstream in the bottom layer and close to the outfall diffuser location. The contour maps (Figure 4.31) demonstrate how turbidity observations are distributed in the surface layer around the diffuser location.

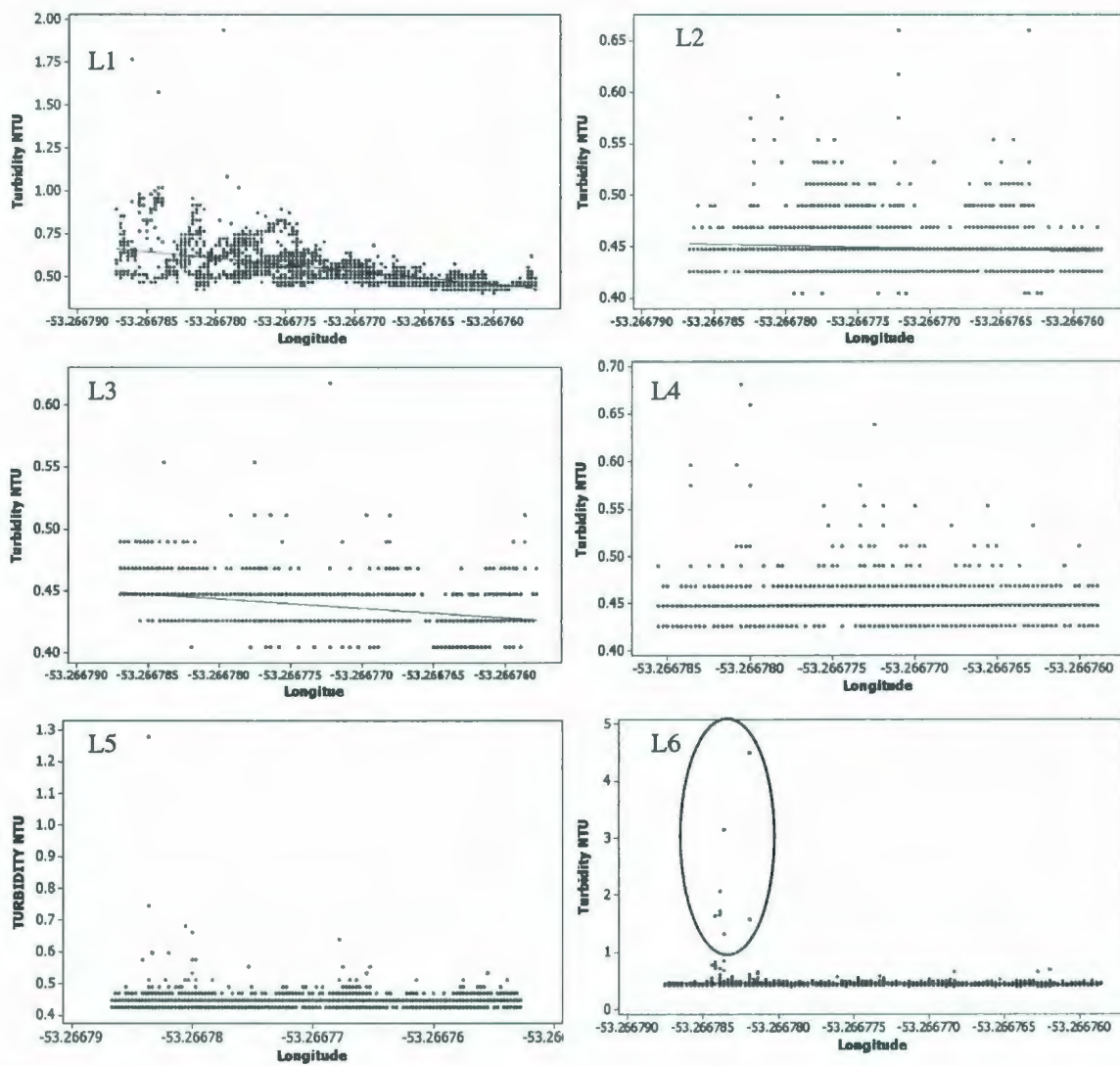


Figure 4.30. Sensor Towing Experiment 1 Downstream Turbidity Distribution Plots

4.3.4. Sensor Towing Experiment 2

In this experiment, the turbidity sensor was replaced by the chlorophyll *a* sensor. The same characterization procedures applied in sensor towing experiment 1 were applied to this experiment.

4.3.4.1. Salinity

With the exception of a few outliers, the integrated salinity observation has shown a weakly stratified water column. Figure 4.32 demonstrates a weak positive salinity correlation with depth, where the correlation coefficient $R^2 = 0.316$. The longitudinal salinity distribution plots (Figure 4.33) demonstrate that the highest salinity variations can be identified at the surface layer, and as the plume travels in a downstream direction the salinity values decrease. Such observations indicate that the effluent plume rose to the surface and advected in a downstream direction. With the exception of a few low salinity observations located upstream in layer 5 and 6, homogenous salinity layers are observed in the layers 2,3,4,5 and 6, which indicate that these layers were not affected by the outfall effluent.

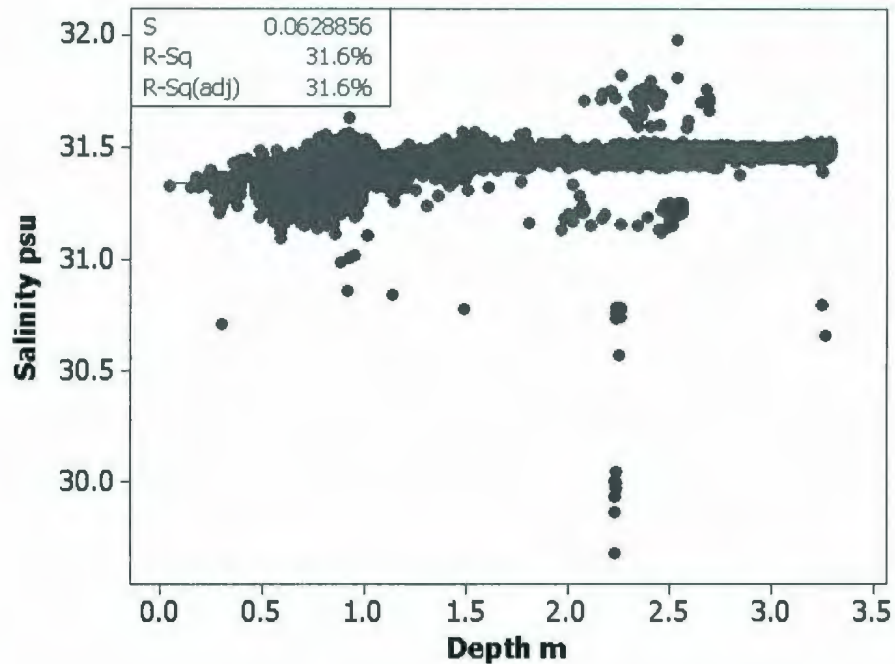


Figure 4.32. Sensor Towing Experiment 2 Salinity - Depth Correlation Plot

Figure 4.33 demonstrates larger salinity variations at surface layer compared to bottom layers. The mean and corresponding standard deviation values were observed as 31.34 and 0.056; 31.37 and 0.55; 31.44 and 0.03; 31.47 and 0.015; 31.44 and 0.045; and 31.48 psu and 0.039 psu. A similar result was observed in sensor towing experiment 1, where the highest variations were observed at the surface layers and the lowest were at the bottom layer. Such similarity of results validates our data. The large salinity variations in the upper layers (L1 and L2) are attributed to the near-field positive buoyancy force (Figure 3.34).

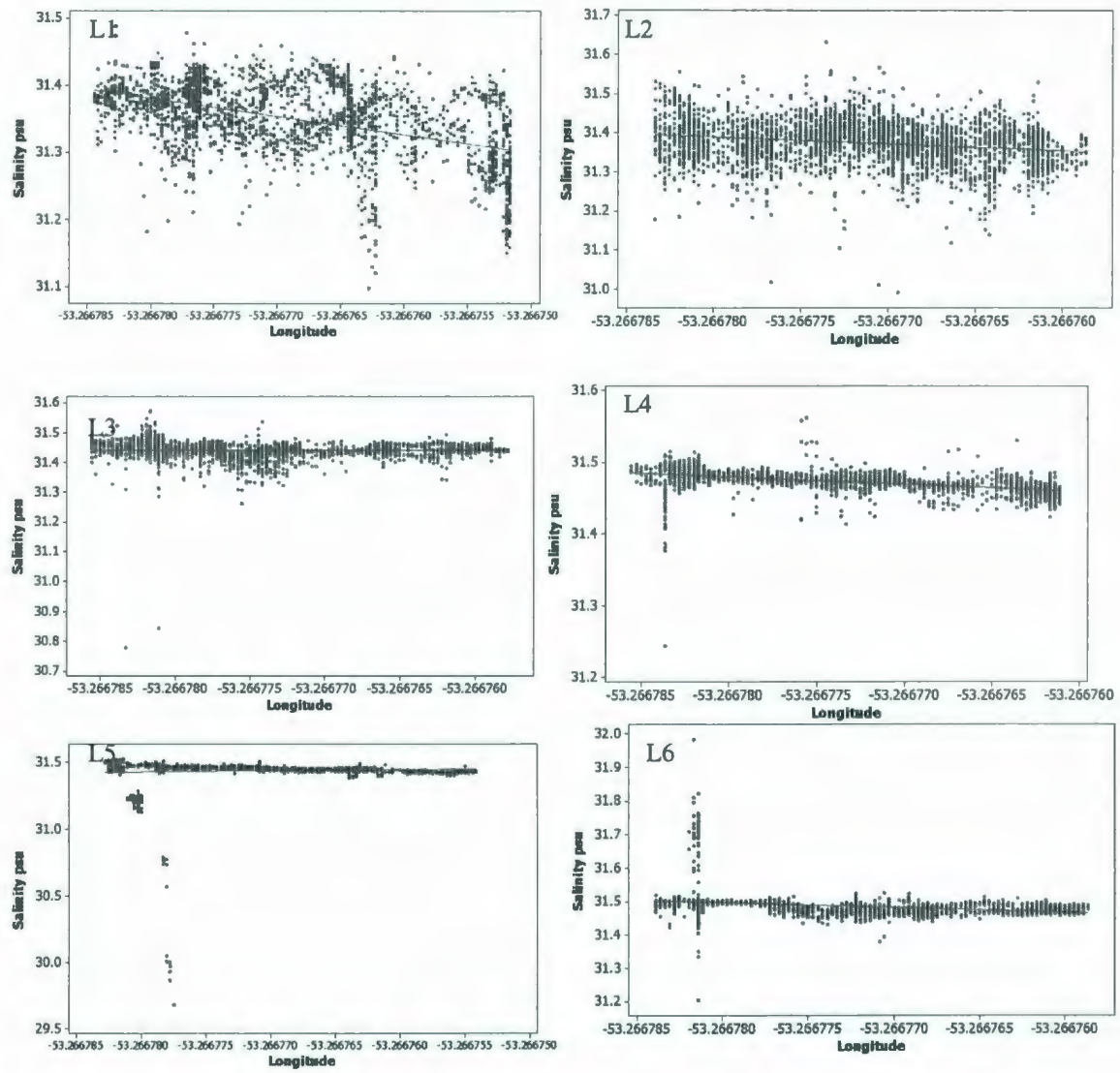


Figure 4.33. Sensor Towing Experiment 2 Downstream Salinity Distribution Plots

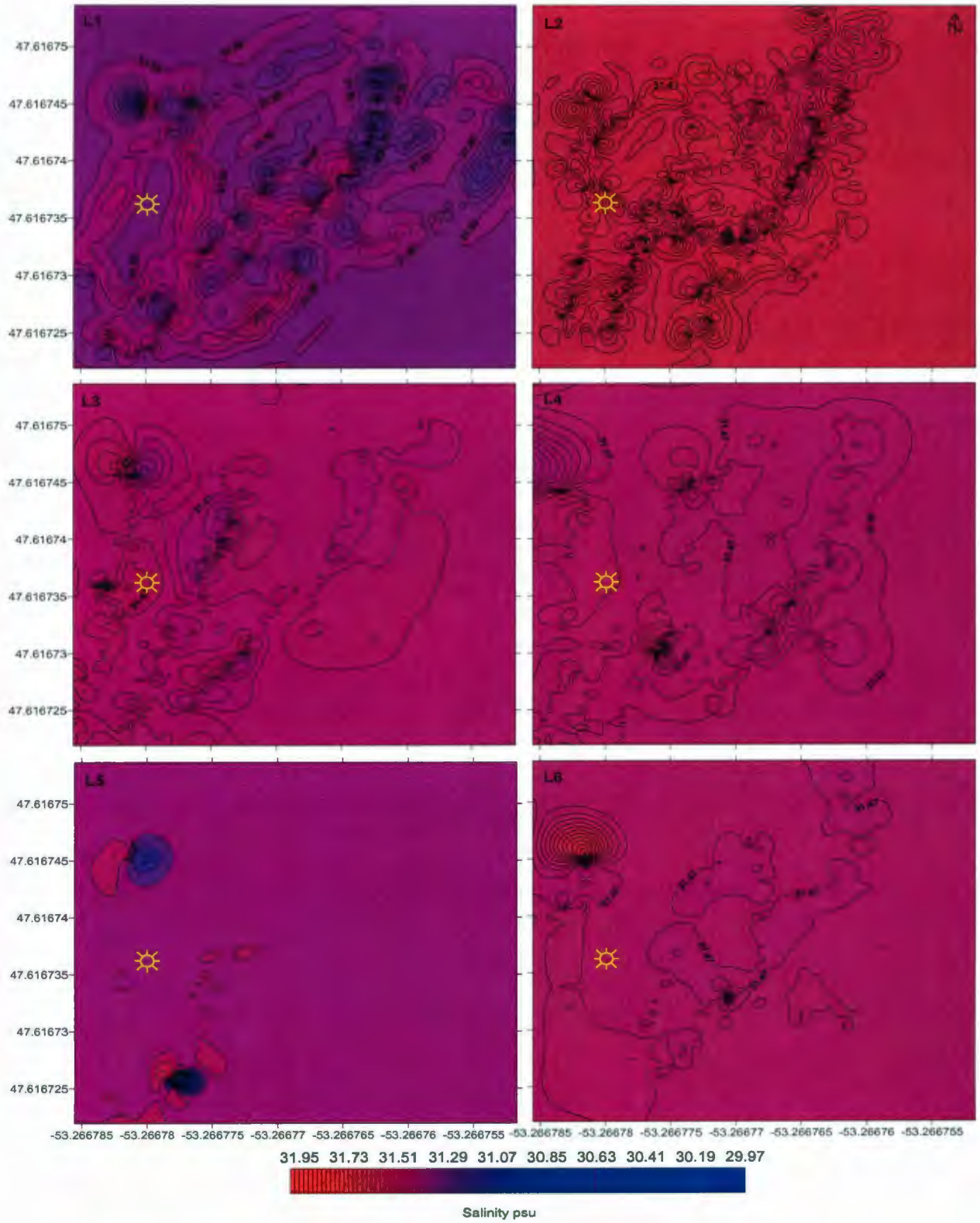


Figure 4.34. Sensor Towing Experiment 2 Water Column Salinity Contour Maps

4.3.4.2. Temperature

Figure 4.35 shows a strong negative temperature correlation with depth, where $R^2 = 0.779$ as compared to $R^2 = 0.579$ in sensor towing experiment 1. These observations indicate temperature stratification. The temperature observations varied from 9.0 °C at 0.86 m to 7.0 °C at 2.8 m depth, with 7.88 °C overall mean and 0.48 °C standard deviation.

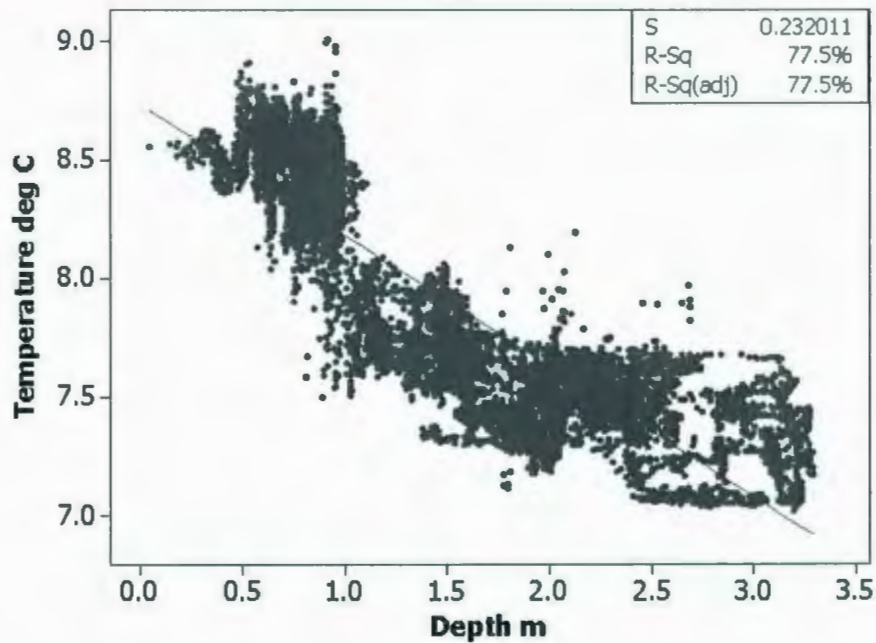


Figure 4.35. Sensor Towing Experiment 2 Temperature - Depth Correlation Plot

The highest temperature values were identified in the upper 1 m (L1 and L2). L1 and L2 of Figure 4.36 demonstrate higher upstream temperature variations compared to downstream. Figure 4.37 demonstrates the water column temperature distribution. The plots show lower temperature at bottom layers and close to the outfall diffuser. It is speculated that at 4.4 m depth, the outfall discharges lower temperature effluent than the

ambient, and as the effluent plume is mixed with the ambient, the plume temperature gradually reaches that of the ambient.

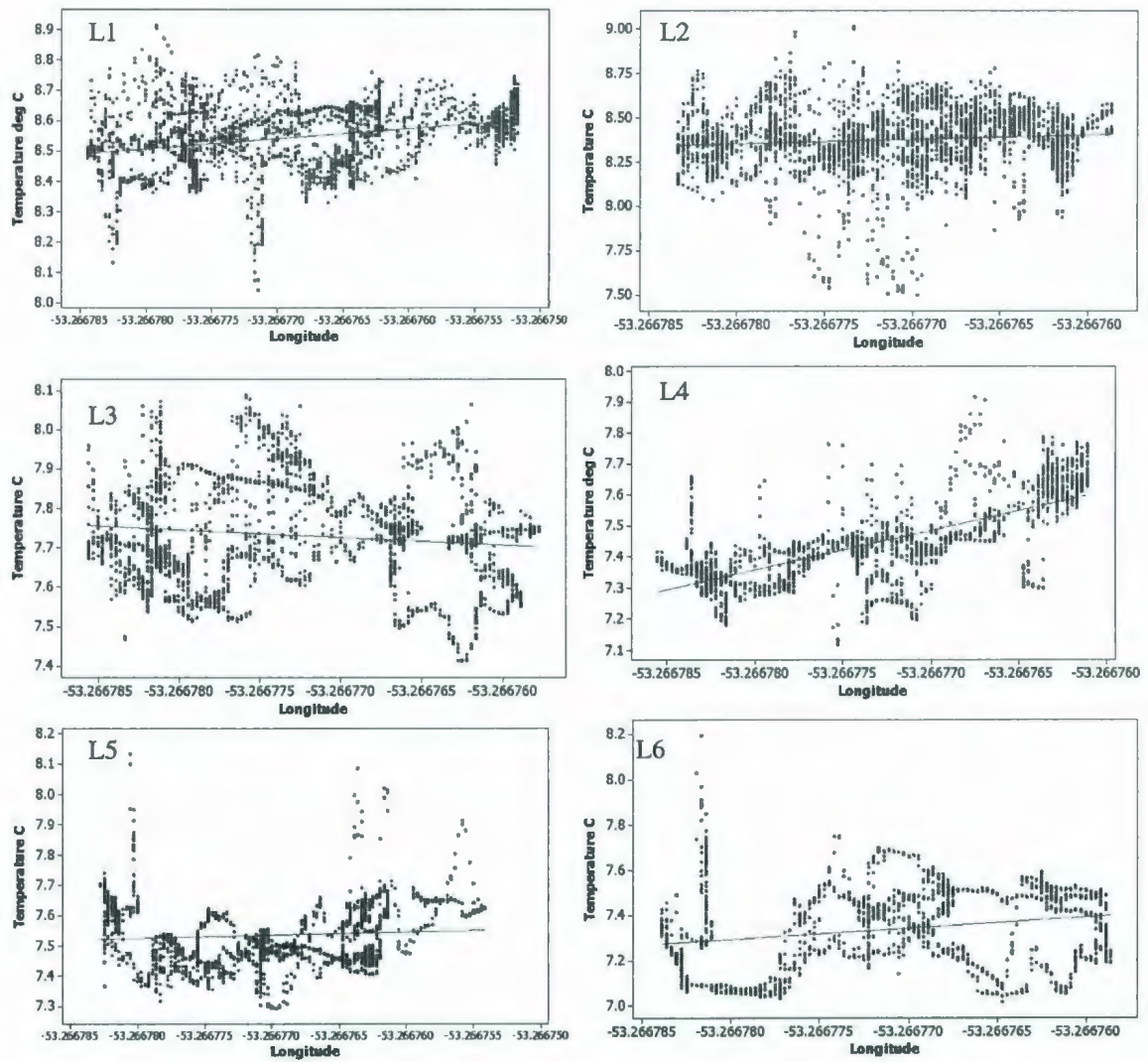


Figure 4.36. Sensor Towing Experiment 2 Downstream Temp Distribution Plots

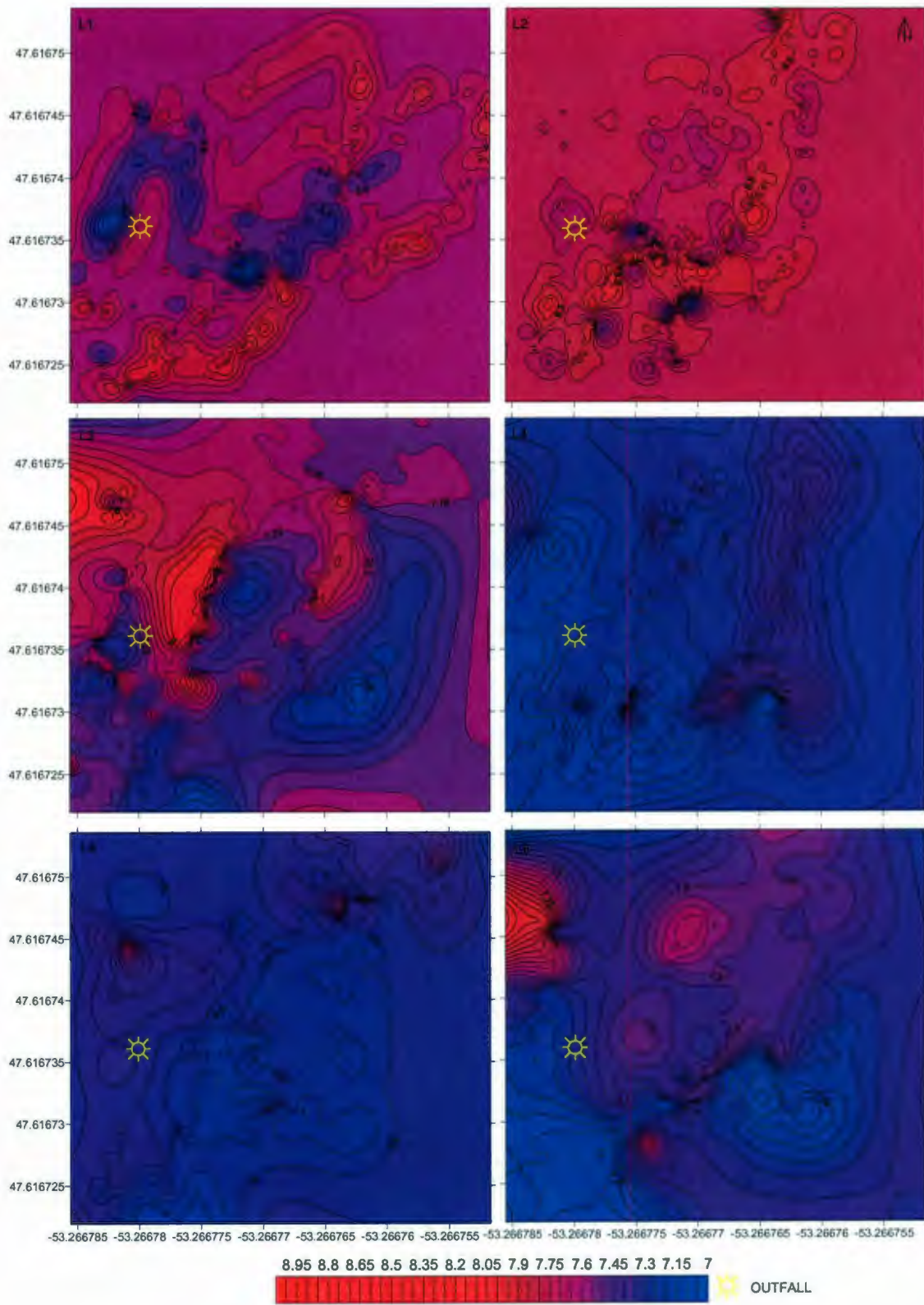


Figure 4.37. Sensor Towing Experiment 2 Water Column Temperature Contour Maps

4.3.4.3. Dissolved Oxygen

DO concentration is highly correlated with temperature and salinity concentrations. At higher temperature and salinity, DO is depleted. During the summer season, coastal water has higher temperatures at the surface layer. Figure 4.38 demonstrates a slightly positive DO correlation with depth, where $R^2 = 0.18$. In this experiment, the DO concentrations ranged from 118% to 142.5% saturation, which were acquired at bottom layer. The overall DO mean was 131 % saturation and the standard deviation was 2.78%.

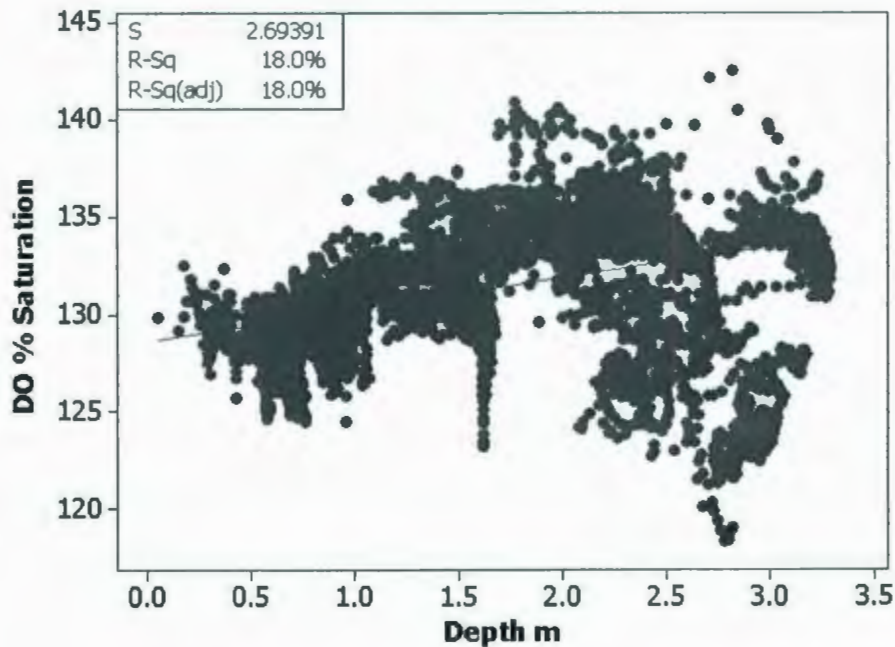


Figure 4.38. Sensor Towing Experiment 2 DO - Depth Correlation Plot

Figure 4.39 illustrates a negative DO correlation with longitudinal distributions, where R^2 was found 0.23, 0.083, 0.12, 0.582, and 0.58, respectively, and a weak positive correlation in the bottom layer with $R^2 = 0.03$. As observed in sensor towing experiment 1, the result revealed that the sewage waste decomposition process was exponential with

time. Initially, the fresh raw sewage effluent has DO concentrations close to that of the fresh water, but when it's exposed to surface and advected by the surface current, the aerobic bacteria present at the surface biodegrade the organic waste exponentially with time. At the bottom layer, the low DO concentrations around the outfall area occurred from the anaerobic process of the organic waste deposited at the seabed. In Figure 4.40, the bottom layer (L6) demonstrates the highest and lowest DO concentrations are present around the outfall diffusers.

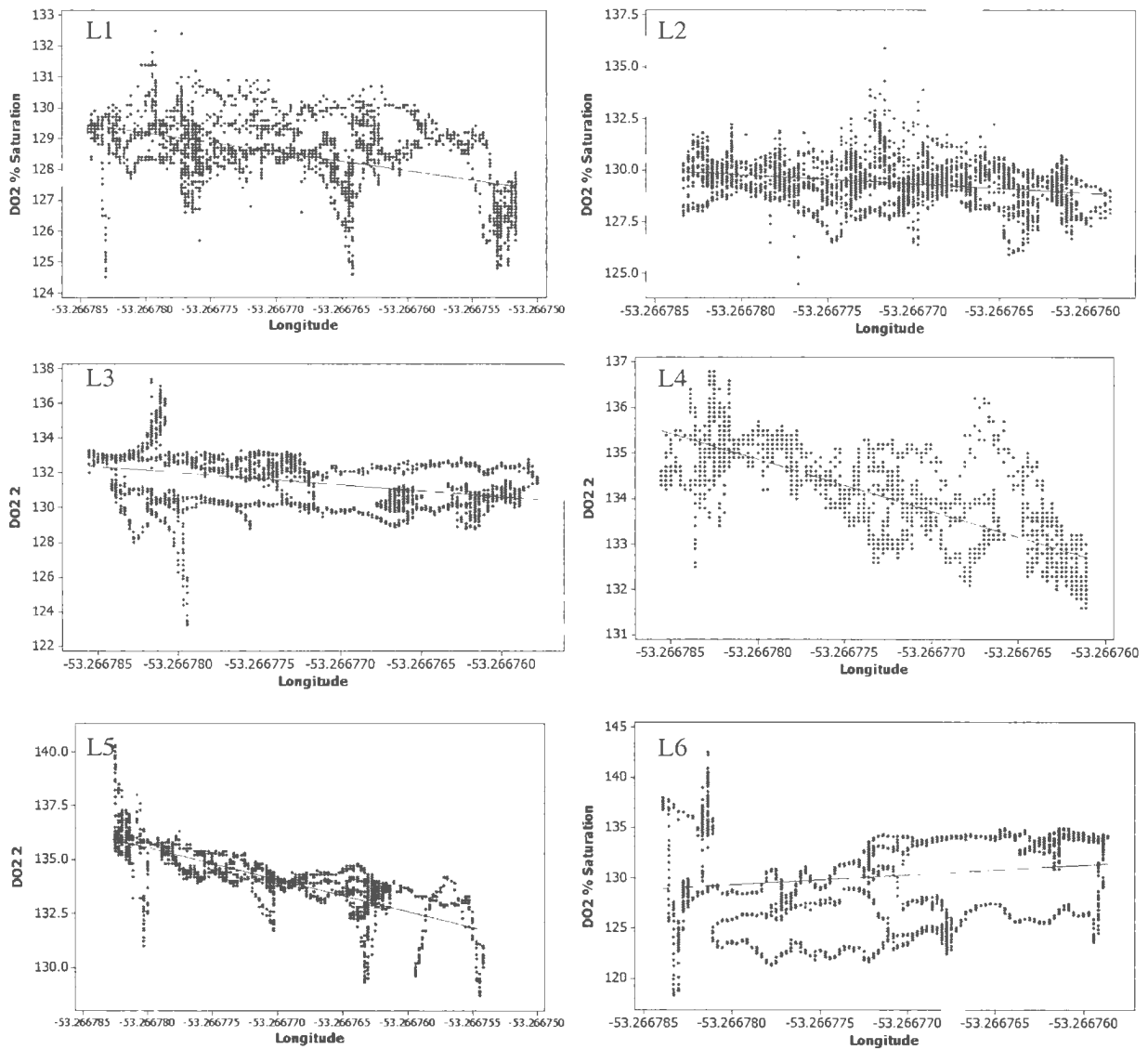


Figure 4.39. Sensor Towing Experiment 2 DO Distribution Plots

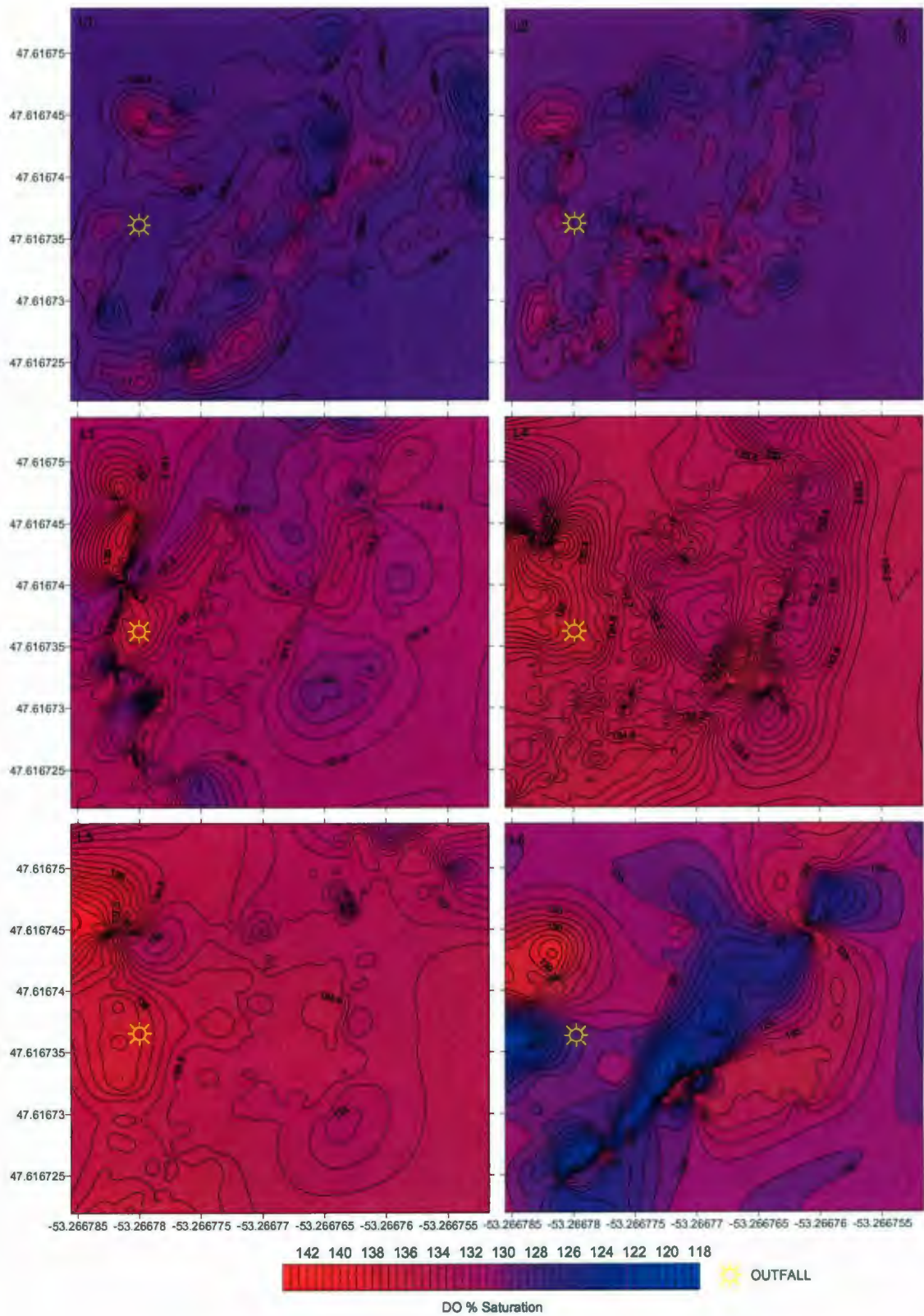


Figure 4.40. Sensor Towing Experiment 2 Water Column DO Contour Maps

4.3.4.4. Chlorophyll a

As described earlier in Chapter 2, chlorophyll *a* is a plant pigment used to determine the amount of algal biomass present in the water body. An excessive amount can indicate algal bloom conditions, which may deplete dissolved oxygen levels. Generally, algal blooms tend to increase with higher nutrient concentrations. The experiment did not indicate any algal bloom in the region. Few isolated high level concentrations were detected at the bottom layer. The chlorophyll *a* concentrations demonstrated a weak positive correlation with depth, where $R^2 = 0.11$ (Figure 4.41).

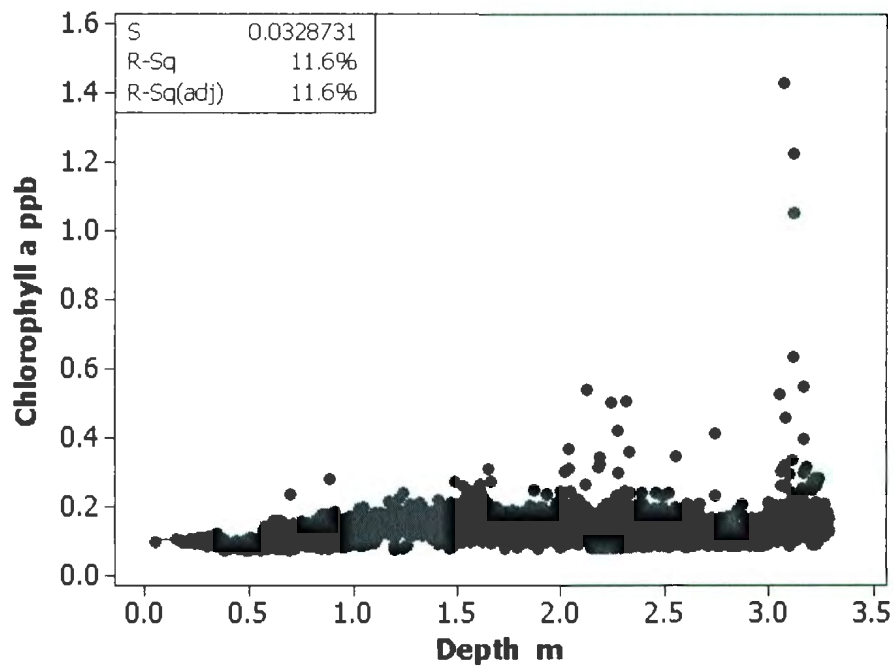


Figure 4.41. Sensor Towing Experiment 2 Chlorophyll *a* - Depth Correlation Plot

This observation can be explained by two factors. The first is that during the summer season sunlight can easily penetrate to 3 m depth, and the second is that nutrient concentrations around the outfall area are high due to settling organic pollutants. The overall mean concentration was found 0.12 ppb with a standard deviation of 0.0034. The mean and the corresponding standard deviations in ppb were 0.1 and 0.014, 0.11 and 0.015, 0.15 and 0.018, 0.0143 and 0.025, 0.13 and 0.03, and 0.13 and 0.056 from top to bottom, respectively. From Figures 4.42 and 4.43 it was observed that higher chlorophyll *a* concentrations can be identified in the central and northwest grids of layers 5 and 6. These higher observations were attributed due to the high nutrient depositions around the outfall location.

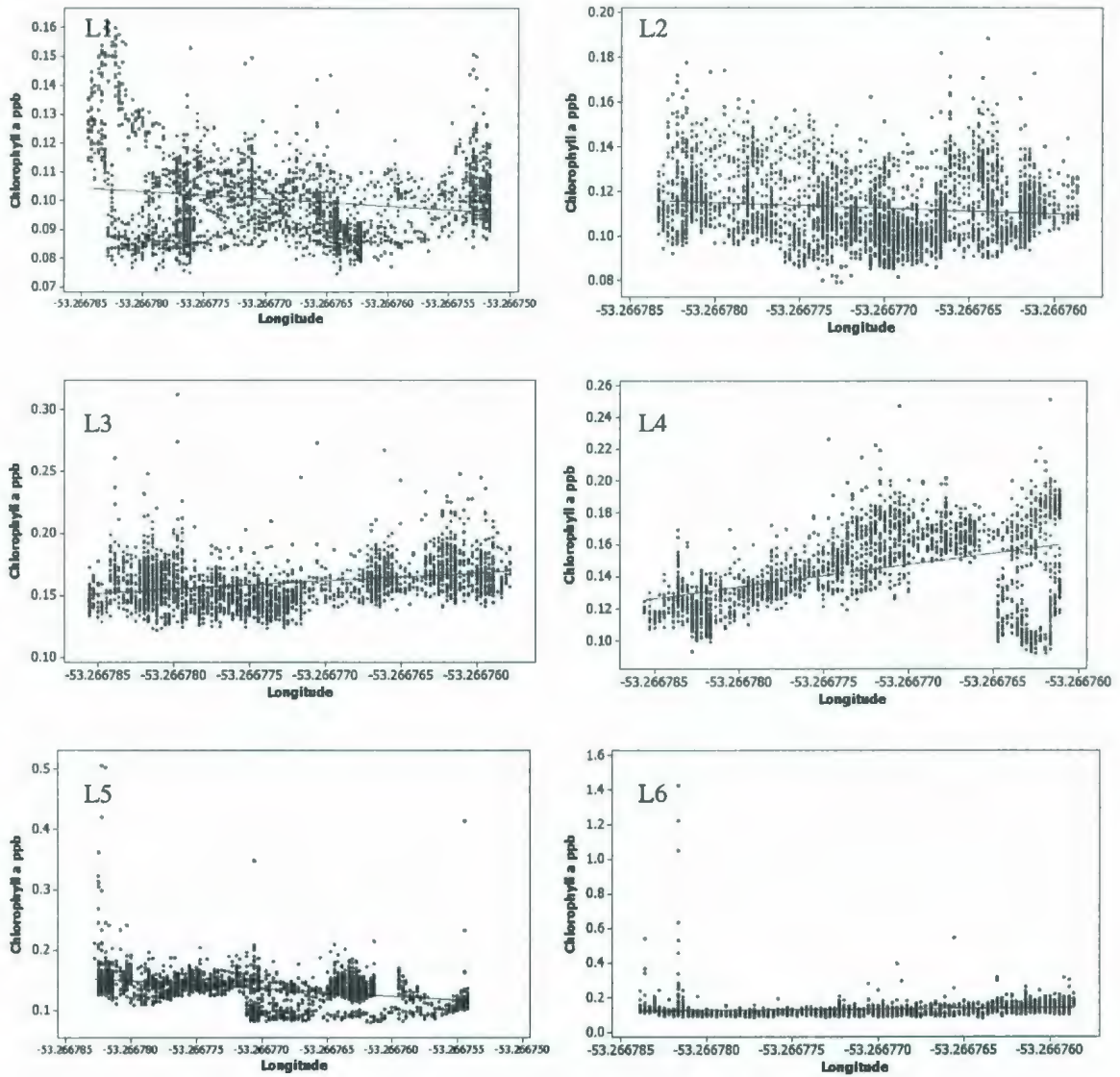


Figure 4.42. Sensor Towing Experiment 2 Chlorophyll Distribution Plots

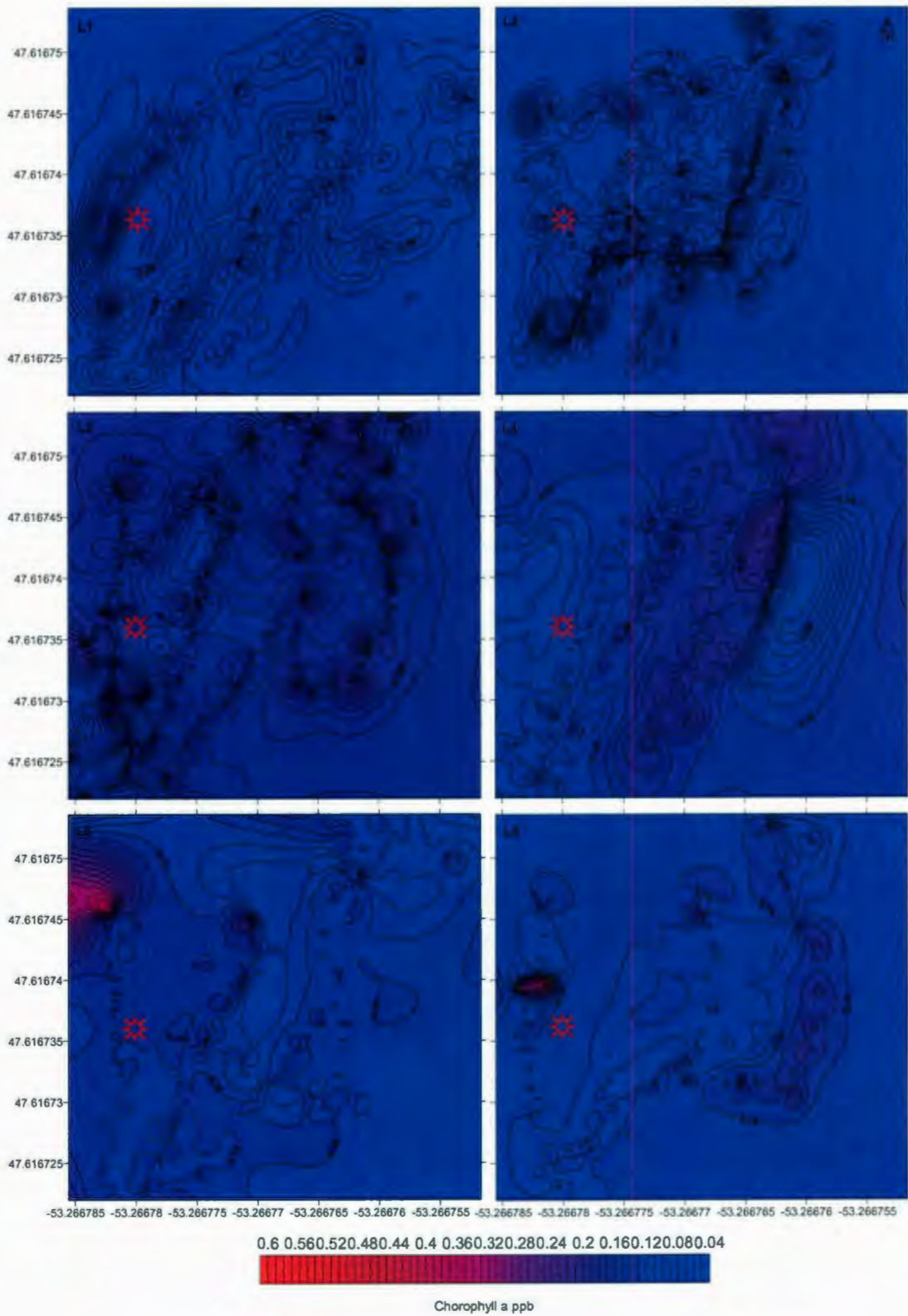


Figure 4.43. Sensor Towing Experiment Chlorophyll a Contour Maps

Chapter 5. Discussion

5.1. Outfall Modeling

As discussed in Chapter 2, both the length scale CORMIX and RSB models are widely used for municipal and industrial outfall designs. The two designs were compared to investigate which design demonstrates better mixing within the near-field boundary. The existing staged diffuser design was evaluated using the CORMIX model and the alternative T-Shape diffuser design was evaluated using the RSB model.

5.1.1. CORMIX Model

The near-field CORMIX model predicted dilution at the edge of the near-field (11.58 m) as 35.6, the turbidity concentration as 0.43 NTU, the plume height (Z) as 4.4 m, the plume half-width (BH) as 11.45 m, and the plume thickness (BV) as 0.71 m.

The model characterized the effluent flow based on the ambient conditions and diffuser geometry. It considered the density stratification as weak relative to the discharge conditions and dynamically unimportant; hence, the effluent will behave as if the ambient conditions were unstratified. The effluent is positively buoyant and will tend to rise toward the surface due to the density difference between the ambient and the effluent. The net horizontal momentum flux controls the flow. However, lateral entraining and diffusion lead to a spreading of the diffuser plume and additional mixing. Initially, the plume is cross-flowing, but it is progressively deflected into the direction of the ambient current. At a certain distance, stratification may take place depending on the strength and direction of the plume buoyancy. The near-field will experience instability conditions with full vertical mixing. There may be a benthic impact of high pollutant concentration.

In the far-field the plume becomes vertically fully mixed within the near-field at 0 m downstream, but re-stratifies later and is not mixed with the far-field. The plume in the unbounded sections will contact the nearest bank at 74.99 m downstream. The plume spreads laterally along the surface layer boundary while it is being advected by the ambient current and the plume thickness may decrease during this phase with a small mixing rate.

5.1.2. CORMIX Outfall Design Recommendations

In the CORMIX model a drastic change in the flow configuration may occur as a result of small change in the ambient or design parameters. The model treated the two nozzle group for each riser as one single nozzle with orientation that represented an average of two nozzles. Also, it described the spacing between adjacent ports/nozzles as equal to or less than the local water depth, therefore the slot diffuser approximation held well. Most of CORMIX recommendations are motivated by the desire of improving the mixing zone conditions (i.e., minimizing concentration and or/areal extents).

In order to improve the mixing process, the model recommended the following:

Diffuser location: It is recommended moving the outfall farther offshore to deeper water in order to delay interaction with the banks/shore and improve the near-field mixing.

Diffuser Type: The diffuser type is dictated by its nozzle/port arrangement and alignment. The diffuser choice is often dictated by local bathymetry and other safety conditions, e.g. clearness for navigation or fishing. The existing staged diffuser provides a directed momentum input; therefore, it can lead to strong induced currents, with plume contact at the bottom. The perpendicular alignment with the current is a good design for

shallow water conditions in the coastal environment under weak or strong reversing currents. Under weak currents it gives good offshore transport, and it efficiently captures the ambient flow under strong current conditions. As for the port or riser spacing, given the other constraints on diffuser mixing (i.e. diffuser length and discharge velocity), the spacing is a dynamically unimportant variable that has a limited effect on overall mixing. However, the spacing plays a major role in the plume/jet merging process, and thus may affect the very initial mixing in the toxic dilution zone (TDZ) predictions. In most cases the port height is not important except for negatively buoyant discharges; the port height may control the amount of initial mixing prior to benthic contact.

5.1.3. Alternative T-Shape Diffuser Risers Design

In the T-Shape design, the same riser spacing of the existing staged diffuser was assumed, but the two ports discharged horizontally in opposite directions. Table 5.1 shows that the existing staged diffuser requires less mixing height than the T-Shape design but a larger mixing zone boundary.

Table 5.1. Comparison between Stage and T- Risers Diffuser Design

Diffuser Design	Centerline dilution Sn	Centerline length Xn (m)	Centerline Height Zn (m)
Staged	35.6	11.58	4.4
T-Shape Riser	22.038	5.06	5.1

The table does not demonstrate a significant difference between the two designs. Nevertheless, if the objective of the regulator is to achieve less than a 35.6 dilution ratio

within or less than an 11.58 m near-field boundary, then the existing staged diffuser design is considered acceptable. But, if the regulator requires achieving a less than 22 dilution ratio within a 5 m near-field boundary, then the T-Shape Riser design is preferable. Often other considerations are also taken into account in the final assessment, such as the ecological vulnerability and the future use of coastal zones.

5.2. Water Quality Monitoring

The initial intention of this study was to use the AUV as an innovative environmental monitoring platform. However, when the propeller motor was damaged during the second experiment, the sensor towing platform was used as an alternative technique. Using this technique has proven to be more practical and safer than the AUV for monitoring surface and shallow coastal areas. But, for deep water monitoring, this technique suffers from many problems, including platform drifting and risk of hitting the seabed. As a summary, it was learned that both platforms have advantages and limitations. Table 5.2 demonstrates some advantages and limitations of both techniques.

Table 5.2. Comparison between AUV and Towed Sensor Platforms

	AUV	Sensor Towing
1	Accumulates spatial and environmental data simultaneously	Accumulates only environmental data
2	Ideal for deep water monitoring	Ideal for shallow water monitoring
3	Minimizes human safety risks in harsh weather conditions	Not convenient to use and dangerous during harsh weather conditions
4	Vehicle safety is a major concern for shallow coastal water	Easy to maneuver around structures and coastal water
5	Requires highly trained staff to operate	Does not require trained staff to operate
6	Minimizes human health exposure in a contaminated environment	Risks of human exposure in a contaminated environment
7	Spatial and temporal data are collected simultaneously	Correlation of spatial and temporal data is tedious and subjected to human error
8	Very expensive	Relatively cheap to assemble

5.3. Plume Tracking

Rhodamine dye is a commonly used tracer for plume tracking and leak detection applications. Some environmental regulators are concerned about the extensive use of this tracer for environmental monitoring. Based on a set of criteria for human and acute toxicity, Field et al. (1995) reported from their experiment on fluorescent tracer dyes used for groundwater tracing that these tracer have low to moderate levels of environmental concern. Furthermore, it may not always possible to inject artificial tracers into a

wastewater stream, such as the produced water and drilling mud. Using the effluent constituents can be considered as an alternative option for plume tracking and hydrodynamic model validation. Ramos et al (2001) integrated a CTD with an AUV for near-field plume tracking and model validation using salinity as a natural tracer. They concluded from their experiment that these techniques can improve validation between collected data and model predictions, allowing model performance evaluation.

In this experiment, both salinity and turbidity parameters were used as primary constituents of an untreated sewage outfall. Observing the behavior of these constituents in the water column revealed a good correlation between low salinity and high turbidity values. During the Spaniard's Bay monitoring experiment, the salinity and turbidity observations revealed a negative correlation, where $R^2 = 0.52$ (Figure 5.1). By comparing the longitudinal turbidity and salinity observations, it was found that variations decreased in a downstream direction (Figure 5.2). These findings show that the low salinity and high turbidity outfall effluent plume can be traced using *in-situ* sensors. Such reduction in variations indicates that plume was dispersed in a downstream direction.

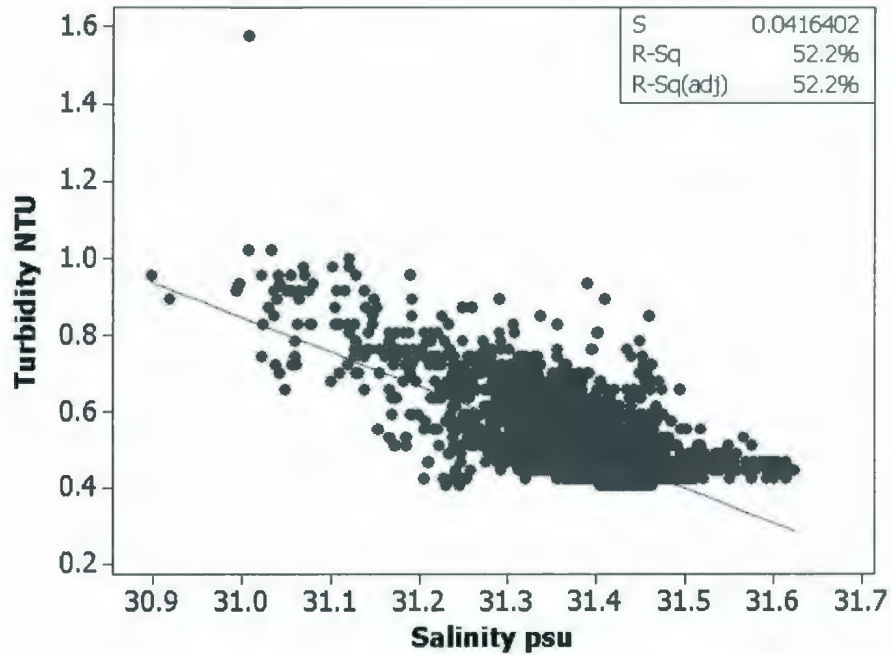


Figure 5.1. Sensor Towing Experiment 1 Turbidity - Salinity Correlation

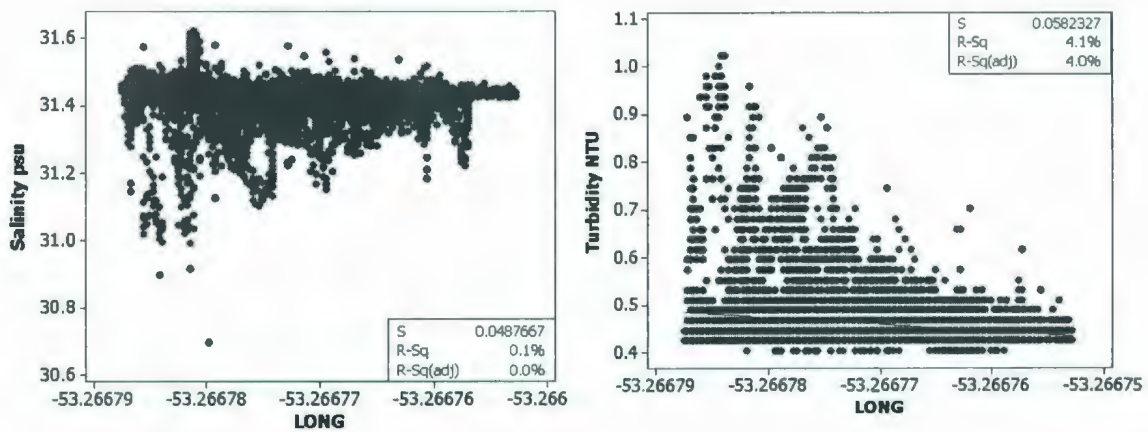


Figure 5.2. Sensor Towing Experiment 1 Salinity and Turbidity Distribution Plots

5.4. Water Quality Assessment

Three dimensional maps were generated to assess the water quality of the Spaniard's Bay outfall water column. Based on the 3-D contour maps of five common parameters present

in typical municipal and industrial effluents, it was possible to understand the impact of outfall effluent on the marine environment.

DO and chlorophyll *a* concentrations are good indicators of water quality. When the DO is under-saturated, this may indicate eutrophication resulting from excessive nutrients. Figure 5.3 demonstrates that DO values are oversaturated and the lowest value observed was 118 % saturation. This observation was present at the lowest layer and close to the outfall diffuser. However, presence of large variations the bottom layer may indicate instabilities resulting from organic matter biodegradation at seabed. Another important indicator of excessive nutrients disposal is Chlorophyll *a* concentration. The monitoring experiment of chlorophyll *a* did not show any algal bloom where concentrations ranged from 0.4 to 0.6 ppb (Figure 5.4).

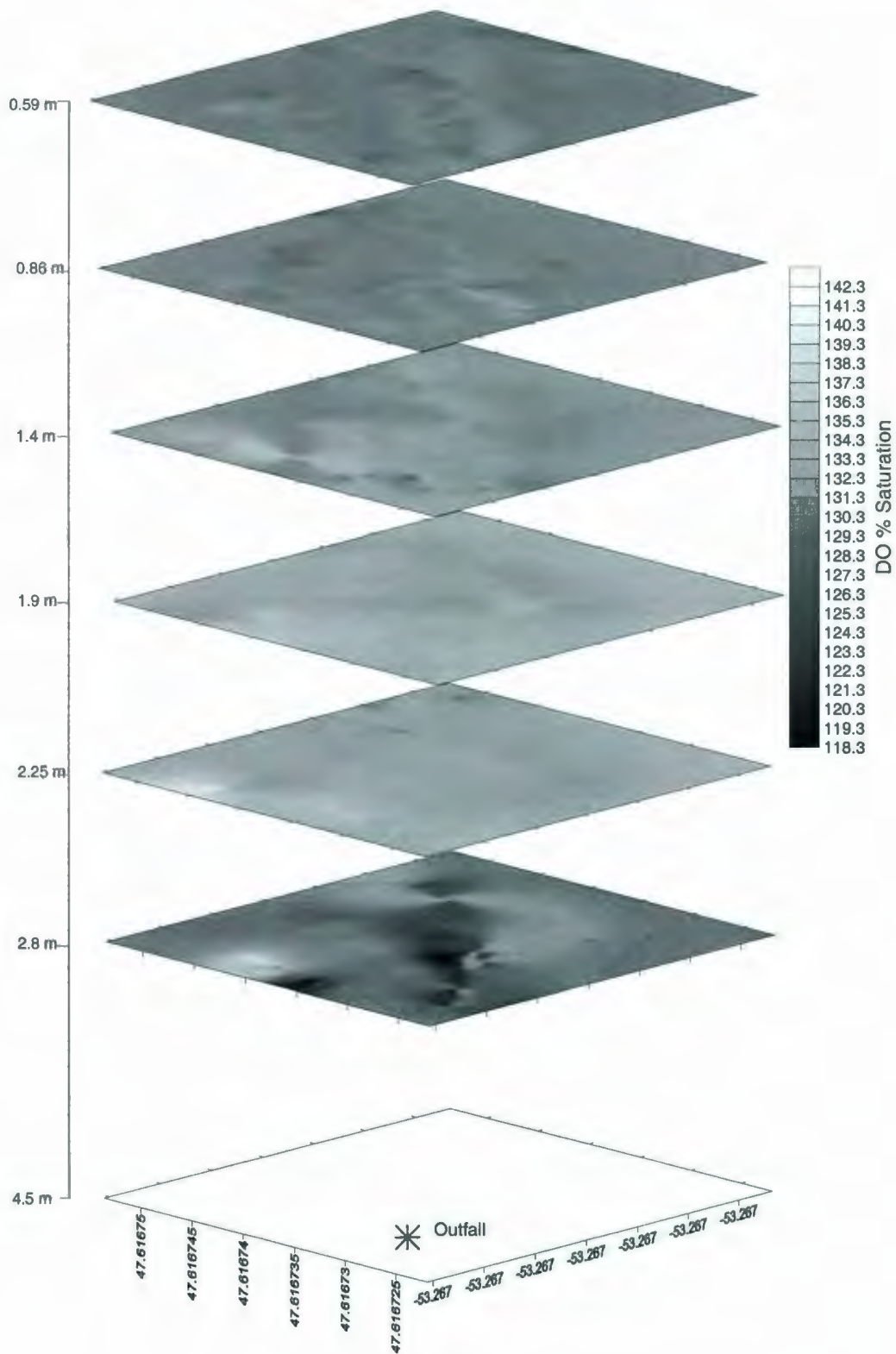


Figure 5.3. 3-D DO % Saturation Concentration

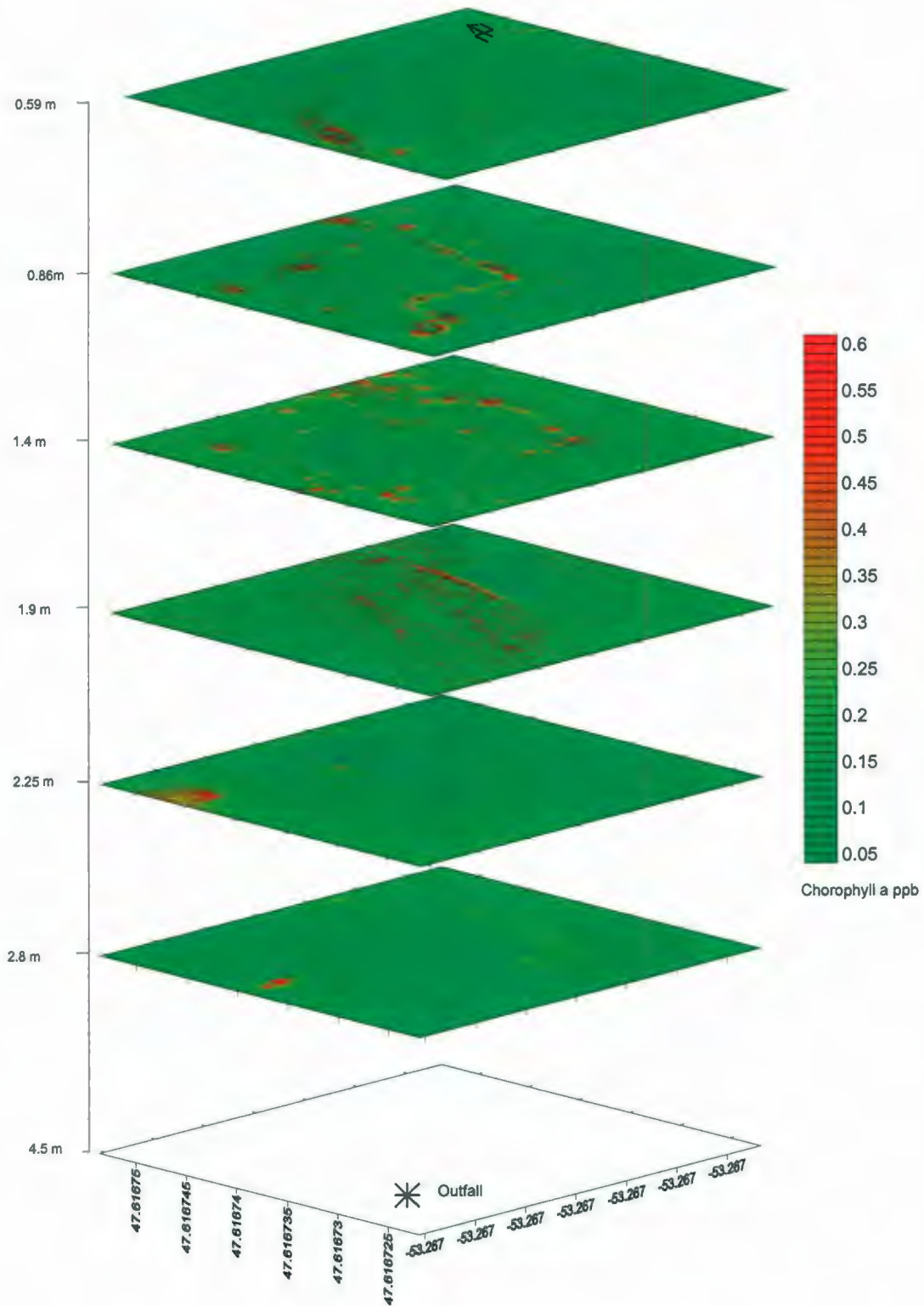


Figure 5.4. 3-D Chlorophyll a Concentration

5.5. Model Validation

Gridding is the process of using original data points (observations) in an XYZ data file to generate calculated data points on a regularly spaced grid file. Based on known observations, an interpolation scheme estimates values at locations where no original data exists. The advantages of a grid based approach outweigh the disadvantages. Tasks such as drawing contour lines are much faster with the grid based approach. Surfer 8 is a grid based mapping software. Most of the gridding methods in Surfer use a weighted average interpolation. This means that, the closer a data point is to a grid node, the more weight it carries in determining the Z value at a particular grid node. The CORMIX model predictions were validated using the grid file generated from Surfer. CORMIX model predictions were compared with the surface layer turbidity field data. The longitudinal and latitudinal field data were distributed over 100 by 100 grids representing the 100 by 100 m experiment boundaries. Figure 5.5 shows the grid map and the magnified near-field turbidity observations. The field data demonstrated that at the center of the boil (0 m) the turbidity was 1.29 NTU, and at 11 m downstream (edge of the near-field) the turbidity value decreased to 0.59 NTU.

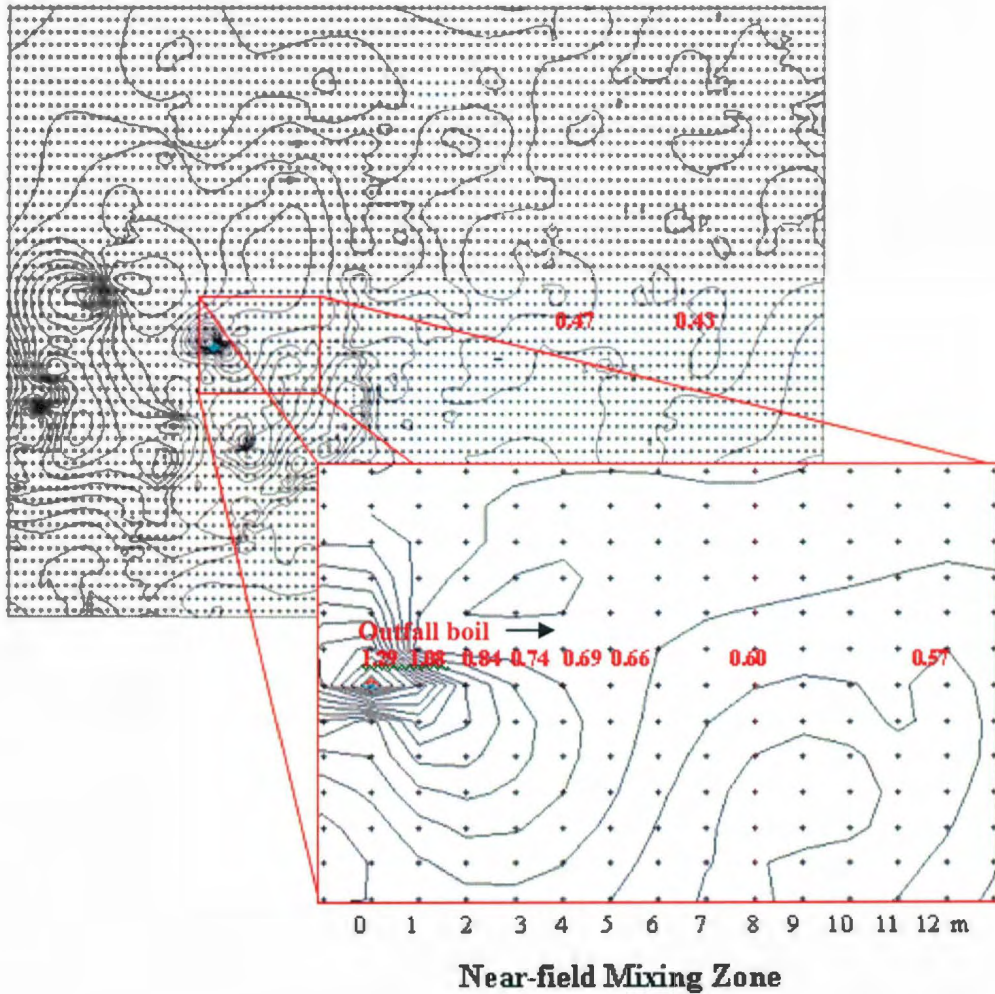


Figure 5.5. Downstream Turbidity Observations

Table 5.3 demonstrates a comparison between CORMIX turbidity predictions and field observations. At the center of the boil, CORMIX predicted the turbidity value as 0.82 NTU and 0.44 NTU at the edge of near-field (Appendix A). The CORMIX model dilution ratio was from the center of the boil to 11.58 m downstream distance as 3.56 times, where the field data measurements demonstrated 3 times.

Table 5.3. CORMIX Model & Field Data Comparison

	Near-field & Far-field Turbidity Concentrations NTU		
Downstream Distance (X) m	CORMIX Model Predictions	Field Data	Standard Deviation
0	0.82	1.29	0.33
1	0.71	1.08	0.26
2	0.65	0.84	0.13
3	0.60	0.74	0.09
4	0.57	0.69	0.08
5	0.54	0.66	0.08
6	0.52	0.64	0.08
7	0.5	0.62	0.08
8	0.48	0.60	0.08
9	0.46	0.59	0.09
10	0.45	0.59	0.09
11	0.44	0.59	0.10
50	0.28	0.47	0.13
75	0.23	0.43	0.14

By comparing turbidity concentrations in this experiment, it was observed that the CORMIX model has underestimated the near-field predictions. Figure 5.6 demonstrates the deviation between CORMIX turbidity predictions and field data observations. Figure

5.7 shows a good correlation of near-field model predictions with field data, where R^2 is 0.859.

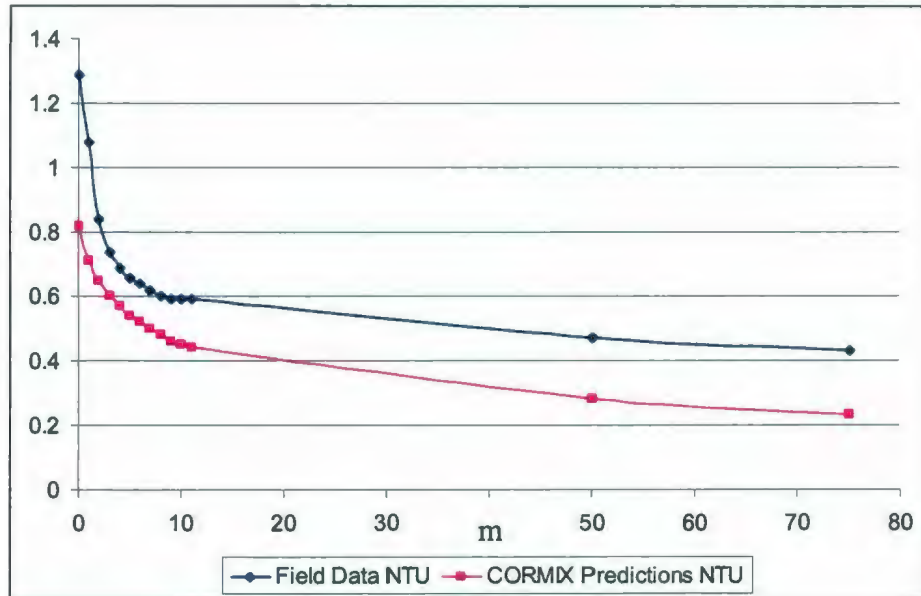


Figure 5.6. Field Data and CORMIX Model Plots

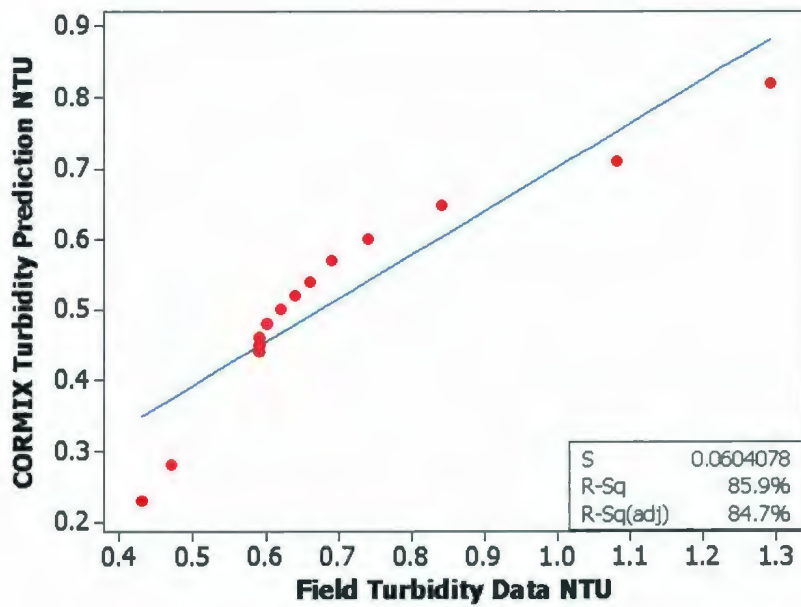


Figure 5.7. Field Data and CORMIX Model Correlation

Chapter 6. Conclusions and Recommendations

6.1. Conclusions

It was concluded from this study that the positive buoyancy force and current velocity are the main factors enhancing the dilution process of the Spaniard's Bay outfall effluent. The performance of the existing staged diffuser design was evaluated using the CORMIX submerged multiport diffuser model and compared with the RSB T-shape diffuser design model. The CORMIX predicted the near-field boundary at 11.58 m with a dilution ratio of 35.6, while the RSB predicted the near-field boundary at 5.06 m with a dilution ratio of 22.03. These results revealed that the existing staged diffuser demonstrated a better dilution than the T-shape diffuser, where at 5 m distance the staged diffuser demonstrated 28.5 times dilution ratio (Appendix A). This concludes that for shallow coastal waters, such as the Spaniard's Bay, the staged diffuser design achieves a better dilution than the T-Shape diffuser design.

Due to a technical fault that occurred with the current meter during the July experiment, it was not possible to retrieve any measurements. Therefore, the May data was used for the July experiment as the only available information. Using this information has added a degree of uncertainty to the model. However, the field data observations were in good agreement with model predictions results.

AUV is a promising technology for environmental monitoring. It was possible in this experiment to collect *in-situ* spatial and environmental information autonomously at 16 m depth. Due to sensor drifting issues, it would be difficult to obtain accurate spatial information at such a depth using the towed sensor platform. Furthermore, monitoring

with the AUV reduces time and human error while correlating the GPS with the CTD data. However, in shallow coastal waters less than 7 m depth, it is safer to maneuver the towed sensor platform close to the outfall structure than using the AUV. For surface monitoring experiments (less than 1m depth), when the vehicle moves against the surface current, it tends to resist the current and rise up to the surface, where the sensors are exposed to ambient air causing rapid noise. Also, using the towed sensor platform at a low collection frequency (1 hz) has generated less noisy data compared to high collection frequency (10 hz) used with the AUV.

In many situations where it is not possible to use dye tracers for plume tracking studies, natural constituents of the effluent can be used instead. This experiment has demonstrated that *in-situ* monitoring of salinity and turbidity parameters could be used for plume tracking studies. From the July monitoring experiments it was observed that high turbidity and low salinity values, which represent sewage effluent characteristics, were positively correlated. The experiment has also demonstrated lower turbidity and higher salinity values while moving in a downstream direction from the outfall boil.

DO and Chlorophyll *a* concentrations are good indicators of water quality. Due to the relatively small effluent flow and the dynamical flushing process caused by surface currents and tides, it was observed that the Spaniard's Bay outfall effluent has a minimal environmental impact on the marine water. The three dimensional water quality maps did not indicate any DO depletion and high chlorophyll *a* concentrations around the outfall area. The lowest DO percent saturation was found to be 118.9 at about 3m depth. Also, no algal blooms were observed in the region, where the lowest chlorophyll *a*

concentration was 0.05 and the highest was 0.6 ppb. These low values indicate low nutrient concentrations in the bay.

6.2. Recommendations

As a result of conducting this study, the following is recommended for similar future studies:

- For water quality assessment, far-field modeling is recommended as an extension to near-field models.
- There is a great potential in using the AUV for deep water monitoring and quality assessment, particularly for produced water impact assessment and model validation. As described in Chapter 2, it is recommended to conduct offshore monitoring experiments using underwater analytical systems, such as Underwater Mass Spectrometry.
- Both the CORMIX model results and DO field data observations have indicated slight instabilities at the bottom layer, which may cause some benthic impacts. It is possible that fish and other benthic communities are feeding on the raw sewage waste, which may result in ecological and health problems. Therefore, it is recommended to conduct further studies on the biological and toxic impacts of the raw sewage on the marine environment.
- The resolution of control maps will improve as more *in-situ* spatial and temporal data is collected. When conducting similar future studies, it is recommended to obtain more information for more precise water column assessment.

- Conduct future studies using the AUV and *in-situ* sensor to monitor salinity and turbidity as natural tracers of produced water and drilling mud generated from offshore operations.
- In future environmental monitoring experiments, it is recommended to maintain the AUV at minimum depth to 1 meter to ensure that sensors are fully submerged and not affected by surface currents and waves.
- It is recommended to investigate different options to minimize the impact of a coastal outfall on the marine ecosystem, such as outfall relocation or construction of a wastewater treatment plant.
- It would be recommended to safeguard the AUV propeller to avoid similar accidents in future monitoring experiments.

References:

- Adams, S. (2005). Environmental monitoring of effluent plumes in coastal Newfoundland. Master Thesis. Faculty of Engineering and Applied Science, Memorial University of Newfoundland.
- Alai, M., L. Glascoe, A. Love, M. Johnson, and W. Einfeld. 2005. Sensor Acquisition for Water Utilities: A Survey and Technology List. Technical Report for the Department of Energy, US.
- Analytica Chimica Acta. 469(2): 235-242.
Aravamudhan, S., S. Bhat, B. Bethala, S. Bhansali. 2005. MEMS Based Conductivity-Temperature-Depth. Proceedings of MTS/IEEE OCEANS 2005.2:1785-1789.
- Applied Microsystems. Accessed Feb, 2007 (www.appliedmicrosystems.com)
- Battisto, G.M. 2002. Field Measurement of Mixed Grain Size Suspension In The Near Shore Under Waves. Master Thesis. The Faculty of Marine Science, College of William and Mary in Virginia.
- Beyer, T., P.Hahn, S.Hartwing, W.Konz, S.Scharring, A.Katzir, H.Steiner, M.Jakusch, M.Kraft, B. Mizaikoff. 2003. Mini Spectrometer with Silver Halide Sensor Fiber For In Situ Detection of Chlorinated Hydrocarbons. Sensor and Actuators B-Chemical. 90: 319-323.
- Biro, D., A. Daniel, H. Floch, M. Lehaitre, B. Leide, and E. Menut. 1994. Evaluation Of Flow Injection Analysis Based Method For *In Situ* Chemical Measurements. Oceans Engineering. 2: 13-16.
- Bleninger and G.H.Jirka. Near-and far-field model coupling methodology for wastewater discharges. 2004. Proceedings of the 4th International Symposium on Environmental Hydraulics and 14th Congress of Asia and Pacific Division, International Association of Hydraulic Engineering and Research, Hong Kong, China.
- Brerton, R.G. 2002. Design of Water Quality Monitoring Programs. In: Environmental Monitoring Handbook. Edited by Burden F., Ian McKelvie, Ulrich Forster, Alex Guenther. McGraw-Hill, New York.
- Buffle J. and G. Horvai. 2000. General Concept. In: in situ Monitoring of Aquatic Systems, Chemical Analysis and Speciation Volume 6. Edited by J. Buffle, G. Horvai. Published by John Wiley & Sons Ltd, USA.

- Campbell, C.G., W. Hopes, T Nguyen , and F. G Tran. 2006. High Concentration Suspended Sediment Measurement Using Continuous Fiber Optic In-Stream Transmissiometer. Earth Science Division, Lawrence Berkeley National Laboratory.
- Carder, K., D. Costello, H. Warrior, L. Langebrake, W. Hou, J. Patten, and E. Kaltenbacher. 2002. Ocean-Science Mission Needs: Real-Time AUV Data for Command, Control, And Model Inputs. *Journal of Ocean Engineering* 26(4):742 – 751.
- Chelsea Group. Accessed Dec, 2006. www.chelsea.co.uk/Instruments.htm
- Controls systems & solutions. Accessed Feb, 2007. www.contros.eu/sensors
- Creed, E.L., A. M. Pence, and K. L. Rankin. 2000. Inter-Comparison of Turbidity and Sediment Concentration Measurement from an ADP, an OBS-3, and A LISST. MTS 0-933957-2809:1750-1754.
- Crimmins, D.,E. Hinchey, M. Chintala, G. Cicchitti, C. Deacutis, and D. Blidberg. 2005. Use of al long endurance solar powered autonomous underwater vehicle (SAUV II) to measure dissolved oxygen concentration in Greenwich bay, Rhode Island, U.S.A. *Proceedings of Oceans-Europe 2005 IEEE/Xplore*.2:896-900.
- D'Sa, E. J., S. E. Lohrenz, and V L. Asper.1997. Time Series Measurement Of Chlorophyll Fluorescence In The Oceanic Bottom Boundary Layer With Multisensor Fiber-Optic Fluorometer. *Journal of Atmospheric and Ocean Technology* 14(4):1889-1995.
- Daviero, G.J. and P.J.W.Robers. 2006. Marine Wastewater Discharges from Multiport Diffuser.III. Stratified Stationary Water. *Journal of Hydraulic Engineering* 132(4):404-410.
- Davis,L.R.1999. Fundamentals of Environmental Discharge Modeling. Boca Raton:CRC Press.165.
- Doneker and Jirka.1991. Expert System for Mixing-Zone Analysis and Desing of Pollution Discharges. *Journal of Water Resources Planning and Management* 117(6):679-697.
- Doneker, R.L. and G.H.Jerka.2002 . Boundary Schematization in Regulatory Mixing Zone Analysis. *Journal of Water Resources Planning and Management* 128(1):46-56.

- Doneker, R.L. and G.H.Jirka.2004. Pollutant Transport and Mixing Zone Simulation of Sediment Density Currents. *Journal of Hydraulic Engineering* 130(4):349-359.
- Doneker, R.L. and Jirka.2001. CORMIX-GI System for Mixing Zone Analysis of Brine Wastewater Disposal. Presented at the European Conference on Desalination and the Environment:Water Shortage. *Desalination* 139(1):263-274.
- Fench, M.S., D. J. Hydes, C. H. Clayson, J. Dakin, P. Gwilliam.1998. A Low Power Ultra Violet Spectrophotometer for Measurement of Nitrate in Seawater: Introduction, Calibration, and Initial Sea Trials. *Analytica Chimica Acta* 377: 167 – 177.
- Field, M.S., R.G. Wilhelm, J. Quinlan, and T. Aley.1995. Fluorescent Tracer Dyes for Groundwater Tracing. *Environmental Monitoring and Assessment* 38:75-96.
- Fleming, L.E., K. Broad, A. Clement, E. Dewailly, S. Elmir, A. Knap, S.A. Pomponi, S. Smith, H. Solo Gabriele, P. Walsh. 2006. Ocean and human health: Emerging public health risks in marine environment. *Marine Pollution Bulletin*. 53: 545-560.
- Fleming, M. C. and J.G. Nellis.2000. *Principals of Applied Statistics* 2nd Edition. Thomson Learning. 474.
- Fraher, P.M., D. W.Clark.1998. Fouling Detection and Compensation in Clark-Type Dox Sensors. *IEEE Transactions on Instrumentation and Measurement* 47(3):686-691.
- Fujinawa, Y., Y.Tsuji, I.Watabe, K.Sasaki, M.Nomotoj, T.Haraj, and Y.Tsuji. Testing of a Towed CTD.1980.*Journal of Oceanography* 36(5):253-258.
- Gartner J. W. Estimation Of Suspended Solids Concentrations Based On Acoustic Backscatter Intensity: Theoretical Background. 2002. *Turbidity And Other Surrogates Workshop*, April30-May2,2002, Reno, NV.
- Glud, R. N., A. Tengberg, M. Kuhl, P.O. Hall, I. Klimant, G. Holst. 2001. An *In Situ* Instrument For Planar Optode Measurement At Benthic Interfaces. *Limnology And Oceanography* 46(8):2073-2080.
- Gowda, R. N.1992. Field and Laboratory Studies of Mixing Tubes for Marine Outfall. Master Thesis. Faculty of Engineering and Applied Science, Memorial University of Newfoundland.

- Gray, S., G. Hanrahan, I. Mckelvie, A. Tappin, F. Tse, and P. Worsfold. 2006. Flow Analysis Techniques for Spatial and Temporal Measurement of Nutrients in Aquatic System. *Environmental Chemistry* 3(1):3-18.
- Griffiths, G., N.W. Millard, S.D. McPhail, P.Stevenson, M.Pebody, J.R. Perrett and A.T. Webb.2001. Multidisciplinary measurement with autosub autonomous underwater vehicle. Paper Presented at Hydro 2001, The 12th Biennial Conference of the Hydrographic Society.2001. Norwich,UK.
- Guidelines for the Design, Construction and Operation of Water and Sewerage Systems. Accessed March, 2008. Department of Natural Resources, Government of Newfoundland and Labrador.
- Hart, B. Water Quality Guidelines.2002. Water Quality Guidelines. Environmental Monitoring Handbook. Edited by Burden, F. and I, McKelvie. Mc Graw Hill, USA.
- Hanson, A K.2007. An Investigation Of The Role Of Nutrient Gradient In Episodic Formation, Maintenance And Decay Of Thin Plankton Layers In Coastal Waters. Subchemical Systems, Inc.
- Hendrikse, J., W. Olthuis, and P. Bergveld.1998. The MOSFET as A Potentiometric Trasducer in an Oxygen Sensor. *Sensors and Actuators B: Chemical* 47(1):1-8.
- Ishikawa, K., M. Kumagai, and R. F.Walker.2005. Application Of Autonomous Underwater Vehicle And Image Analysis For Detecting The Three-Dimensional Distribution of Fresh Red Tide *Uroglena Americana(Chrysophyceae)*. *Journal of Plankton Research* 27 (I):129 – 134.
- Issac, M. T., S. Adams, N. Boss, C. D. Williams, R. Bachmayer, and T. Crees.2007. Maneuvering Experiment Using the MUN Explorer AUV. *Proceedings of IEEE Underwater Technology 2007*:256-262.
- Jannasch, H.W., K.S. Johnson, and C.M. Sakamoto. 1994. Submersible, Osmotically Pumped Analyzers for Continuous Determination Of Nitrate *In Situ* .1994. *Analytica Chimica Acta*.66: 3352-3361.
- Jirka, G.H. and R.L.Doneker.1991. Hydrodynamic Classification of Submerged Singel-Port Discharges. *Journal of Hydraulic Engineering* 117(9):1995-1112.

- Johnson, K.S. and L.J.Coletti. 2002. *In Situ* Ultraviolet Spectrometry For High Resolution and Long-Term Monitoring of Nitrate, Bromide and Bisulfide in the Ocean. *Deep-Sea Research I* 49: 1291-1305.
- Kohls, O. and T. Scheper.2000. Setup of a Fiber Optical Oxygen Multisensor-System and its Applications in Biotechnology. *Sensor and Actuators B: Chemical* 70(1):121 – 130.
- Koneke, R., A. Gomte, H. Jurgens, O. Kohls, H. Lam, and T. Scheper. 1999. Fiber Optic Oxygen Sensor for Use In Biotechnology, Environmental And Food Industries. *Chemical Eng. Technology*.21:666- 671.
- Kraft, M., M. Jakusch, M. Karlowatz, A. Katzir, B. Mizaikoff. 2003. In Situ Sensing of Volatile Organic Compounds in Groundwater: First Field Tests of a Mid-Infrared Fiber-Optic Sensing System. *Applied Spectroscopy*. 57(6):607-613.
- Kraft, M., M. Jakusch, M. Karlowatz, A. Katzir, B. Mizaikoff. 2003. New Frontiers for Mid-Infrared Sensor: Toward Deep Sea Monitoring with a Submarine FT-IR Sensor System. *Society for Applied Spectroscopy*.57(6):591-599.
- Kumagai, M., T. URA, Y. Kuroda, R. Walker.2002. New AUV Design for Lake Environmental Monitoring. *Advanced Robotics*. 16(1):17-26.
- Laser Diffraction Turbidity Sensor, Sequoia Scientific. Accessed Oct, 2006
[Http://Www.Sequoiasci.Com/Research/Yogesh.AspX](http://Www.Sequoiasci.Com/Research/Yogesh.AspX)
- Lembit, N. And G. Compton. 1996. An Improved Clark-Type Galvanic Sensor For Dissolved Oxygen. *Sensors and Actuators B: Chemical* 30 (2):83-87.
- Maher, W. and G. Batley. 2002. Design of Water Quality Monitoring Programs. In: Environmental Monitoring Handbook. Edited by Burden F., Ian McKelvie, Ulrich Forster, Alex Guenther. McGraw-Hill, New York.
- Malinowska, E., V.Oklejas, R.W.Hower, R.B.Brown, and M.E. Meyerhoff.1995. Enhanced Electrochemical Performance of Solid-State Ion Sensor Based on Silicon Rubber Membrane. The 8th International Conference on Solid-State Sensors and Actuators, and Eurosensors IX. Stockholm, Sweden, 1995.
- McMurry, G.M., J.C.Wiltshire, A. Bossuyt. 2005. Hydrocarbon seep monitoring using *in situ* deep sea mass spectrometry. *Proceedings of IEEE Oceans2005 –Europe*.1:395-400.

- Mendez-Diaz, M.M. and G.H.Jirka.1996. Buoyant Plumes From Multiport Diffuser Discharges in Deep Co-flowing Water. *Journal of Hydraulic Engineering* 122(8):428-435.
- Mizaikoff, B.1999. Mid-infrared evanescent wave sensors-a novel approach for subsea monitoring. *Meas.Sci. Technol.*10:1185-1194.
- Mohan, A., P. Ajay, S. Aravamudhan, S. Bhansali. 2004. Piezoresistive MEMS Pressure Sensor and Packaging for Harsh Oceanic Environment. *Proceedings of Electronic Components and Technology Conference 2004.* 1:948-959.
- Mukhtasor. 1998. Probabilistic Ocean Outfall Design. Master Thesis. Faculty of Engineering and Applied Science, Memorial University of Newfoundland.
- Niu, H., T. Husain, T. Veitch, N. Boss, S. Adams, M. He, and K. Lee. 2007. Ocean Outfall Mapping Using an Autonomous Underwater Vehicle. *Proceedings of IEEE Oceans 2007 Conference:*1-4.
- Novic, M., S. Tezak, B. Pihlar, and V. Hudnik. 1994. Error Sources in Simultaneous Nitrate/Nitrite Determinations Using Copperised Cadmium as Nitrate Reducing Agent.
- Pennell, V., B. Veitch, K. Howboldt, T. Husain, N. Bose. 2003. Use of an autonomous underwater vehicle for environmental effects monitoring. Presented at the 13th International Symposium on Unmanned Untethered Submersible Technology.
- Prien, R.D. and D.J.Hydes.2003.A full ocean depth UV-Spectrophotometer for nitrate measurement. *Proceedings of IEE Oceans 2003.*1:18-21.
- Ramos, P., N. Cruz, A. Matos, M.V. Neves, F.L. Pereira. 2001. Presented at Medcoast01, the fifth international conference on the Mediterranean Coastal Environment, Tunisia.
- Rasmussen, P.Bennett, K.S. Wichita, C. Lee, and V. G. Christensen.2002. Continuous *In Situ* Measuring of Turbidity In Kansas Streams. 2002. Turbidity And Other Surrogates Workshop, April30-May2,2002, Reno, NV.
- Rudnick, D., R. E. Davis, C.C. Eriksen, D.M. Fratantoni, and M. J. Perry. 2004. Underwater gliders for ocean research. *Marine Technology Society Journal* 38(1):48-59.
- Sea Bird Electronics. Accessed Nov, Jan, 2006.
<http://www.seabird.com/products/profilers.htm>.

Sequoia Scientific. Accessed Oct, 2006 www.sequoiasci.com

Shannon, A., M.J. Atkinson, and A.M. Tarrant. 2003. Estrogens from Sewage in Coastal Marine Environment. *Environmental Health Perspectives* 111(4): 531-535.

Sharp, J. J. 1989, Spaniard's Bay Outfall Monitoring Study, Final Report – Dec, Memorial University of Newfoundland – Civil/Sanitary Environmental Engineering Division, Department of Environmental & Land, Government of Newfoundland & Labrador.

Short, R.T., D.P. Fries, S.K. Toler, C.E. Lembke, and R.H. Byrne. 1999. Development of Underwater Mass-Spectrometer for In situ Chemical Analysis. *Meas. Sci. Technol.* 10:1195-1201.

Sibenac, M., W. J. Kirkwood, R. McEwen, F. Shane, R. Henthorn. D. Gashler, and H. Thomas. 2002. Modular AUV for routine deep water science operations. *Proceedings of Oceans 02 MTS/IEEE* 1:167 – 172.

Sicardi, A., R. Bozzano, R. Mantovani, F. Grosso. 1997. A Multiple Input Fiber Optic Fluorometer for A Coastal Cost-Effective AUV. *Proceedings of MTS/IEEE Ocean'97 Conference*. 1: 651 – 654.

Siccardi, A., R. Bozzano, R. Mantovani, and F. Grosso. 1997. Multiple Input Fiber Optic Fluorometer for a Coastal Cost-Effective AUV. *Proceedings of IEEE Oceans 07 Conference Proceeding*. 1: 651-654.

Stokey, B.R., T. Austin, N. Forster, R. Goldborough, and M. Purcell, C. Von. 1997. A Small, Low Cost AUV; System Description, Field Trials and Performance Results *Proceedings of MTS/IEEE Oceans 97.2*: 994 – 1000.

Sub Chemical Pack Systems Inc. Accessed Dec, 2006. Nutrient Subchemical Pack Analyzer <http://www.subchem.com/prod01.htm>

Tegberg, A.J., J.Hovdenes, J.H. Andersson, O. Brocandel, R. Diaz, Hebert, T. Arnerich, C. Huber, A. Kortzinger, A. Khriponunoff, F. Rey, C. Ronning, J. Schimanski, S. Sommer, and A. Stangelmayer. 2006. Evaluation of a lifetime-based optode to measure oxygen in aquatic systems. Published by the American Society of Limnology and Oceanography Inc 4(NUM): 7-17.

Tervalon, N. and R. Henthom. 2002. Ice profiling sonar for AUV: Experience in the Arctic. *Proceedings of Ocean'02 MTS/IEEE*. 1:305 – 310.

- Tian, X, P. J.W. Robarts, and G. J.Daviero.2004-a). Marine Wastewater Discharges from Multiport Diffuser. I:Unstratified Stationary Water. Journal of Hydraulic Engineering 130(12):1137-1146.
- Tian, X, P. J.W. Robarts, and G. J.Daviero.2004-b). Marine Wastewater Discharges from Multiport Diffuser. II:Unstratified Flowing Water. Journal of Hydraulic Engineering 130(12):1147-1155.
- Tian, X, P. J.W. Robarts, and G. J.Daviero.2006. Marine Wastewater Discharges from Multiport Diffuser. VI: Stratified Flowing Water. Journal of Hydraulic Engineering 132(4):411-419.
- Torvar, A., C. Moreno, M. P Manuel-Vez, M.G.Vargas. 2002. A simple automated method for the speciation of dissolved inorganic nitrogen in seawater. Analytica Chemica Acta 469(3): 235-242.
- UNEP, 2002.Seas in Asia, North West Pacific and West Africa at Highest Risk from Land-Based Pollution.
- Ura T., M Kumagai, T. Sakakibara, Y. Kimura, T. Okumura, S Kazuyoshi, M. Sasaki, M. Mutsuushima. 2002. Construction and operation of four autonomous underwater vehicles for lake survey. Proceedings of IEEE 2002 International Symposium on Underwater Technology: 24- 29.
- Vestgard, K. and R. Hansen.2001. The Hugin 3000 survey AUV-Design and Field results. Proceedings from underwater intervention 2002 in Tampa, Florida.
- Wernli R. 2000. AUV commercialization – Who’s leading the pack. Intl Conf. on Robotics and Automation, pp. 85-90, 2000.
- Wesson, J. and K. D. Sauners. 1999. A Miniature Fluorometer For Oceanographic Applications. Journal Of Atmospheric And Ocean Technology. Volume 16(11):1630-1634.
- Wet Labs, Inc and sub *champak Systems Inc*. Accessed in 2006. (<http://www.wetlabs.com/appdescs/nutrientstudy.htm>)
- Woolsey, J. R., T. M. McGee, and R. C. Buchannon.2001. A Remote, Multi-Sensor to Monitor Conditions Near the Sea Floor with the Hydrate Stability Zone. Proceedings of MTS/IEEE Oceans 2001 Conference.4:2389-2395.
- Worsfold, P.J. 2006. Challenges in the Determination of Nutrient Species in Natural Waters. Microchimica Acta.154: 45-48.

- Worsfold, P.J.2006. Challenges in the determination of nutrient species in natural waters. *Microchim Acta* 154(1-2):45-48.
- Wu, C.C., T. Yasukawa, H. Shiku, and T. Matsue. 2005. Fabrication Of Miniature Clark Oxygen Sensor Integrated With Microstructure. *Sensors and Actuators* 110(2):342-349.
- Zhaoying, Z. Discussion On CTD Measurement Technology. 2004. *Proceedings MT/IEEE Techno-Ocean 2003*. 3: 1391 – 1

Appendix A. CORMIX Model Prediction File

 BEGIN MOD274: ACCELERATION ZONE OF STAGED DIFFUSER

In this laterally contracting zone the diffuser plume becomes VERTICALLY FULLY

MIXED over the entire layer depth (HS = 4.40m).

Full mixing is achieved after a plume distance of about five layer depths from the diffuser.

Profile definitions:

BV = layer depth (vertically mixed)

BH = Gaussian 1/e (37%) half-width in horizontal plane normal to trajectory

ZU = upper plume boundary (Z-coordinate)

ZL = lower plume boundary (Z-coordinate)

S = hydrodynamic centerline dilution

C = centerline concentration (includes reaction effects, if any)

X	Y	Z	S	C	BV	BH
0.00	2.50	0.60	1.0	0.155E+02	0.00	0.00
0.00	2.40	0.63	3.5	0.439E+01	0.02	0.02
0.00	2.30	0.66	4.6	0.338E+01	0.04	0.03
0.00	2.20	0.70	5.4	0.288E+01	0.06	0.05
0.00	2.10	0.73	6.1	0.255E+01	0.08	0.06
0.00	2.00	0.76	6.7	0.233E+01	0.10	0.08
0.00	1.90	0.79	7.2	0.215E+01	0.12	0.09
0.00	1.80	0.82	7.7	0.201E+01	0.14	0.11
0.00	1.70	0.86	8.2	0.190E+01	0.16	0.12
0.00	1.60	0.89	8.6	0.180E+01	0.18	0.14
0.00	1.50	0.92	9.0	0.172E+01	0.20	0.15
0.00	1.40	0.95	9.4	0.165E+01	0.22	0.17
0.00	1.30	0.98	9.8	0.159E+01	0.24	0.18
0.00	1.20	1.02	10.1	0.153E+01	0.26	0.20
0.00	1.10	1.05	10.5	0.148E+01	0.28	0.21
0.00	1.00	1.08	10.8	0.143E+01	0.30	0.23
0.00	0.90	1.11	11.1	0.139E+01	0.32	0.24
0.00	0.80	1.14	11.4	0.135E+01	0.34	0.26
0.00	0.70	1.18	11.7	0.132E+01	0.36	0.27
0.00	0.60	1.21	12.0	0.129E+01	0.38	0.29
0.00	0.50	1.24	12.3	0.126E+01	0.40	0.30
0.00	0.40	1.27	12.6	0.123E+01	0.42	0.32
0.00	0.30	1.30	12.9	0.120E+01	0.44	0.33
0.00	0.20	1.34	13.1	0.118E+01	0.46	0.34
0.00	0.10	1.37	13.4	0.116E+01	0.48	0.36
0.00	0.00	1.40	13.7	0.113E+01	0.50	0.37
0.00	-0.10	1.43	13.9	0.111E+01	0.52	0.39

0.00	-0.20	1.46	14.2	0.109E+01	0.54	0.40
0.00	-0.30	1.50	14.4	0.108E+01	0.56	0.42
0.00	-0.40	1.53	14.6	0.106E+01	0.58	0.43
0.00	-0.50	1.56	14.9	0.104E+01	0.60	0.45
0.00	-0.60	1.59	15.1	0.103E+01	0.62	0.46
0.00	-0.70	1.62	15.3	0.101E+01	0.64	0.48
0.00	-0.80	1.66	15.5	0.997E+00	0.66	0.49
0.00	-0.90	1.69	15.8	0.983E+00	0.68	0.51
0.00	-1.00	1.72	16.0	0.969E+00	0.70	0.52
0.00	-1.10	1.75	16.2	0.957E+00	0.72	0.54
0.00	-1.20	1.78	16.4	0.945E+00	0.74	0.55
0.00	-1.30	1.82	16.6	0.933E+00	0.76	0.57
0.00	-1.40	1.85	16.8	0.921E+00	0.78	0.58
0.00	-1.50	1.88	17.0	0.911E+00	0.80	0.60
0.00	-1.60	1.91	17.2	0.900E+00	0.82	0.61
0.00	-1.70	1.94	17.4	0.890E+00	0.84	0.63
0.00	-1.80	1.98	17.6	0.880E+00	0.86	0.64
0.00	-1.90	2.01	17.8	0.871E+00	0.88	0.66
0.00	-2.00	2.04	18.0	0.861E+00	0.90	0.67
0.00	-2.10	2.07	18.2	0.852E+00	0.92	0.69
0.00	-2.20	2.10	18.4	0.844E+00	0.94	0.70
0.00	-2.30	2.14	18.5	0.835E+00	0.96	0.72
0.00	-2.40	2.17	18.7	0.827E+00	0.98	0.73
0.00	-2.50	2.20	18.9	0.819E+00	1.00	0.75

Cumulative travel time = 34. sec

Plume centerline may exhibit slight discontinuities in transition to subsequent far-field module.

END OF MOD274: ACCELERATION ZONE OF STAGED DIFFUSER

BEGIN MOD252: DIFFUSER INDUCED PLUME IN WEAK CROSS-FLOW

Phase 1: Vertically mixed, Phase 2: Re-stratified

Phase 1: The diffuser plume is VERTICALLY FULLY MIXED over the entire layer depth.

This flow region is INSIGNIFICANT in spatial extent and will be by-passed.

Phase 2: The flow has RESTRATIFIED at the beginning of this zone.

Profile definitions:

BV = top-hat thickness, measured vertically

BH = Gaussian 1/e (37%) half-width in horizontal plane normal to trajectory

ZU = upper plume boundary (Z-coordinate)

ZL = lower plume boundary (Z-coordinate)

S = hydrodynamic centerline dilution

C = centerline concentration (includes reaction effects, if any)

X	Y	Z	S	C	BV	BH	
0.00	-2.50	4.40	18.9	0.819E+00	4.40	0.58	
0.16	-2.81	4.40	19.4	0.799E+00	2.46	1.09	
0.32	-3.12	4.40	19.8	0.781E+00	1.99	1.41	
0.49	-3.43	4.40	20.3	0.763E+00	1.73	1.68	
0.65	-3.74	4.40	20.7	0.747E+00	1.57	1.94	
0.83	-4.05	4.40	21.2	0.732E+00	1.45	2.18	
1.00	-4.36	4.40	21.6	0.717E+00	1.35	2.42	
1.18	-4.66	4.40	22.0	0.704E+00	1.28	2.65	
1.37	-4.97	4.40	22.4	0.691E+00	1.22	2.87	
1.55	-5.28	4.40	22.8	0.679E+00	1.18	3.09	
1.74	-5.59	4.40	23.2	0.667E+00	1.13	3.31	
1.94	-5.90	4.40	23.6	0.656E+00	1.10	3.52	
2.13	-6.21	4.40	24.0	0.646E+00	1.07	3.73	
2.33	-6.52	4.40	24.4	0.636E+00	1.04	3.94	
2.53	-6.83	4.40	24.7	0.626E+00	1.02	4.15	
2.74	-7.14	4.40	25.1	0.617E+00	0.99	4.36	
2.95	-7.45	4.40	25.5	0.609E+00	0.97	4.56	
3.16	-7.76	4.40	25.8	0.600E+00	0.96	4.77	
3.37	-8.07	4.40	26.2	0.592E+00	0.94	4.97	
3.59	-8.38	4.40	26.5	0.585E+00	0.92	5.18	
3.81	-8.68	4.40	26.8	0.577E+00	0.91	5.38	
4.03	-8.99	4.40	27.2	0.570E+00	0.90	5.58	
4.26	-9.30	4.40	27.5	0.563E+00	0.89	5.78	
4.49	-9.61	4.40	27.8	0.556E+00	0.87	5.99	
4.72	-9.92	4.40	28.2	0.550E+00	0.86	6.19	
4.95	-10.23	4.40	28.5	0.544E+00	0.85	6.39	
5.19	-10.54	4.40	28.8	0.538E+00	0.84	6.59	
5.43	-10.85	4.40	29.1	0.532E+00	0.84	6.79	
5.67	-11.16	4.40	29.4	0.526E+00	0.83	7.00	
5.91	-11.47	4.40	29.7	0.521E+00	0.82	7.20	
6.16	-11.78	4.40	30.0	0.516E+00	0.81	7.40	
6.41	-12.09	4.40	30.3	0.511E+00	0.81	7.60	
6.66	-12.40	4.40	30.6	0.506E+00	0.80	7.80	
6.91	-12.70	4.40	30.9	0.501E+00	0.79	8.00	
7.17	-13.01	4.40	31.2	0.496E+00	0.79	8.21	
7.43	-13.32	4.40	31.5	0.492E+00	0.78	8.41	
7.69	-13.63	4.40	31.8	0.487E+00	0.77	8.61	
7.95	-13.94	4.40	32.1	0.483E+00	0.77	8.81	
8.22	-14.25	4.40	32.4	0.479E+00	0.76	9.01	
8.49	-14.56	4.40	32.6	0.475E+00	0.76	9.22	

8.76	-14.87	4.40	32.9	0.471E+00	0.75	9.42
9.03	-15.18	4.40	33.2	0.467E+00	0.75	9.62
9.30	-15.49	4.40	33.5	0.463E+00	0.74	9.82
9.58	-15.80	4.40	33.7	0.459E+00	0.74	10.03
9.86	-16.11	4.40	34.0	0.456E+00	0.74	10.23
10.14	-16.42	4.40	34.3	0.452E+00	0.73	10.43
10.43	-16.72	4.40	34.5	0.449E+00	0.73	10.64
10.71	-17.03	4.40	34.8	0.445E+00	0.72	10.84
11.00	-17.34	4.40	35.1	0.442E+00	0.72	11.04
11.29	-17.65	4.40	35.3	0.439E+00	0.72	11.25
11.58	-17.96	4.40	35.6	0.436E+00	0.71	11.45

Cumulative travel time = 555. sec

END OF MOD252: DIFFUSER INDUCED PLUME IN WEAK CROSS-FLOW

 ** End of NEAR-FIELD REGION (NFR) **

The initial plume WIDTH values in the next far-field module will be CORRECTED by a factor 2.04 to conserve the mass flux in the far-field! The correction factor is quite large because of the small ambient velocity relative to the strong mixing characteristics of the discharge! This indicates localized RECIRCULATION REGIONS and internal hydraulic JUMPS.

 BEGIN MOD241: BUOYANT AMBIENT SPREADING

Profile definitions:

- BV = top-hat thickness, measured vertically
- BH = top-hat half-width, measured horizontally in y-direction
- ZU = upper plume boundary (Z-coordinate)
- ZL = lower plume boundary (Z-coordinate)
- S = hydrodynamic average (bulk) dilution
- C = average (bulk) concentration (includes reaction effects, if any)

Plume Stage 1 (not bank attached):

X	Y	Z	S	C	BV	BH	ZU	ZL	
11.58	-17.96	4.40	35.6	0.436E+00	1.45	23.38	4.40	2.95	
12.85	-17.96	4.40	36.7	0.422E+00	1.32	26.49	4.40	3.08	
14.12	-17.96	4.40	37.7	0.410E+00	1.23	29.42	4.40	3.17	
15.39	-17.96	4.40	38.6	0.401E+00	1.15	32.21	4.40	3.25	
16.65	-17.96	4.40	39.5	0.392E+00	1.08	34.88	4.40	3.32	
17.92	-17.96	4.40	40.2	0.385E+00	1.03	37.45	4.40	3.37	
19.19	-17.96	4.40	40.9	0.378E+00	0.98	39.93	4.40	3.42	
20.46	-17.96	4.40	41.6	0.372E+00	0.94	42.33	4.40	3.46	
21.73	-17.96	4.40	42.3	0.367E+00	0.90	44.67	4.40	3.50	

23.00	-17.96	4.40	42.9	0.361E+00	0.87	46.94	4.40	3.53
24.26	-17.96	4.40	43.5	0.356E+00	0.84	49.15	4.40	3.56
25.53	-17.96	4.40	44.0	0.352E+00	0.82	51.31	4.40	3.58
26.80	-17.96	4.40	44.6	0.347E+00	0.80	53.43	4.40	3.60
28.07	-17.96	4.40	45.1	0.343E+00	0.78	55.50	4.40	3.62
29.34	-17.96	4.40	45.7	0.339E+00	0.76	57.53	4.40	3.64
30.60	-17.96	4.40	46.2	0.335E+00	0.74	59.52	4.40	3.66
31.87	-17.96	4.40	46.7	0.332E+00	0.73	61.47	4.40	3.67
33.14	-17.96	4.40	47.2	0.328E+00	0.71	63.40	4.40	3.69
34.41	-17.96	4.40	47.7	0.325E+00	0.70	65.29	4.40	3.70
35.68	-17.96	4.40	48.2	0.321E+00	0.69	67.15	4.40	3.71
36.94	-17.96	4.40	48.7	0.318E+00	0.67	68.98	4.40	3.73
38.21	-17.96	4.40	49.3	0.314E+00	0.66	70.79	4.40	3.74
39.48	-17.96	4.40	49.8	0.311E+00	0.65	72.57	4.40	3.75
40.75	-17.96	4.40	50.3	0.308E+00	0.65	74.33	4.40	3.75
42.02	-17.96	4.40	50.8	0.305E+00	0.64	76.07	4.40	3.76
43.29	-17.96	4.40	51.3	0.302E+00	0.63	77.78	4.40	3.77
44.55	-17.96	4.40	51.8	0.299E+00	0.62	79.47	4.40	3.78
45.82	-17.96	4.40	52.3	0.296E+00	0.62	81.15	4.40	3.78
47.09	-17.96	4.40	52.9	0.293E+00	0.61	82.80	4.40	3.79
48.36	-17.96	4.40	53.4	0.290E+00	0.60	84.43	4.40	3.80
49.63	-17.96	4.40	53.9	0.287E+00	0.60	86.05	4.40	3.80
50.89	-17.96	4.40	54.5	0.284E+00	0.59	87.65	4.40	3.81
52.16	-17.96	4.40	55.0	0.282E+00	0.59	89.24	4.40	3.81
53.43	-17.96	4.40	55.5	0.279E+00	0.58	90.81	4.40	3.82
54.70	-17.96	4.40	56.1	0.276E+00	0.58	92.36	4.40	3.82
55.97	-17.96	4.40	56.7	0.273E+00	0.58	93.90	4.40	3.82
57.23	-17.96	4.40	57.2	0.271E+00	0.57	95.42	4.40	3.83
58.50	-17.96	4.40	57.8	0.268E+00	0.57	96.93	4.40	3.83
59.77	-17.96	4.40	58.4	0.265E+00	0.57	98.43	4.40	3.83
61.04	-17.96	4.40	59.0	0.263E+00	0.56	99.91	4.40	3.84
62.31	-17.96	4.40	59.6	0.260E+00	0.56	101.39	4.40	3.84
63.57	-17.96	4.40	60.2	0.257E+00	0.56	102.85	4.40	3.84
64.84	-17.96	4.40	60.8	0.255E+00	0.56	104.30	4.40	3.84
66.11	-17.96	4.40	61.5	0.252E+00	0.56	105.73	4.40	3.84
67.38	-17.96	4.40	62.1	0.249E+00	0.55	107.16	4.40	3.85
68.65	-17.96	4.40	62.8	0.247E+00	0.55	108.57	4.40	3.85
69.92	-17.96	4.40	63.4	0.244E+00	0.55	109.98	4.40	3.85
71.18	-17.96	4.40	64.1	0.242E+00	0.55	111.37	4.40	3.85
72.45	-17.96	4.40	64.8	0.239E+00	0.55	112.76	4.40	3.85
73.72	-17.96	4.40	65.4	0.237E+00	0.55	114.13	4.40	3.85
74.99	-17.96	4.40	66.1	0.234E+00	0.55	115.50	4.40	3.85

Cumulative travel time = 2930. sec

Plume is ATTACHED to LEFT bank/shore.

Plume width is now determined from LEFT bank/shore.

Plume Stage 2 (bank attached):

X	Y	Z	S	C	BV	BH	ZU	ZL	
74.99	97.50	4.40	66.1	0.234E+00	0.55	230.92	4.40	3.85	
79.49	97.50	4.40	68.3	0.227E+00	0.55	235.46	4.40	3.85	
83.99	97.50	4.40	70.5	0.220E+00	0.56	239.94	4.40	3.84	
88.49	97.50	4.40	72.8	0.213E+00	0.57	244.39	4.40	3.83	
92.99	97.50	4.40	75.2	0.206E+00	0.58	248.79	4.40	3.82	
97.49	97.50	4.40	77.6	0.200E+00	0.59	253.15	4.40	3.81	
101.99	97.50	4.40	80.1	0.193E+00	0.59	257.47	4.40	3.81	
106.49	97.50	4.40	82.7	0.187E+00	0.60	261.76	4.40	3.80	
110.99	97.50	4.40	85.4	0.181E+00	0.61	266.01	4.40	3.79	
115.49	97.50	4.40	88.1	0.176E+00	0.62	270.23	4.40	3.78	
119.99	97.50	4.40	91.0	0.170E+00	0.63	274.41	4.40	3.77	
124.49	97.50	4.40	93.9	0.165E+00	0.64	278.57	4.40	3.76	
128.99	97.50	4.40	96.9	0.160E+00	0.65	282.69	4.40	3.75	
133.49	97.50	4.40	99.9	0.155E+00	0.67	286.78	4.40	3.73	
137.99	97.50	4.40	103.1	0.150E+00	0.68	290.85	4.40	3.72	
142.49	97.50	4.40	106.3	0.146E+00	0.69	294.89	4.40	3.71	
146.99	97.50	4.40	109.6	0.141E+00	0.70	298.90	4.40	3.70	
151.49	97.50	4.40	113.0	0.137E+00	0.71	302.89	4.40	3.69	
155.99	97.50	4.40	116.5	0.133E+00	0.72	306.86	4.40	3.68	
160.49	97.50	4.40	120.1	0.129E+00	0.74	310.80	4.40	3.66	
164.99	97.50	4.40	123.7	0.125E+00	0.75	314.72	4.40	3.65	
169.49	97.50	4.40	127.4	0.122E+00	0.76	318.61	4.40	3.64	
173.99	97.50	4.40	131.3	0.118E+00	0.78	322.49	4.40	3.62	
178.49	97.50	4.40	135.2	0.115E+00	0.79	326.34	4.40	3.61	
182.99	97.50	4.40	139.2	0.111E+00	0.80	330.18	4.40	3.60	
187.49	97.50	4.40	143.3	0.108E+00	0.82	333.99	4.40	3.58	
191.99	97.50	4.40	147.4	0.105E+00	0.83	337.79	4.40	3.57	
196.49	97.50	4.40	151.7	0.102E+00	0.85	341.56	4.40	3.55	
200.99	97.50	4.40	156.1	0.992E-01	0.86	345.32	4.40	3.54	
205.49	97.50	4.40	160.5	0.965E-01	0.88	349.06	4.40	3.52	
210.00	97.50	4.40	165.1	0.938E-01	0.89	352.78	4.40	3.51	
214.50	97.50	4.40	169.7	0.913E-01	0.91	356.49	4.40	3.49	
219.00	97.50	4.40	174.4	0.888E-01	0.92	360.18	4.40	3.48	
223.50	97.50	4.40	179.3	0.864E-01	0.94	363.85	4.40	3.46	
228.00	97.50	4.40	184.2	0.841E-01	0.96	367.51	4.40	3.44	
232.50	97.50	4.40	189.2	0.819E-01	0.97	371.15	4.40	3.43	
237.00	97.50	4.40	194.3	0.797E-01	0.99	374.78	4.40	3.41	
241.50	97.50	4.40	199.5	0.776E-01	1.01	378.39	4.40	3.39	
246.00	97.50	4.40	204.8	0.756E-01	1.02	381.98	4.40	3.38	
250.50	97.50	4.40	210.2	0.737E-01	1.04	385.57	4.40	3.36	



